AD/A-006 588

ON THE PROBLEM OF SHAPING AN AXISYMMETRIC BODY TO OBTAIN LOW DRAG AT LARGE REYNOLDS NUMBERS

J. L. Hess, et al

McDonnell Douglas Corporation

REPORT DOCUMENTATION PAGE		READ INSTRUCTIONS BEFORE COMPLETING FORM
1. REPORT NUMBER MDC J6791	2. GOVT ACCESSION NO.	3. RECIPIENT'S CATALOG NUMBER ADA-006588
4. TITLE (and Subtitle) ON THE PROBLEM OF SHAPING AN AXISYMMETRIC BODY TO OBTAIN LOW DRAG AT LARGE REYNOLDS NUMBERS		5. TYPE OF REPORT & PERIOD COVERED Final Technical 6/73 - 1/75
		6. PERFORMING ORG. REPORT NUMBER MDC J6791
7. AUTHOR(s) J. L. Hess and R. M. James		8. CONTRACT OR GRANT NUMBER(s) N00014-73-C-0502
9. PERFORMING ORGANIZATION NAME AND ADDRESS McDonnell Douglas Corporation Douglas Aircraft Company 3855 Lakewood Boulevard Long Beach, California 90801		10. PROGRAM ELEMENT, PROJECT, TASK AREA & WORK UNIT NUMBERS NR061-219/4-23-75 code 438
11. CONTROLLING OFFICE NAME AND ADDRESS Office of Naval Research Department of the Navy Arlington, Virginia 22217		12. REPORT DATE January 1975
		13. NUMBER OF PAGES 124
14. MONITORING AGENCY NAME & ADDRESS(if different from Controlling Office) Office of Naval Research Department of the Navy Arlington, Virginia 22217		15. SECURITY CLASS. (of this report) Unclassified
		15a. DECLASSIFICATION/DOWNGRADING SCHEDULE

16. DISTRIBUTION STATEMENT (of this Report)

Approved for public release; distribution unlimited. Reproduction in whole or in part is permitted for any purpose of the United States Government.

17. DISTRIBUTION STATEMENT (of the abstract entered in Block 20, if different from Report)

18. SUPPLEMENTARY NOTES

19. KEY WORDS (Continue on reverse side if necessary and identify by block number)

Axisymmetric
Body Shape
Boundary Layer
Drag
Inverse Methods
Optimization
Potential Flow
Turbulence

20. ABSTRACT (Continue on reverse side if necessary and identify by block number)

This report describes attempts at the analytic design of an axisymmetric body having low drag with a fully turbulent boundary layer in incompressible flow. The drag is to be made small solely by proper shaping of the body. Several theoretical studies of various types are performed in an attempt to determine what body shapes have low drag. The principal conclusion is that the drag coefficient is not very sensitive to body shape and thus that no significant drag reductions can be obtained from shaping alone.

DD FORM 1473 1 JAN 73   EDITION OF 1 NOV 65 IS OBSOLETE
S/N 0102-014-6601

PRICES SUBJECT TO CHANGE

ON THE PROBLEM OF SHAPING AN AXISYMMETRIC BODY
TO OBTAIN LOW DRAG AT LARGE REYNOLDS NUMBERS

Prepared by: John L. Hess and R. M. James

Approved by:

John L. Hess
Section Manager
Theoretical Aerodynamics

A. M. O. Smith
Chief Aerodynmics Engineer
Aerodynamics

O. R. Dunn
Director of Aerodynamics

DOUGLAS AIRCRAFT COMPANY

MCDONNELL DOUGLAS

CORPORATION

1.0 ABSTRACT

This report describes an attempt to design by analytic means a class of axisymmetric bodies having low drag in incompressible flow for the case where the boundary layer is fully turbulent over the entire body. The drag is to be made small solely by proper shaping of the body, and the drag coefficient to be minimized is that based on a reference area equal to the two-thirds power of the body's volume. A comparison of various drag-calculation methods shows that the Truckenbrodt formula, which expresses drag as an integral of a power of the potential-flow surface velocity, is sufficiently accurate, and this formula is adopted as the chief analytic tool. Among the consequences of this choice is that bodies with low drag at one Reynolds number have low drag at all. Drag performances of various types of bodies are compared, including those of "cavitation shapes" derived from a new inverse potential-flow program. Two-dimensional optimization studies are carried out using an integral formula for drag analagous to that of Truckenbrodt. The principal conclusion is that the drag coefficient is not very sensitive to body shape and thus that no significant drag reductions can be obtained from shaping alone.

2.0 TABLE OF CONTENTS

3.0 INDEX OF FIGURES

3

4.0 PRINCIPAL NOTATION

A area enclosed by the profile curve of a two-dimensional body

C_D drag coefficient; based on two-thirds power of volume for axisymmetric bodies; based on square root of A for two-dimensional bodies

c_f skin friction coefficient

D drag; used in some figures for body diameter

H ratio of boundary-layer displacement thickness to momentum thickness

I integral defined by (13)

J integral defined by (19)

L body length

Re Reynolds number based on body length

r radial coordinate, distance from symmetry axis

S reference area equal to two-thirds power of body volume

U potential-flow velocity on the body surface

U_∞ free-stream velocity

u velocity component in boundary layer. On the body it is parallel to the local body surface. In the wake it is parallel to the free-stream direction

x coordinate parallel to free-stream direction. For axisymmetric flow the x-axis is the symmetry axis.

y in section 6.0; denotes distance in the boundary layer measured normal to the body surface. In section 7.1 and in all two-dimensional analysis it denotes a coordinate perpendicular to the free-stream direction

α slope angle of the profile curve of the body with respect to the x-axis

δ boundary-layer thickness

δ^* boundary-layer displacement thickness

θ boundary-layer momentum thickness

ρ fluid density — a constant

χ momentum area

χ_∞ momentum area of the wake far downstream

5.0 INTRODUCTION AND SUMMARY

This report presents results of a study whose object has been the design of axisymmetric bodies having low drag at high Reynolds number. More precisely the problem may be stated as follows. Consider an axisymmetric body at zero angle of attack in an incompressible flow whose Reynolds number is so large that the boundary layer on the body may be taken fully turbulent over the entire length of the body. Let the drag coefficient be based on a reference area defined as the two-thirds power of the body's volume. It is desired to minimize this drag coefficient solely by proper shaping of the body without resort to suction, compliant surfaces, additives, etc. Moreover, this minimization should be performed for a range of Reynolds number. While the problem is easy to state, it is difficult to formulate in a manner that admits of fruitful analysis. Accordingly, the present work has consisted of several investigations designed to shed light on the mechanisms leading to low drag and also to determine a number of bodies having as low a drag as possible. The chief emphasis has been on the axisymmetric problem, but the related two-dimensional problem has been considered also. The latter is more tractable in some ways, and the results obtained have definite implications for the axisymmetric case.

The first part of the study concerns methods of computing the drag of an axisymmetric body (section 6.0). The ideas and formulas for calculating drag from a momentum deficit approach are presented. These formulas are implemented with two different types of boundary-layer calculation methods and also with a set of simplifying assumptions that eliminates the need for an explicit boundary-layer calculation and calculates drag from an integral over the body of a power of the potential flow velocity. Drags computed by all three methods are compared with experimental drags obtained for a set of bodies in water. It is concluded that the simplified integral method of computing drag is sufficiently accurate and so much simpler than the others that it is used in all subsequent calculations. A particularly desirable feature of this method is the fact that the Reynolds number enters only in a multiplicative factor. Thus, if a particular body has the lowest drag at one Reynolds number, it has the lowest drag at all Reynolds numbers, and the investigation need not concern itself with Reynolds number directly.

6

The drag performance of a wide variety of bodies has been compared using the simplified integral drag formula (section 7.0). The drag coefficient for a general prolate spheroid can be written down analytically. The curve of drag coefficient versus fineness ratio for prolate spheroids has proven a very useful device for correlating drags for all bodies, because all "good" shapes have drags that plot near this curve. The curve has a shallow minimum, and thus there is a preferred range of fineness ratio from about three to four. Oddly, the simplified integral drag formula does not strictly apply to prolate spheroids, from which the flow is presumed to separate at their blunt aft ends. However, the separation can be removed by a small amount of aft streamlining or "boattailing" with a very small effect on drag. In any case the unseparated "good" bodies have relatively low drags that essentially follow the curve.

Unlike certain two-dimensional applications, there is no information on what properties of the body shape, its pressure distribution, or its skin-friction distribution lead to low drag. Thus the use of inverse boundary-layer or potential-flow methods is of limited value in the present problem. Nevertheless, some investigation along this line has been carried out. In particular "cavitation" bodies having extensive regions of constant pressure were studied on the ground that they should have relatively low maximum velocities and thus possibly low values of the drag integral. Unfortunately, this proved not to be true (section 7.3).

In implementing the above investigation a new method of solution for the axisymmetric potential flow problem was discovered and developed. This solution, which is applicable to completely general shapes, is based on a conformal transformation of the body to a circle and obtains the solution as a series of Chebyshev and Legendre polynomials. Both direct and inverse problems can be treated. While the application of this procedure to the low-drag problem appears to be of limited usefulness, the development of such a method is felt to be important in itself.

Two-dimensional analysis has been used in section 8.0 to attempt to determine shapes that minimize the drag coefficient calculated from the simplified drag integral. For this study the two-dimensional drag coefficient has been based on the square root of the area enclosed by the body profile as

the closest analogy to the normalization based on the two-thirds power of the volume that is used in the axisymmetric case. Slender-body theory is shown to be inadequate. General solutions based on conformal transformations yield bodies having minimum drag coefficients. However, the drags thus obtained are only very slightly less than those for simple bodies selected at random. Probably the same is true for the axisymmetric problem.

6.0 DIRECT DRAG CALCULATION FOR AXISYMMETRIC BODIES

6.1 Theory for Drag Calculation Based on Momentum Deficit

Because the straightforward calculation of drag by integration of surface pressure and skin friction turns out to be inaccurate [1], the drag of a body must be obtained by considering the deficit of momentum far downstream in the wake. The basic analysis, which is given in [2], is merely outlined here.

Consider an axisymmetric body at zero angle of attack as shown in Fig. 1. The boundary layer on the body continues into the wake and far downstream there is a deficit of momentum due to viscous retardation of the flow along the body surface. From momentum considerations the drag of the body is given by

$$D = 2\pi\rho \int_0^\infty u(U_\infty - u)r\,dr = 2\pi\rho \int_0^\delta u(U_\infty - u)r\,dr \tag{1}$$

where ρ is fluid density (a constant in the present study), U_∞ is free stream velocity, u is the local velocity component parallel to the symmetry axis (x-axis), r is radial distance from the symmetry axis, and δ is the radius of the wake. The integral in (1) is taken in an x = constant plane which for convenience is taken as far downstream. The momentum area of the wake far downstream is defined as

$$X_\infty = 2\pi \int_0^\delta \frac{u}{U_0} \left(1 - \frac{u}{U_0}\right) r\,dr \tag{2}$$

so that

$$D = \rho U_\infty^2 X_\infty \tag{3}$$

the drag coefficient is

$$C_D = \frac{D}{(1/2)\rho U_\infty^2 S} = \frac{2X_\infty}{S} \tag{4}$$

9

where S is some reference area, which in the present study is equal to the two-thirds power of the volume of the body. It is desired to compute this drag in terms of quantities evaluated on the body, and this is where the first approximation must be introduced.

The momentum thickness of the boundary layer at any point of the body is

$$\theta = \int_0^\delta \frac{u}{U}\left(1 - \frac{u}{U}\right)\left(1 + \frac{y}{r}\cos\alpha\right) dy \tag{5}$$

In (5) the various quantities have their customary definitions, which are somewhat different than those of equation (1), which applies to a location in the wake. Specifically, y denotes distance normal to the body surface, δ is boundary-layer thickness, u is the velocity component parallel to the surface, and U is the value of u for $y = \delta$. Moreover, r is radial distance from the symmetry axis to a point on the body surface, and α is the local slope angle of the surface with respect to the symmetry axis. The momentum area of the boundary layer at any location on the body is defined as

$$\chi = 2\pi r\theta \tag{6}$$

Finally define

$$H = \frac{\delta^*}{\theta} \tag{7}$$

where δ^* is the usual boundary-layer displacement thickness

$$\delta^* = \int_0^\delta \left(1 - \frac{u}{U}\right)\left(1 + \frac{y}{r}\cos\alpha\right) dy \tag{8}$$

Now the required approximation is introduced. Young's analysis [2] leads to the relationship

$$\chi_\infty = \chi\left(\frac{U}{U_\infty}\right)^{(H+5)/2} \tag{9}$$

where χ, U, and H in (9) are all evaluated at a particular location on the body — usually "near" the trailing edge. This gives for the drag coefficient

$$C_D = \frac{4\pi r \theta}{S} \left(\frac{U}{U_\infty}\right)^{(H+5)/2} \tag{10}$$

Granville [3] has an alternate form of (9) which gives as an alternative to (10) the form

$$C_D = \frac{4\pi r \theta}{S} \left(\frac{U}{U_\infty}\right)^{(7/8)H+(17/8)} \tag{11}$$

However, for most of the present work (10) has been used. The various quantities appearing in (10) must be evaluated by means of a boundary-layer calculation. During the present study three boundary-layer methods were considered, one of which evaluates these quantities directly in terms of potential-flow quantities.

6.2 Finite-Difference Boundary-Layer Method

The most general and elaborate type of boundary-layer method is that which solves a partial differential equation for flow in the boundary layer. The numerical solution is effected by some type of finite-difference scheme, usually beginning with the front stagnation point and proceeding downstream along the body. The calculation terminates if separation is encountered but othe⋅⋅ise traverses the entire body. In the present study of low-drag bodies it is presumed that all good bodies will indeed have unseparated boundary layers, so that the above is not a serious restriction. In fact one advantage of the finite-difference method is that it predicts separation (or its absence) which some other methods do not. For a laminar boundary layer such a technique may be made numerically exact. However, for a turbulent boundary layer an empirical or semi-empirical "closure" condition is required that usually takes the form of an "eddy-viscosity" law. This assumption renders the calculation approximate. A variety of closure conditions have been proposed. The method used in this study is that due to Cebeci and Smith. Details of the procedure are given in [4].

According to the theory of section 6.1, the drag of a body is obtained by evaluating (10) at the downstream end of the body. However, (10) can be evaluated at any point of the body. If this is done and the results plotted versus position along the body, certain modifications in the use of the formula become evident. There are three different types of cases; examples of which are shown in figures 2, 3 and 4. Figure 2 shows the unambiguous case where the drag coefficient is a smooth function of position all over the body, and extrapolating it to the aft end of the body presents no problem. This extrapolated value is then taken to be the drag of the body. More common, however, is the type of case shown in Figure 3, where the calculated drag coefficient rather suddenly begins to increase more rapidly a short distance ahead of the aft end of the body — about 90% of body length in figure 3. Extrapolating the calculated curve for such a case to the aft end of the body gives a value of drag that is far too large. The most effective procedure appears to consist of extrapolating to the aft end from the smooth portion of the curve upstream of the "break" as shown in figure 3. The third type of case is that shown in figure 4. It is characterized by having a calculated drag coefficient that is not monotonically increasing. Instead there is a maximum a short distance ahead of the aft end of the body, and the drag decreases downstream of this point. The only reasonable procedure is to use the maximum computed value of drag as the drag of the body.

Despite the somewhat striking differences in the procedure for estimating drag in the three cases, there is no real difference in the accuracy of the results as judged by comparison with experimental values. The "nice" case of figure 2 agrees with experiment no better than the "difficult" case of figure 3.

6.3 Momentum-Integral Boundary-Layer Method

Momentum-integral boundary-layer methods are characterized by the fact that they use certain assumptions, such as the form of the velocity profile in the boundary layer, to reduce the partial differential equation of boundary-layer flow to an ordinary differential equation (or set of such equations) along the body surface. Patel [5] has developed a method of this type for calculating thick axisymmetric boundary layers and Nakayama and Patel [6] have used this method together with Granville's formula (11) to calculate drag. As in the third type of case of section 5.2, the drag calculated

12

in this way does not increase monotonically along the body but has a maximum, which is taken as the drag of the body.

6.4 Simplified Integral Drag Calculation

The drag calculation methods of the previous two sections use a boundary-layer calculation procedure to determine the quantities that enter into the drag formula (10). The boundary-layer calculation procedures are approximate but are still fairly elaborate and require computer programs for their implementation. Moreover, the drag calculation must be repeated for each Reynolds number of interest. By making certain additional approximations the quantities in (10) can be obtained directly, and thus the need for a boundary-layer calculation method can be eliminated entirely. In the present study this has been done using the theory of Truckenbrodt [7].

For the case of a fully turbulent boundary layer the theory of [7] gives the momentum thickness at a point on the body as

$$\theta = \frac{c_f}{2} \frac{L^{1/7}}{r(U/U_\infty)^3} I \tag{12}$$

where L is body length, c_f is total skin-friction coefficient, and where

$$I = \left[\int \left(\frac{U}{U_\infty}\right)^{10/3} r^{7/6} ds \right]^{6/7} \tag{13}$$

where s denotes arc length along the body profile curve, and where the range of integration is from the front stagnation point to the point where θ is to be evaluated. If this is used in (10) the drag coefficient is

$$C_D = \frac{2\pi L^{1/7}}{S} c_f I \left(\frac{U}{U_\infty}\right)^{(H-1)/2} \tag{14}$$

Since $H > 1$ it is evident that if the potential-flow velocity is used in (14), then $C_D = 0$ at the aft end of the body. However, since C_D is never negative, it obviously has a maximum value, which generally occurs a short distance ahead of the aft end of the body just as for the methods of sections 6.2 and 6.3. This maximum value is taken as the drag of the body.

13

Calculations obtained from the method of section 6.2 for a large number of bodies, have shown that at the location where (14) is a maximum

$$0.975 < \left(\frac{U}{U_\infty}\right)^{(H-1)/2} < 1.0 \tag{15}$$

for all bodies. Thus it is consistent with the other approximations that have been made to set this quantity equal to unity and to write the drag as

$$C_D = \frac{2\pi L^{1/7}}{S} c_f \left[\int_{body} \left(\frac{U}{U_\infty}\right)^{10/3} r^{7/6} ds\right]^{6/7} \tag{16}$$

where the integral is over the entire body profile. The Reynolds number Re enters only in the skin-friction coefficient c_f which the Prandtl-Schlichting relation [8] gives as

$$c_f = \frac{0.455}{[\log(Re)]^{2.58}} \tag{17}$$

Equation (16) is the simplified integral drag formula, which obtains drag directly from the potential-flow velocity distribution. The fact that the Reynolds number enters only in a multiplicative factor means that if one shape has lower drag than another at one Reynolds number, it will have lower drag at all Reynolds numbers. In particular an optimum shape, if it can be found, is independent of Reynolds number.

6.5 Comparison of the Methods

The relative accuracies of the three methods for computing drag in incompressible flow have been evaluated by comparing calculated drags with the highly accurate experimental results obtained by Gertler for a series of bodies of revolution in a towing tank [9]. For these comparisons eight of the 20 bodies of [9] were selected in such a way that the complete ranges of fineness ratio and drag values are well represented.

First the simplified integral formula (16) is compared with the result of using the finite-difference boundary-layer method of section 6.2 in the basic drag formula (10). Figures 5 and 6 compare these two methods with

14

experiment for Reynolds numbers of 10 million and 20 million, respectively. The simplified integral formula (16) is definitely more accurate. Its RMS errors are approximately 60% of those obtained by the use of the finite-difference boundary-layer method. Formula (16) is thus much to be preferred because of its simplicity.

Next the momentum-integral boundary-layer method of section 6.3 used with Granville's drag formula (11) is compared with the simplified integral formula (16) and with the result of using the finite-difference boundary-layer method of section 6.2 in the basic drag formula (10). These comparisons, which are shown in figures 7 and 8, respectively, are for the same set of bodies from [9] at a Reynolds number of 20 million. The calculation based on the momentum-integral is definitely the most accurate of the three methods studied. Its RMS error is about 57% of that obtained by the simplified integral formula and only 35% of that obtained using the finite-difference boundary-layer method.

Despite the above finding the simplified integral formula (16) has been used for drag calculation in this study. One important consideration was that the momentum-integral method was not obtained by the authors until rather late in the study. The other important factor is the greater simplicity of formula (16), including the fact that Reynolds number need not be considered explicitly in the investigation. Despite the somewhat inferior accuracy of formula (16), it seemed unlikely that any overall conclusions drawn on the basis of this formula would be drastically overturned by use of the momentum-integral method. The finite-difference method has been applied after the fact to the best bodies to verify that their boundary layers are unseparated.

15

7.0 INVESTIGATION OF LOW-DRAG SHAPES USING THE SIMPLIFIED INTEGRAL DRAG CALCULATION

7.1 Comparison of Two-Dimensional and Axisymmetric Formulas

Although the principal interest in the present study is axisymmetric flow, two-dimensional flow has been considered also, because it is simpler from some standpoints and it should be at least qualitatively similar. In fact the similarities between the two-dimensional and axisymmetric cases can most easily be seen by examining the two forms of the simplified drag integral. Spence [10] reduces the drag of a two-dimensional body to an integral of the potential-flow velocity in a manner analogous to the theory of Truckenbrodt, quoted in section 6.4, for axisymmetric bodies. The two-dimensional drag coefficient must be normalized with respect to a reference length that is as analagous as possible to the reference area (two-thirds power of volume) used for the axisymmetric drag coefficient. The length chosen is the square root of the area enclosed by the profile curve of the body. With these choices the drag coefficient for both axisymmetric and two-dimensional bodies may be written

$$C_D = (\text{const}) \frac{\left[\int U^m y^n ds\right]^p}{\left[\int y^q dx\right]^r} \tag{18}$$

where x and y denote, respectively, distance parallel and perpendicular to the free stream. As before U is surface velocity, s is arc length, and the integrals are over the entire body. The exponents are

	Axisymmetric	Two-Dimensional
m	10/3	4
n	7/6	0
p	6/7	5/6
q	2	1
r	2/3	1/2

7.2 Prolate Spheroids and Pointed Shapes

The function to be adjusted to obtain the minimum is of course the body shape y(x). Some direct attacks on the minimization problem are outlined in subsequent sections. In this section attention is concentrated on an attempt to find good shapes simply by using (16) to calculate results for a variety of bodies.

The drag coefficient of (16) can be obtained analytically for prolate spheroids as a function of fineness ratio. This function is graphed in Figure 9. Drag values are shown for a Reynolds number of 10 million, but at other Reynolds numbers only the level of the curve is changed not its shape. It can be seen that there is a shallow minimum at a fineness ratio somewhat greater than three. This curve has proved quite useful in analyzing bodies, because it turns out that on the basis of approximately 50 calculations most good bodies give drags that plot very near this curve. It might be argued that since prolate spheroids have blunt aft ends near which the boundary layer separates, the curve of figure 9 is not meaningful. To investigate this several prolate spheroids were fitted with conical boattails. Equation (16) was evaluated for these bodies and the results lie close to the basic curve as shown in figure 9. Absence of separation was verified for these bodies by finite-difference boundary-layer calculations. By way of example, figure 10 shows results for a 40%-thick prolate spheroid that was fitted with a conical boattail to produce a body of fineness ratio 3.25, the flow about which is effectively unseparated. For fineness ratios below about 3, absence of separation could not be obtained, and it is concluded that the curve of figure 9 is only of theoretical interest to the left of this point. The calculated drags for the Gertler bodies (figure 5) are also shown in figure 9 and they also lie on the basic curve. The calculations imply a preferred range of fineness ratio from 3 to 4. Experimental results may alter this conclusion somewhat — probably in the direction of increased fineness ration.

7.3 Constant-Pressure Bodies Derived from an Inverse Procedure

Since the integrand of the simplified drag integral (16) depends on a higher power of surface velocity than of local body ordinate, it was hypothesized that the search for low drag bodies might better be conducted in terms of velocity distribution rather than in terms of shape directiy. That

17

is, it was thought that certain velocity distributions might have low values
of drag associated with the corresponding shapes. However, no general principles
of this sort could be formulated. It does appear from the form of (16) that
keeping the maximum velocity as small as possible should be desirable. This
leads to consideration of velocity distributions which are constant at their
maximum value over much of the body, i.e., "cavitation shapes." Unfortunately,
it turns out that their performance is not much different from prolate spheroids
(see below).

Suppose a surface velocity distribution can be selected by some criterion.
Determination of the body shape corresponding to this velocity distribution
requires an inverse potential-flow method. When the present study was initiated
the development of such a method for the axisymmetric case was an unsolved
problem. Early in the study [11] appeared, which solves the inverse problem
by iterative use of a direct method. As part of the present study a new type
of direct-and-inverse solution was developed for the problem of axisymmetric
potential flow. The method of solution depends on conformal transformation
and a series solution in terms of Legendre and Chebyshev polynomials. A
detailed presentation is contained in Appendix A.

Based on the reasoning outlined above, "cavitation shapes" were determined
by both the method of [11] and that of Appendix A. The velocity distributions
that were called for had extensive regions of constant velocity. Because of
the details of the inverse procedures the bodies that resulted had velocity
distributions that were almost, but not quite, constant. Figure 11 shows a typ-
ical result.

Figure 12 shows drag coefficients computed by (16) for nine bodies designed
to have virtually constant maximum-velocity regions. Four were obtained directly
by modifying elliptic contours. The other five are products of the inverse
potential-flow methods mentioned above. Four of the five have pointed aft ends
similar to the one shown in Figure 11. The fifth, which has the lowest drag of
all, is symmetric fore-and-aft and has a blunt aft end. Flow about the pointed
shapes is unseparated. From Figures 9 and 12 it may be concluded that the per-
formance represented by the curve for prolate spheroids can actually be obtained
but that shapes with significantly lower drag are difficult to find.

18

8.0 APPLICATION OF MINIMIZATION TECHNIQUES TO THE TWO-DIMENSIONAL
LOW-DRAG PROBLEM BASED ON THE SIMPLIFIED INTEGRAL FORMULA

8.1 Statement of the Problem

One of the principal reasons for concentrating on the simplified integral formula for drag is that application of a rigorous minimization technique to this integral appears to be at least a possibility. According to this formula a body with minimum drag at one Reynolds number has minimum drag at all Reynolds numbers. For simplicity the initial work on minimization was done for the two-dimensional problem. The results obtained were not sufficiently encouraging to justify much additional effort for the axisymmetric case.

The problem is to select a shape $y(x)$ in such a way that the two-dimensional form of (18) is minimized. Alternatively, the function $y(x)$ must be selected to minimize the integral

$$J = D^{6/5} = (const) \int_{body} U^4 ds \tag{19}$$

subject to the constraint that the integral

$$A = \int_{body} y dx \tag{20}$$

take on a specified value. This is not a well-defined calculus-of-variations problem. The difficulty is that, while U depends on y in the sense that given a complete body shape $y(x)$ then $U(x)$ can be determined, there is no relation between local values of U and y.

8.2 Slender-Body Theory

For sufficiently slender bodies the standard aerodynamic techniques yield the following relationship

$$A = \int_0^1 \frac{(U-1)(1-2t)^2 dt}{\sqrt{1-(1-2t)^2}} \qquad t = x/L \tag{21}$$

19

while (19) becomes

$$J = \int_0^1 U^4 dt \qquad (22)$$

Now standard calculus-of-variations techniques can be applied. The result is

$$U = (\text{const}) \frac{(1 - 2t)^{2/3}}{[1 - (1 - 2t)^2]^{1/6}} \qquad (23)$$

This velocity has fore-and-aft symmetry with a 1/6-power singularity at the ends. Clearly the theory has broken down. However, to investigate the possibility that the theory has indicated certain desirable features for low-drag, calculations were performed for bodies having "saddleback" velocity distributions (fore-and-aft peaks of finite size with a lower velocity region in the middle). These bodies consist of semicircles at the front and rear joined by a constant-thickness region, whose length may be varied to give different fineness ratios. Results are discussed in section 8.4 below where the bodies are identified as "circle-flat" bodies. They turned out to have relatively high drag. Thus, slender-body theory was abandoned.

8.3 A General Procedure Based on Conformal Mapping

In two-dimensional potential flow the complete solution for both direct and inverse problems can be expressed in terms of the coefficients of the conformal mapping that maps the body in question to the unit circle. This fact permits a rather general "brute force" solution to the minimization problem.

Let $z(\zeta)$ be the conformal mapping that carries a body shape in the z-plane to the unit circle in the ζ-plane. Then it can be shown that the mapping derivative must satisfy a number of constraints and that a general expression consistent with these constraints can be written down quite simply. This topic is discussed in more detail in appendices A and B, where the general formula in question, viz.

$$\frac{dz}{d\zeta} = \left(1 - \frac{1}{\zeta}\right)^{1 - \tau_1/\pi} \left(1 + \frac{1}{\zeta}\right)^{1 - \tau_2/\pi} \left(1 + \frac{a_1}{\zeta} + \frac{a_2}{\zeta^2} + \ldots\right) \qquad (24)$$

20

is justified. The angles τ_2 and τ_1 are twice the cone angles of the fore and aft end of the body, respectively. Equation (24) defines the mapping coefficients a_n which must be real for application to bodies of revolution by reason of the symmetry. Also closure of the profile requires that $a_1 = (\tau_2 - \tau_1)/\pi$.

Now both the surface velocity on the body and the area enclosed by the profile can be expressed in terms of these coefficients, and thus so can the drag coefficient based on square root of area (18). The most general case of (24) has not been investigated fully, and a detailed account of the various complications is the subject of appendix B. However, for a blunt body $(\tau_1 = \tau_2 = \pi)$ certain important numerical simplifications occur which enable this case to be computed rather simply. Specifically the drag coefficient for such a body can be written

$$C_D = (\text{const}) \frac{1}{G(a_n)} \left[\int_0^\pi \frac{\sin^4 \omega d\omega}{H(\omega, a_n)} \right]^{5/6} \tag{25}$$

where

$$G(a_n) = \left(1 - a_2^2 - \frac{a_3^2}{2} - \frac{a_4^2}{3} - \ldots \right)^{1/2} \tag{26}$$

and

$$H(\omega, a_n) = [(1 + a_2 \cos 2\omega + a_3 \cos 3\omega + \ldots)^2 +$$

$$(a_2 \sin 2\omega + a_3 \sin 3\omega + \ldots)^2]^{3/2} \tag{27}$$

A very simple numerical searching scheme has been developed for finding minimum values of a function of a finite number of real variables which has an obvious application to the problem of minimizing the C_D given by (25) and (26) (see appendix B, section B6). Notice that this is a minimum problem in n variables, not a calculus of variations problem. If only a_2 is retained, the body shape is an ellipse and the procedure gives the analytically correct thickness ratio for minimum drag coefficient. Using a large number of terms gives the result that the optimum shape is actually pointed, because the body obtained has its infinite slope only in a very small region of the fore and aft ends, i.e., the procedure is trying to give a pointed shape. Figure 13 shows the optimum "blunt" body, which appears pointed. Moreover, the coefficients a_n of (26)

for the optimum body appear to be asymptotically equal to those of an expansion for a particular fractional power. The indications are that the true optimum has an equation of the form

$$\frac{dz}{d\zeta} = \left(1 - \frac{1}{\zeta^2}\right)^{1-\tau/\pi} \tag{28}$$

which is the simplest form of (24), namely the one with all $a_n = 0$. The equal fore and aft angles τ appear to be approaching approximately $\pi/3$, i.e., 30° cone angle (see appendix B, section B7). The near-optimum body of figure 13 achieves a drag reduction over the optimum ellipse of 0.15% — a very interesting and discouraging result.

It appears that by using the new type of axisymmetric solution described in appendix A, an analogous minimization procedure could be applied to the axisymmetric case. However, all the indications are that only very small reductions in drag could be obtained.

8.4 Miscellaneous Two-Dimensional Results

While the emphasis of the present study is on axisymmetric bodies, some two-dimensional cases have been investigated also. Most, but not all, of these cases are connected with the optimization studies of the preceeding sections. By analogy with the axisymmetric case, all two-dimensional bodies considered have a right-and-left symmetry with respect to the flow direction and are, of course, nonlifting.

Figure 14 summarizes the drag coefficients obtained for various two-dimensional bodies from the integral formula (18). The curve of figure 14 represents the analytic expression to which (18) reduces for the case of ellipses. The drag of the "near-optimum" body of figure 13 is shown, as well as drags for a set of "circle-flat" bodies that have "saddleback" velocity distributions. As discussed in section 8.2 these bodies were suggested by results from slender-body theory, but it can be seen that their drags are significantly higher than ellipses.

Figure 14 also shows drags for a series of symmetric struts that were designed to have zero skin friction over their aft portions [12]. Despite this their total drag coefficients, as calculated from (18), are higher than those of ellipses.

22

9.0 CONCLUSIONS

1. In computing the drag of an axisymmetric body with fully turbulent boundary layer in incompressible flow the momentum-integral method of Nakayama and Patel [6] is considerably more accurate than either the method based on a finite-difference boundary-layer calculation [4] or the simplified integral formula based on the analysis of Truckenbrodt [7]. Of the latter two methods the simplified integral formula is more accurate than the current finite-difference method and much easier to use.

2. If the simplified integral formula is used to compute drag, the following conclusions can be drawn for axisymmetric bodies with fully turbulent boundary layers in incompressible flow:

   a. A shape having the lowest drag, a one Reynolds number has the lowest drag at all Reynolds numbers.

   b. Shapes with fineness ratios in the range three to four have the lowest drag coefficients based on the two-thirds power of volume.

   c. Drag coefficient is insensitive to shape and no shape has been found with significantly lower drag than a boattailed prolate spheroid. A more accurate drag calculation might modify these conclusions slightly but would probably not drastically revise them.

3. The two-dimensional analogue of the simplified integral formula for drag can be rigorously optimized in terms of mapping coefficients to find a "near optimum" shape that supposedly has the lowest possible. Unfortunately the shape so determined has a drag coefficient almost undetectably less than bodies selected at random.

4. Accurate and very rapid solutions to both the direct and the inverse problems of axisymmetric potential flow can be obtained using the expansion method of appendix A.

10.0 REFERENCES

1. Cebeci, T. and Smith, A.M.O.: Remarks on Methods for Predicting Viscous Drag. AGARD Conf. Paper No. 124, on Aerodynamic Drag, Izmir, Turkey, April 1973.

2. Young, A.D.: The Calculation of Total and Skin Friction Drags of Bodies of Revolution at Zero Incidence. ARC R&M No. 1874, April 1939.

3. Granville, P.S.: The Calculation of Viscous Drag of Bodies of Revolution. David Taylor Model Basin Report No. 849, 1953.

4. Cebeci, T., Smith, A.M.O., and Wang, L.C.: A Finite-Difference Method for Calculating Compressible Laminar and Turbulent Boundary Layers. Douglas Aircraft Co. Rept. No. DAC 67131, March 1969.

5. Patel, V.C.: A Simple Integral Method for the Calculation of Thick Axisymmetric Turbulent Boundary Layers. IIHR Report No. 150, September 1973.

6. Nakayama, A. and Patel, V.C.: Calculation of Viscous Resistance of Bodies of Revolution. IIHR Report No. 151, October 1973.

7. Truckenbrodt, E.: A Method of Quadrature for Calculation of the Laminar and Turbulent Boundary Layer in Case of Plane and Rotationally Symmetrical Flow. NACA TM 1379, May 1955.

8. Schlichting, H.: Boundary-Layer Theory. McGraw-Hill, New York, 1950.

9. Gertler, M.: Resistance Experiments on a Systematic Series of Streamlines Bodies of Revolution for Application to the Design of High-Speed Submarines. David Taylor Model Basin Report C-297, April 1950.

10. Thwaites, B.: Incompressible Aerodynamics. Clarendon Press, Oxford, 1960.

11. Bristow, D.R.: Solution to the Inverse Problem for Incompressible Axisymmetric Potential Flow. AIAA Paper No. 74-520, June 1974.

12. Liebeck, R.H.: A Class of Airfoils Designed for High Lift in Incompressible Flow. AIAA Paper No. 73-86, January 1973.
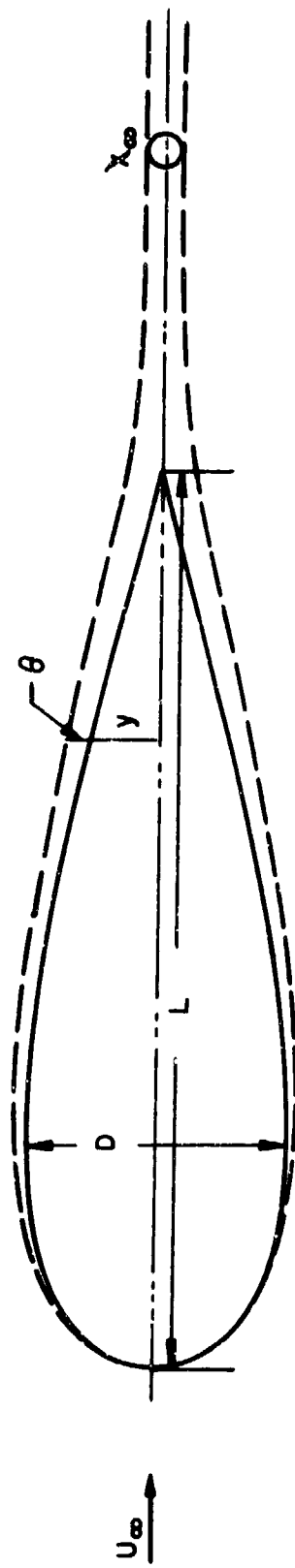
Figure 1. Boundary layer on an axisymmetric body.
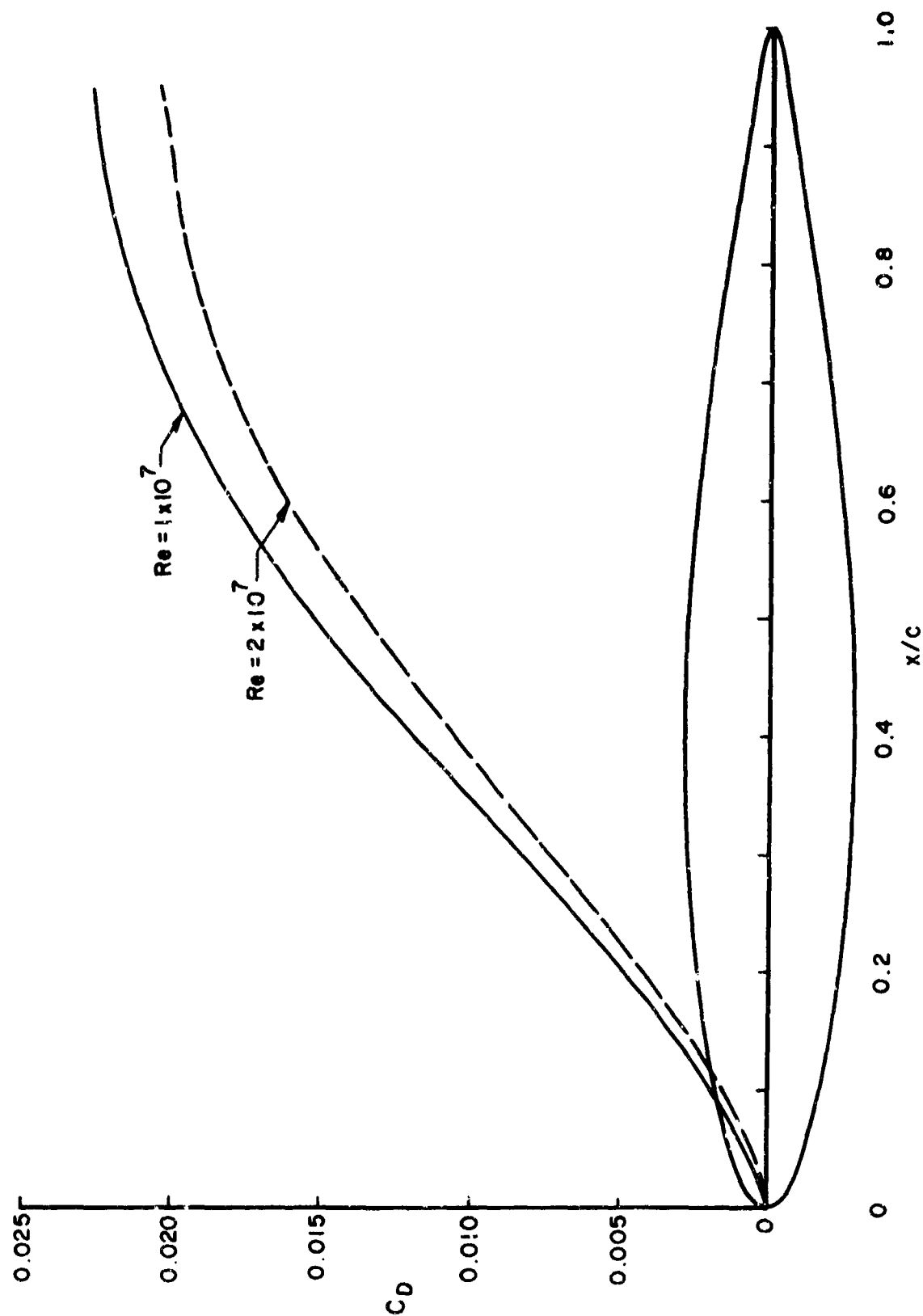
Figure 2. Drag computed by the finite-difference boundary-layer method as a function of location for body 4164 [9].

26
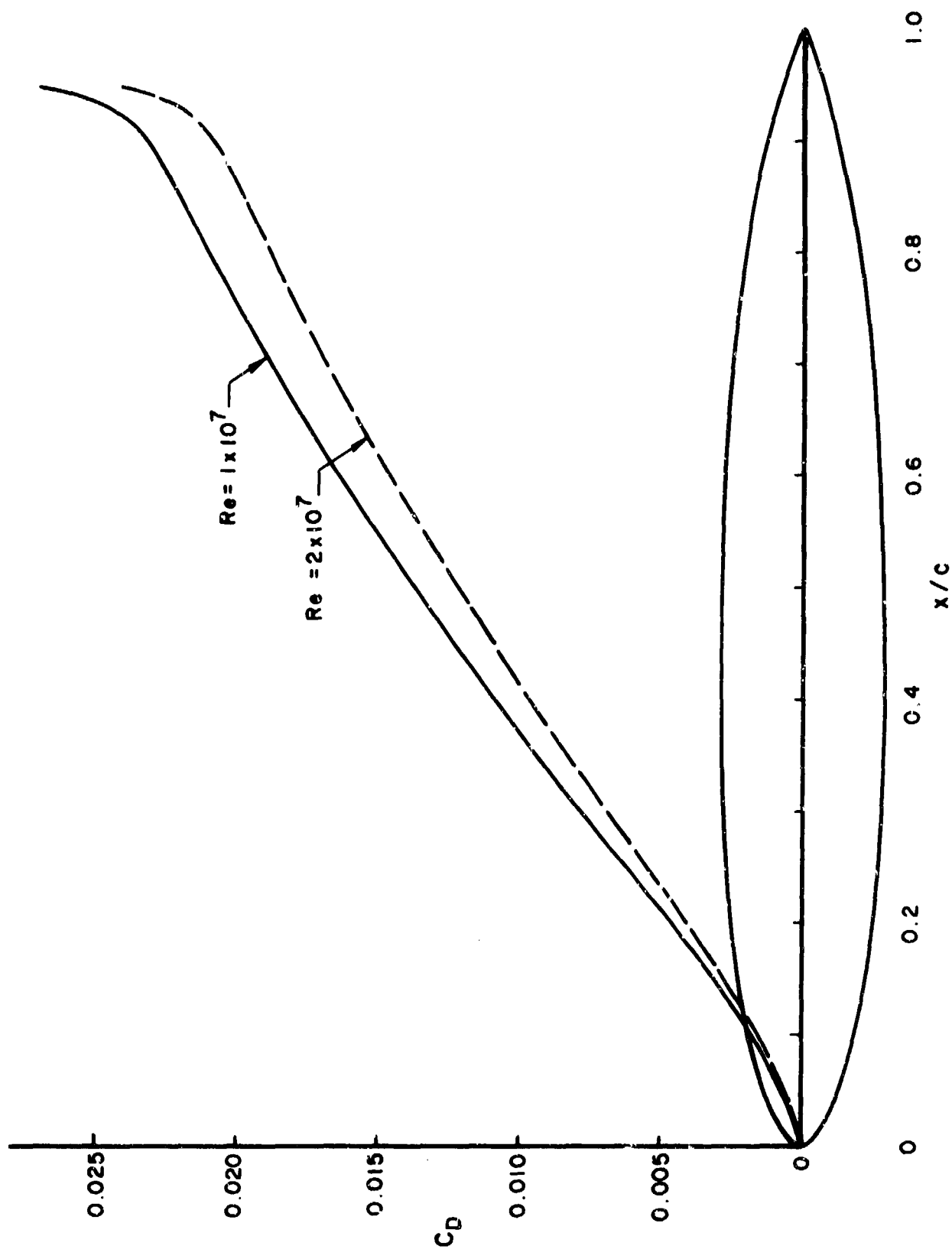
Figure 3. Drag computed by the finite-difference boundary-layer method as a function of location for body 4171 [9].

27
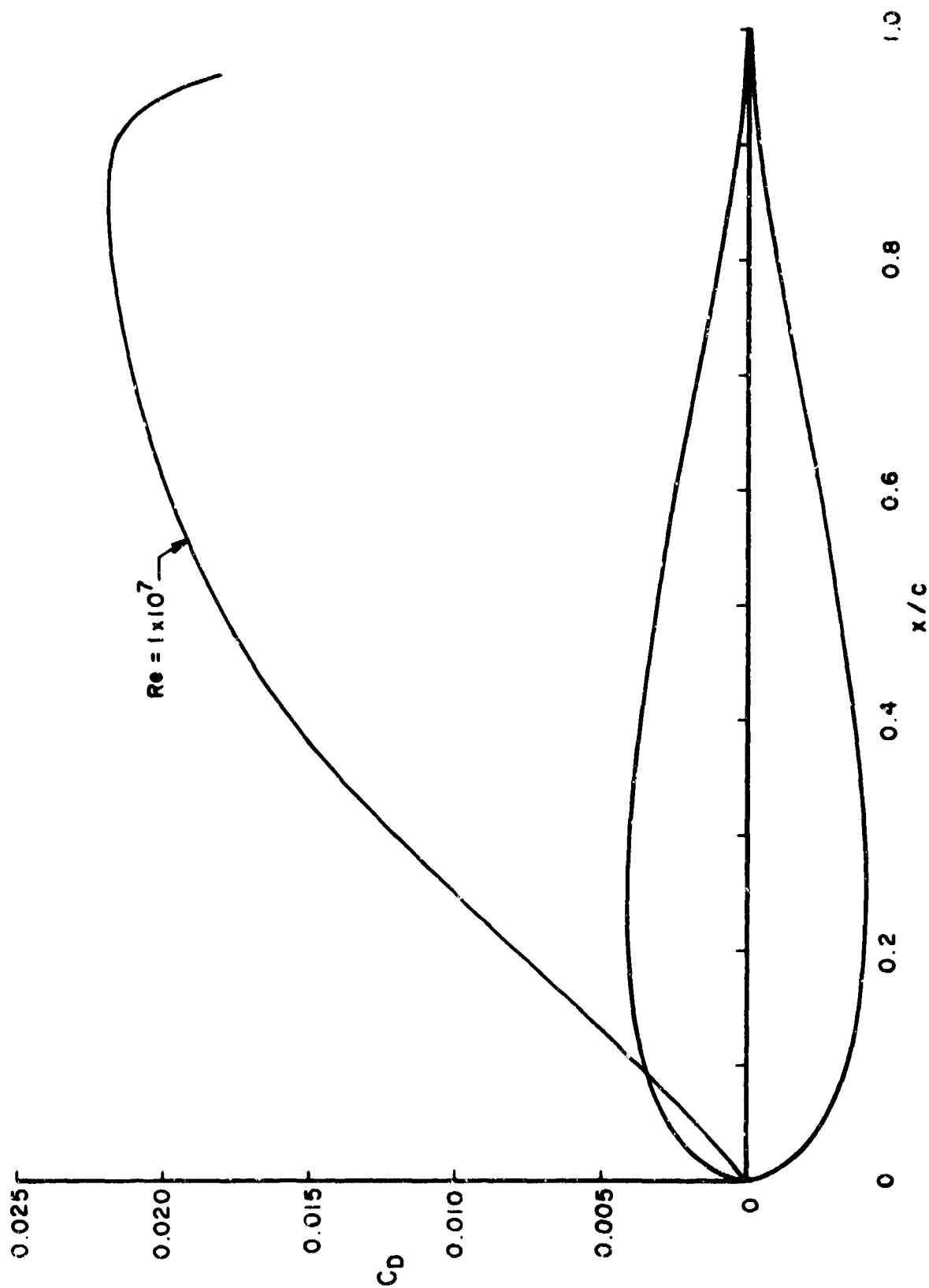
Figure 4. Drag computed by the finite-difference boundary-layer method as a function of location for a body with a cusped aft end.

28
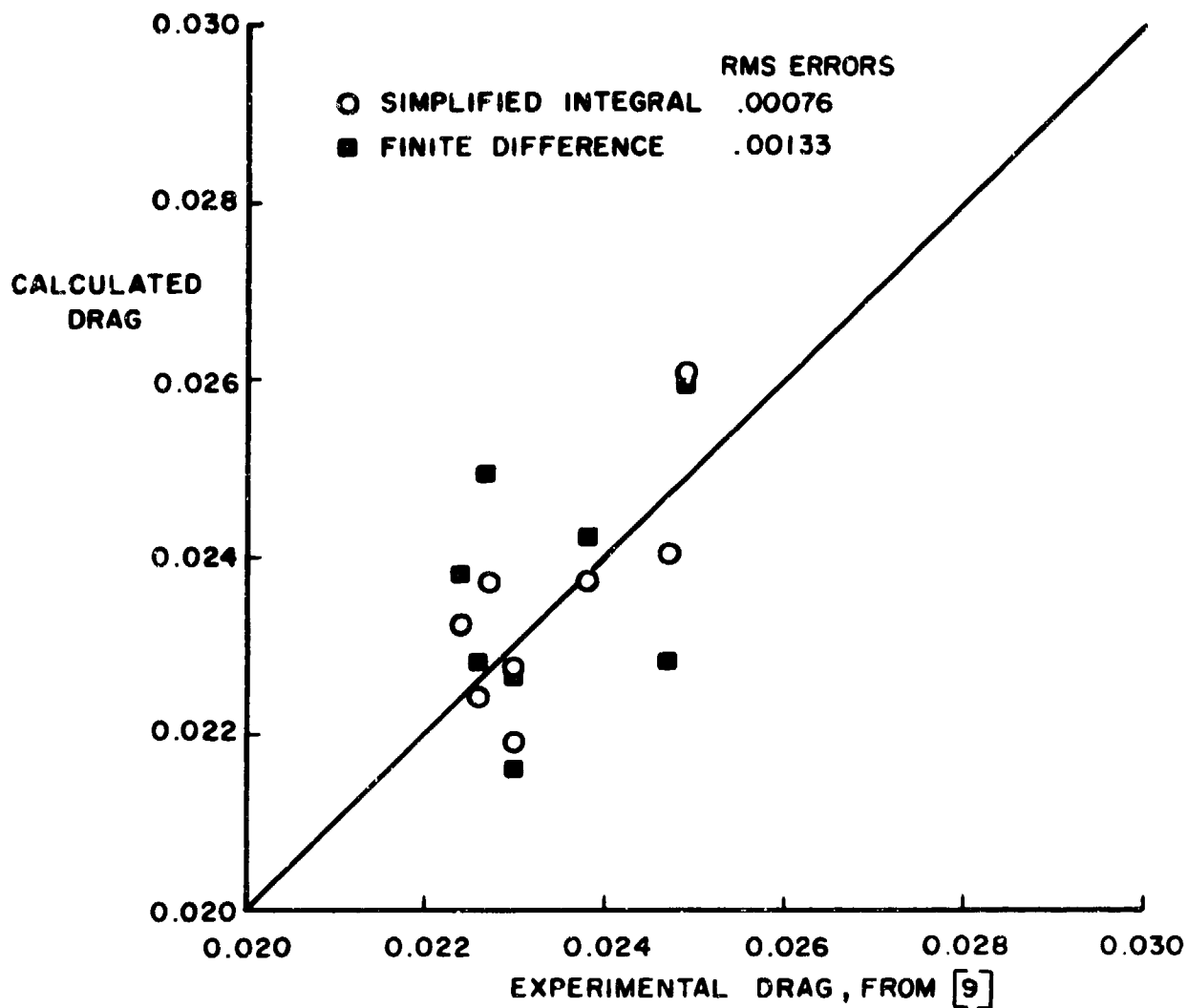
Figure 5. Comparison of drags computed by the finite-difference boundary-
layer method and the simplified integral method with experimental
data for a series of eight bodies at a Reynolds number of 10 million.

29
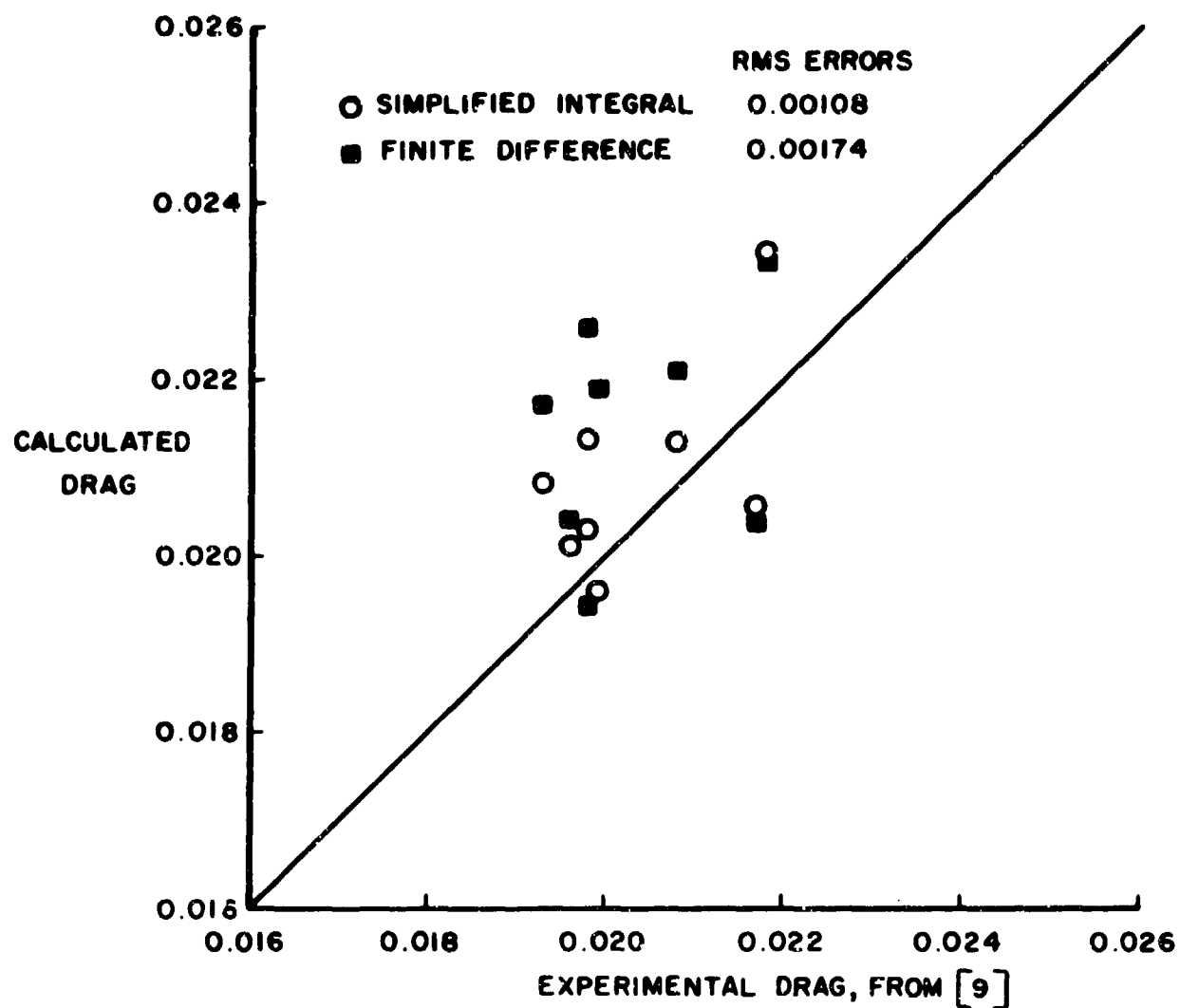
Figure 6. Comparison of drags computed by the finite-difference boundary-layer method and the simplified integral method with experimental data for a series of eight bodies at a Reynolds number of 20 million.
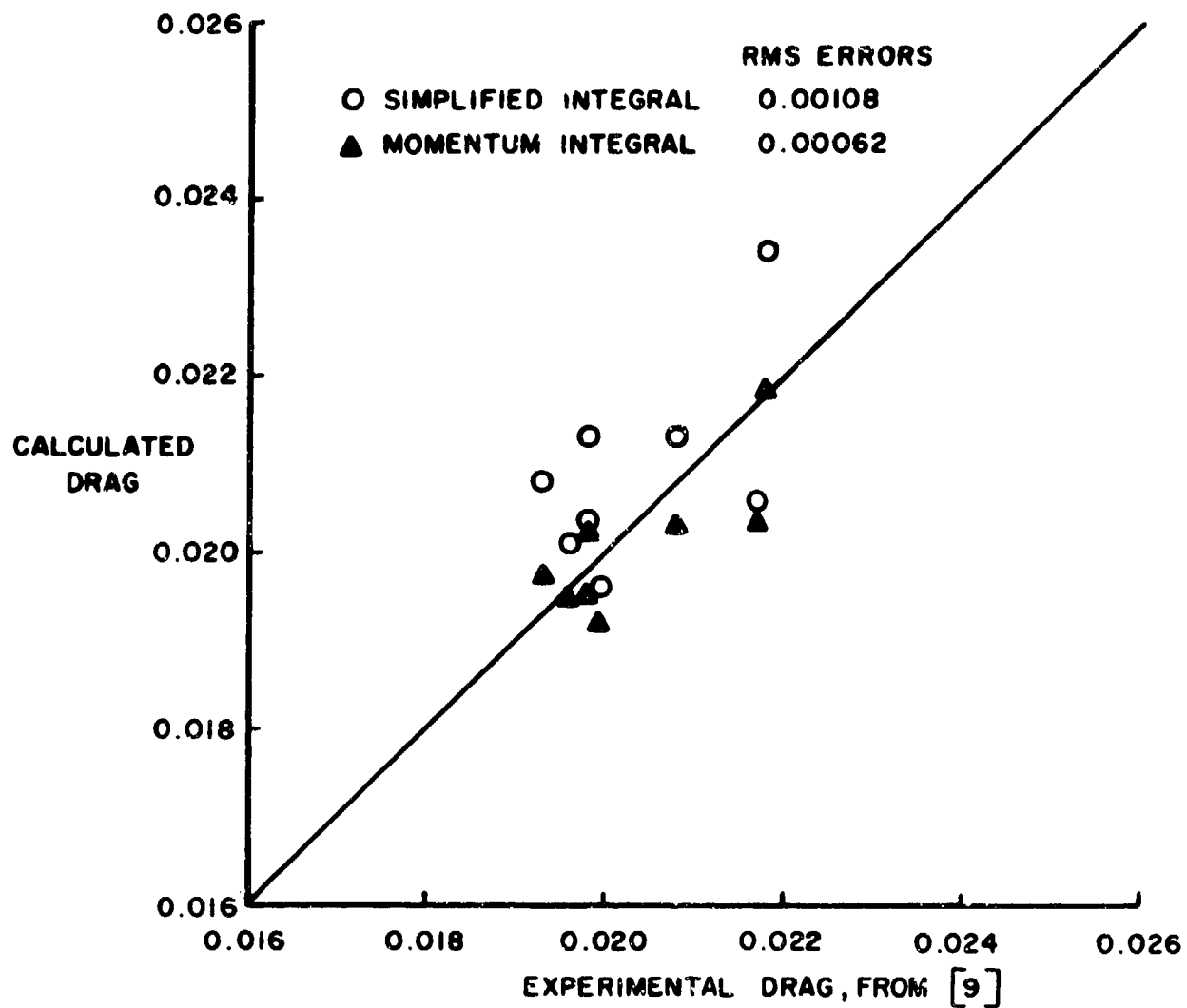
Figure 7.   Comparison of drags computed by the momentum-integral boundary-layer method and the simplified integral method with experimental data for a series of eight bodies at a Reynolds number of 20 million.
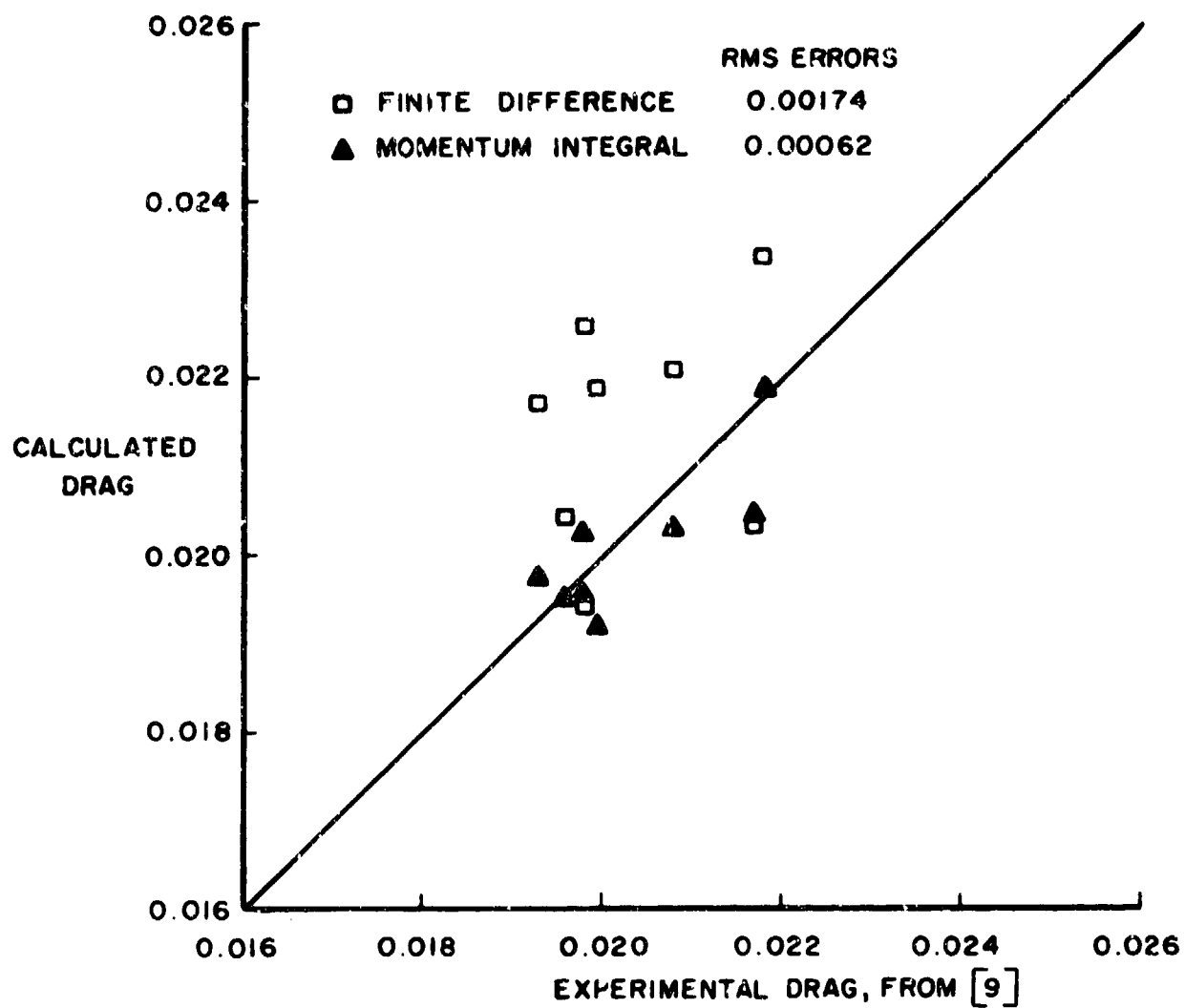
Figure 8. Comparison of drags computed by the momentum-integral boundary-layer method and the finite-difference boundary-layer method with experimental data for a series of eight bodies at a Reynolds number of 20 million.
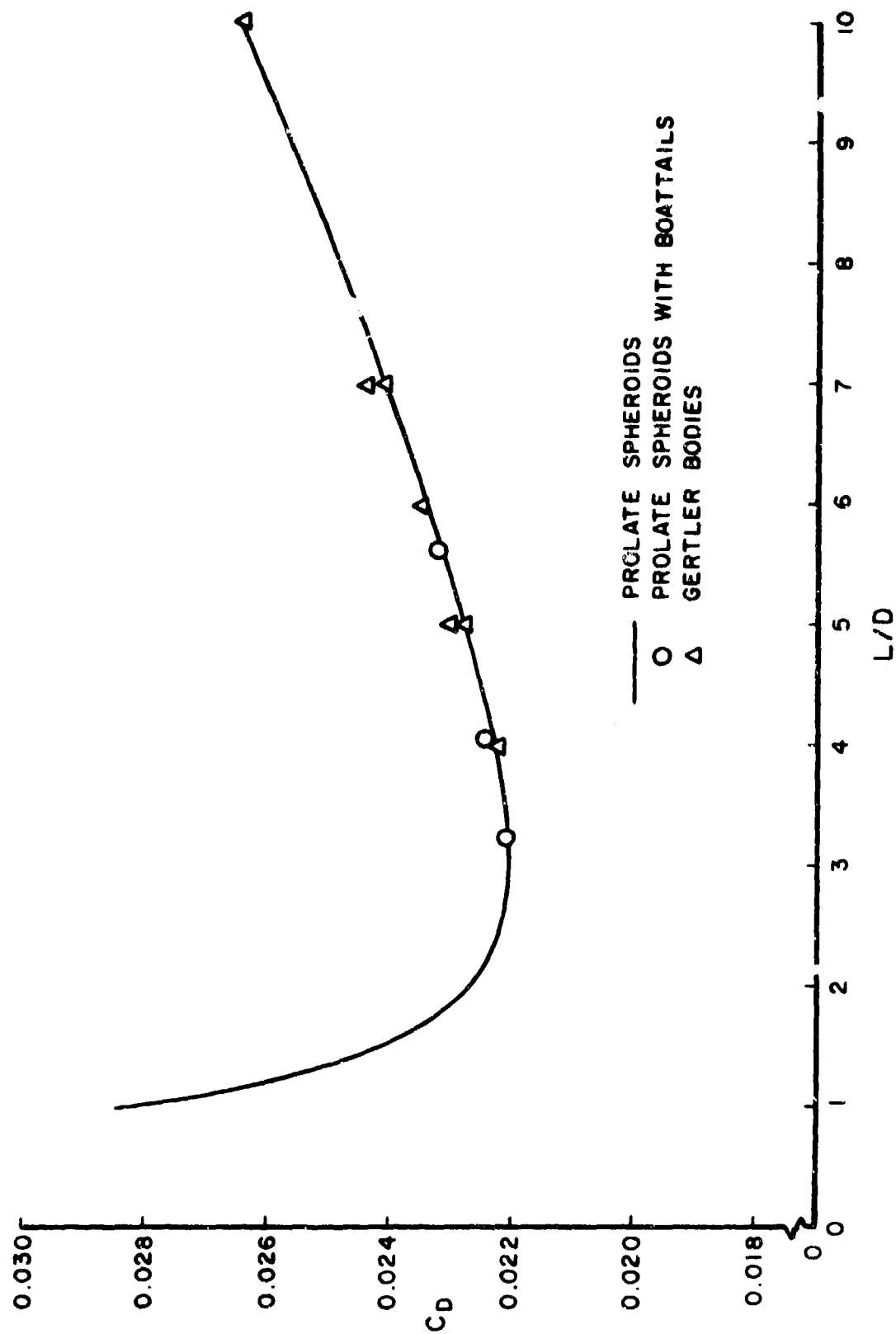
Figure 9. Calculated drag coefficients versus fineness ratio at a Reynolds number of 10 million.

33
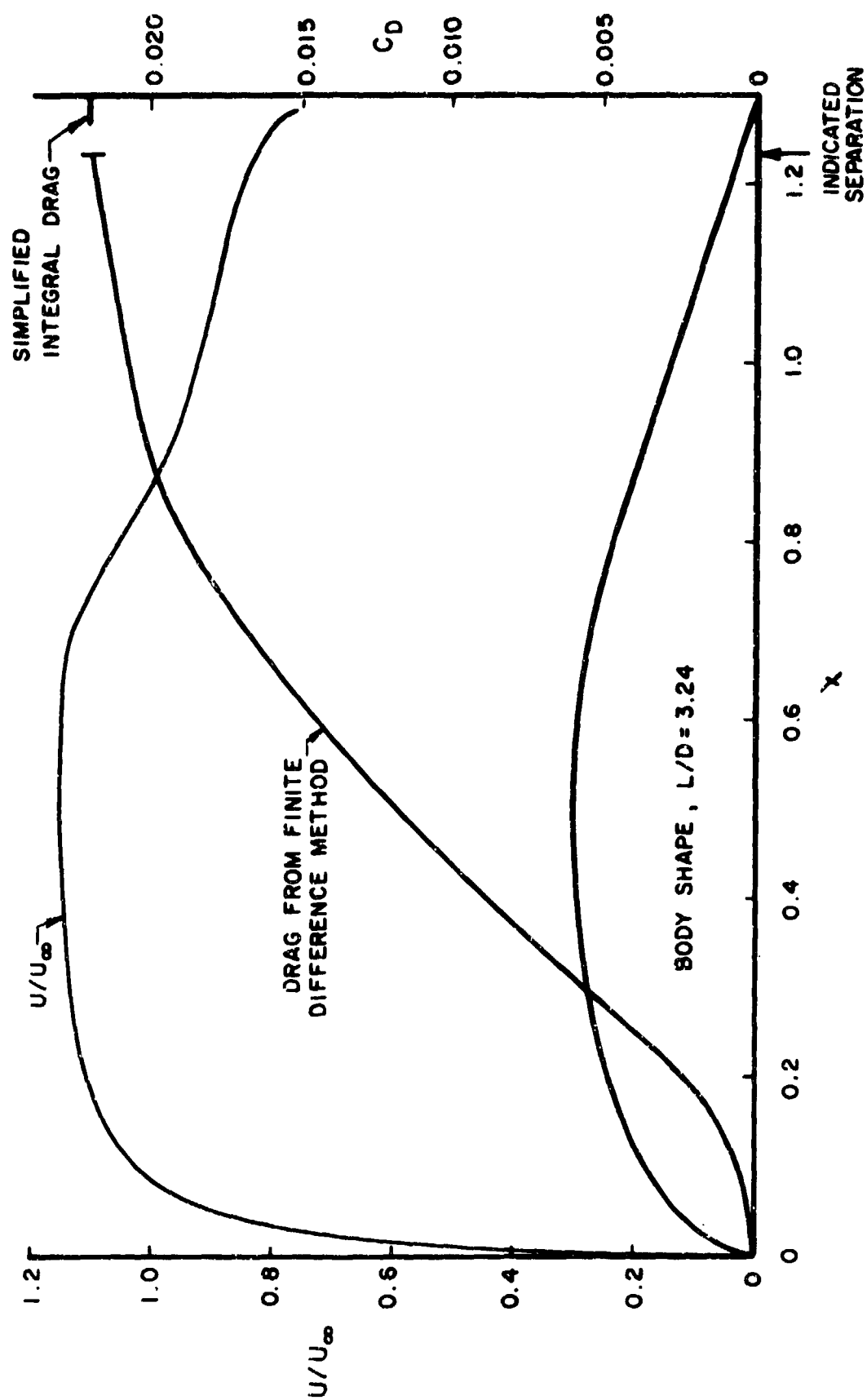
Figure 10. A 40% thick prolate spheroid boattailed by means of a conical afterbody.
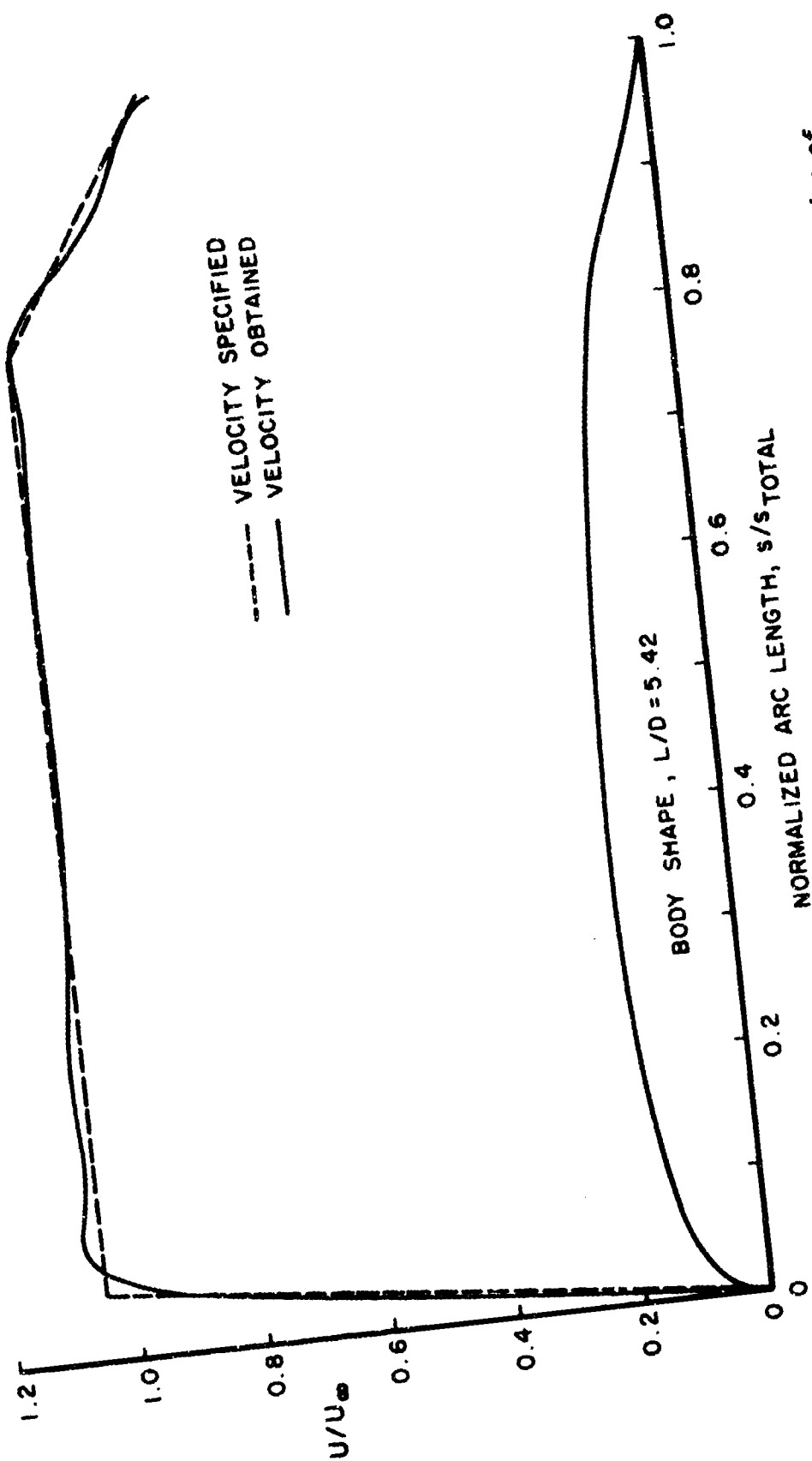
Figure 11. A body designed by an inverse potential-flow method to have a large region of constant pressure.
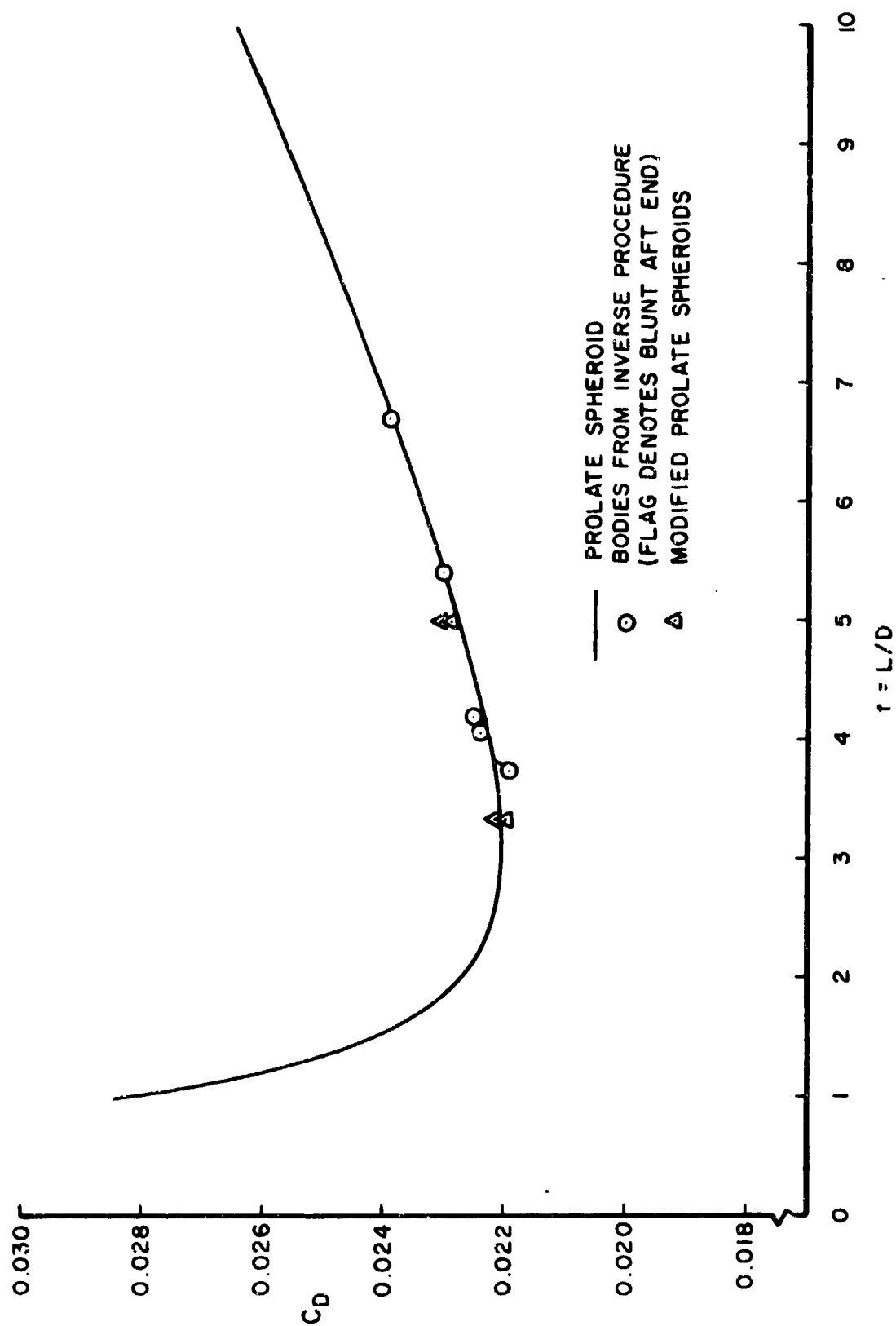
Figure 12. Calculated drag coefficients versus fineness ratio for constant-pressure bodies at a Reynolds number of 10 million.
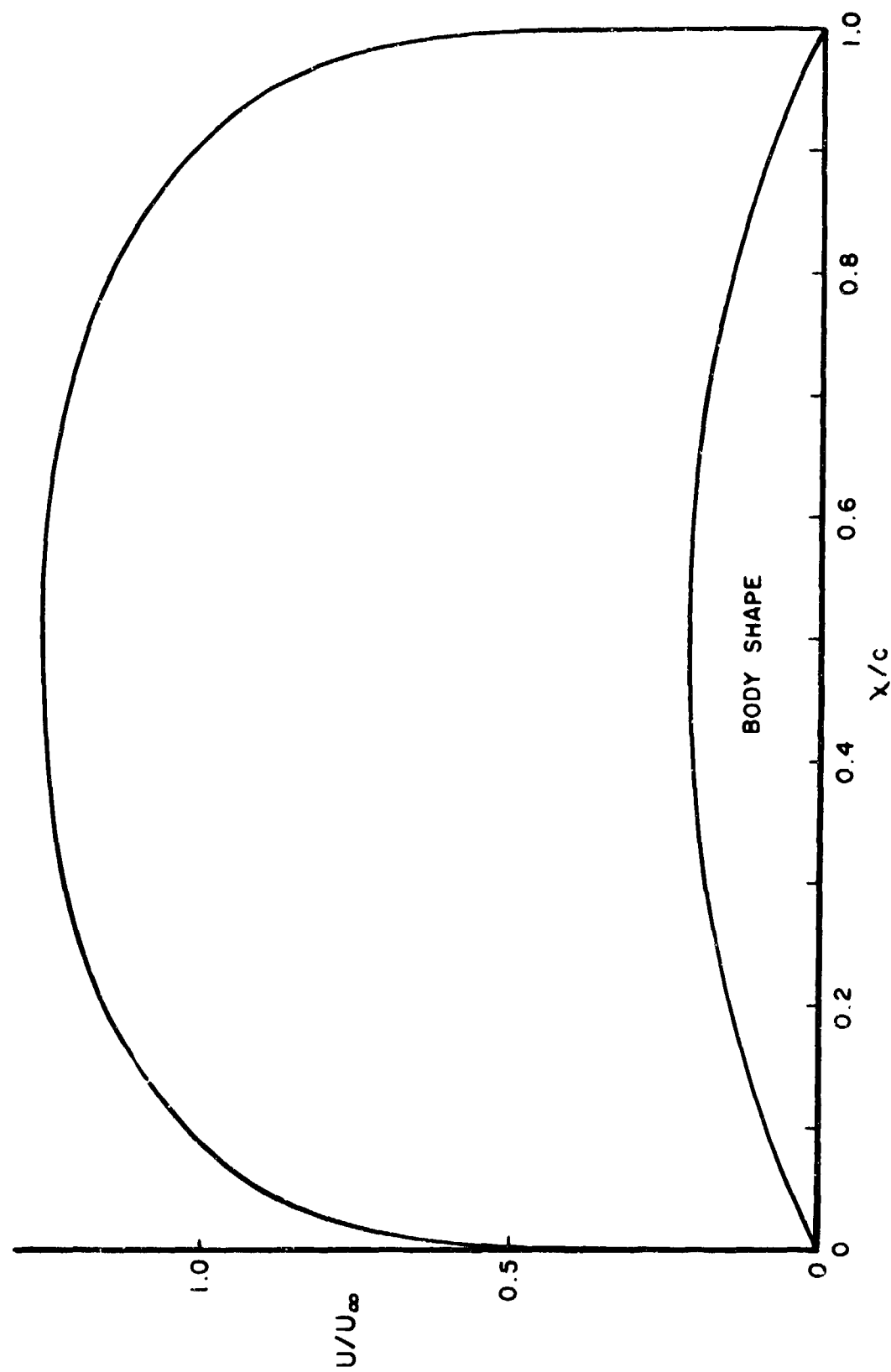
Figure 13. A two-dimensional near-optimum "blunt" body.
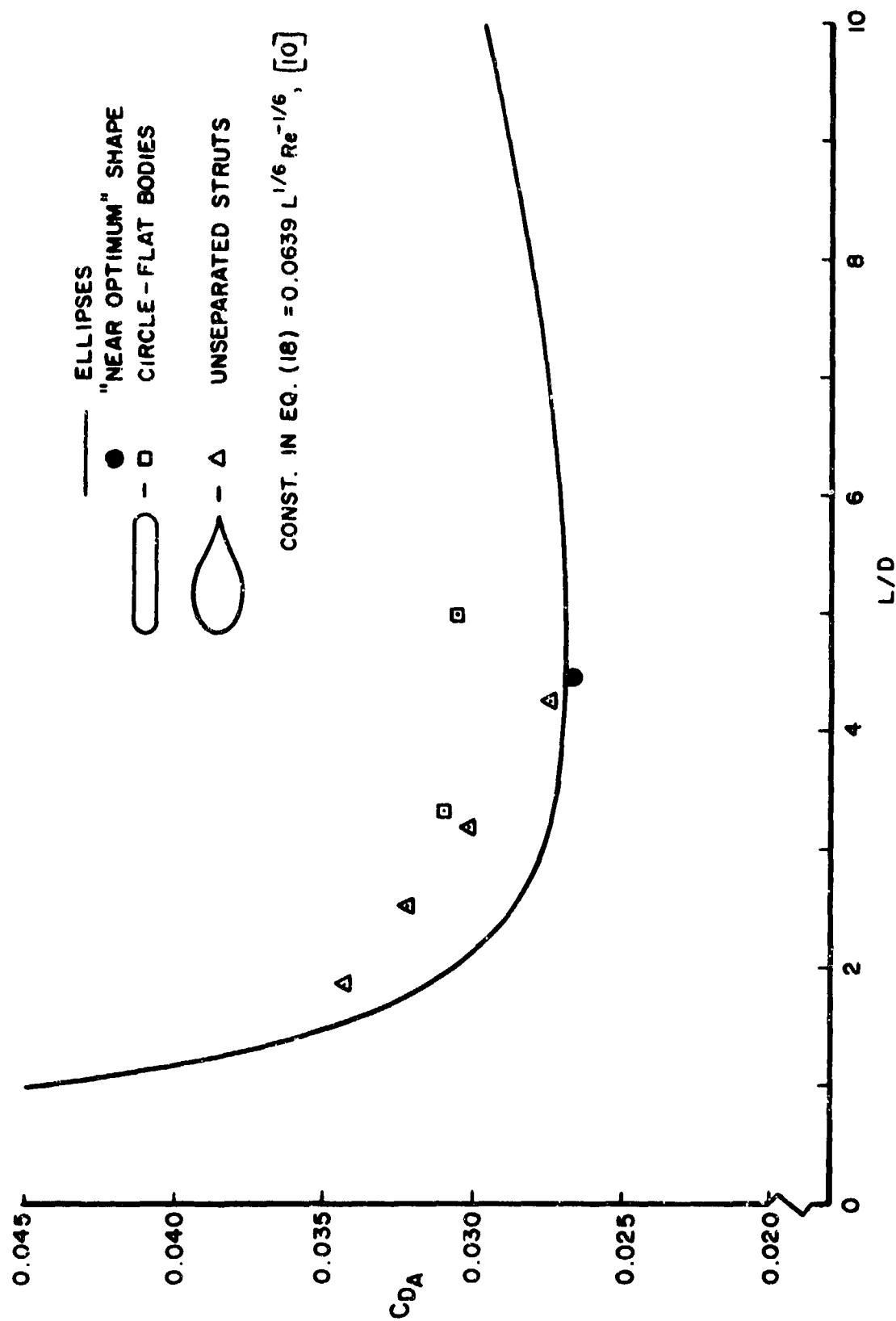
Figure 14. Calculated drag coefficients versus fineness ratio for two-dimensional bodies at a Reynolds number of 10 million.

APPENDIX A
A GENERAL ANALYTICAL METHOD FOR AXISYMMETRIC INCOMPRESSIBLE POTENTIAL FLOW

ABSTRACT

A method is presented for calculating the flow field about bodies of revolution in incompressible potential flow as a sequence of elementary analytic functions (Fourier, Chebyshev and Legendre). For the cases of greatest interest to practical engineering (cusp and blunt trailing edges) comparison with an existing highly accurate numerical method shows that convergence is good. Only ten terms are required to give adequate accuracy for negligible computer usage on bodies with much more character than usually encountered. The theory can be used for design (inverse) operation to produce body shapes associated in some least squares sense with a desired input velocity. It is shown that, when used this way, again good results are obtained with remarkably few terms or iterative cycles.

AI. INTRODUCTION

The literature of axisymmetric incompressible potential flow abounds with numerical methods of the direct type, in which integral equations are solved eventually by matrix methods following some form of discretization. This characteristic traditional path starting from von Karman's [A1] original numerical method and arriving at such sophisticated schemes as the higher-order Neumann method of Hess [A2] has not only spawned no general analytical techniques, but even very few special solutions. In this context "analytical" will be taken to mean solutions in terms of known functions, or a sequence of known functions, such that the convergence and computation of the coefficients allows practically useful calculations to be carried out to arbitrary order. Thus solutions for which only two or three terms can be obtained (e.g., asymptotic series or matched local expansions, etc.) are not considered to be analytical in this sense. This appendix deals with the development of a general analytic method for axisymmetric flow.

In two dimensions there are analytical methods for isolated bodies (airfoils), and experience with them has shown that they have certain clear advantages over the purely numerical schemes — as compensation in a very real sense for loss of generality. For instance — they are usually quicker and more accurate; they frequently provide detailed qualitative insight into far field or special local behavior (near sharp trailing edges as an example), and they often have a much more immediate application to inverse problems. In the case of isolated airfoils this inverse capacity, in which profiles are designed for a prescribed velocity distribution, has proved very valuable.

One of the most important distinctions between the two dimensional and axisymmetric cases from a theoretical point of view is that the former flows can be treated entirely by complex variable methods including conformal mapping; whereas, although the meridian profile of an axisymmetric shape involves only two variables, the flow field itself is not Laplacian in the potential. This means, at best, that one could perhaps treat the geometry by mapping methods; but then a much more sophisticated differential equation would have to be solved. It seems that this largely explains the almost total lack of analytical methods even though the actual equations of motion appear deceptively simple. However, one island in the sea of numerical methods is the work

40

of Kaplan [A3], who did use a mapping for the geometry and then devised an
iterative scheme for the velocity potential. Unfortunately Kaplan's scheme
rapidly becomes very complicated so that it is only feasible to work out the
first three terms in detail, and quite impossible to program a computer to
calculate higher-order terms automatically.

Nevertheless, the underlying principle of this calculation was a good one.
By using recent advances in appreciation of conformal mapping methods (James
[A4]) it is shown below that a very wide class of bodies can be parameterized
in a very simple way, and that, consequently, analytical solutions can be found
for general axisymmetric shapes by a slightly unexpected series assumption —
for which an indefinite number of terms can be computed automatically. From
the examples given it is clear that convergence can be expected to be very
good in general when used to calculate the direct flow about a given body.
However, since this investigation was originally stimulated by recent interest
[A5] in the possibility of a design (inverse) procedure for axisymmetric bodies,
it is even more significant that the convergence was also found to be excellent
on the cases tested when the theory was used in the inverse mode.

A2. EQUATIONS OF MOTION

For an axisymmetric body lying in the (x,y)-plane such that the free-
stream at infinity is parallel to the axis of symmetry (x), the velocity
potential (ϕ) satisfies the well-known differential equation

$$\frac{\partial}{\partial x}\left(y\,\frac{\partial\phi}{\partial x}\right) + \frac{\partial}{\partial y}\left(y\,\frac{\partial\phi}{\partial y}\right) = 0 \tag{A1}$$

with the additional conditions that $\phi \sim x$ in the far field and that the
derivative of ϕ normal to the profile vanishes on the profile. It is quite
standard to seek orthogonal curvilinear transformations $x = x(\xi_1, \xi_2)$,
$y = y(\xi_1, \xi_2)$ in order to either simplify (A1) or the profile representation
(thus making the normal derivative condition more tractable). Such a trans-
formation leads to

$$\frac{\partial}{\partial\xi_1}\left(\frac{h_2}{h_1}\,y\,\frac{\partial\phi}{\partial\xi_1}\right) + \frac{\partial}{\partial\xi_2}\left(\frac{h_1}{h_2}\,y\,\frac{\partial\phi}{\partial\xi_2}\right) = 0 \tag{A2}$$

41

where h_1 and h_2 are the usual metrics, viz.

$$h_1 = \sqrt{\left(\frac{\partial x}{\partial \xi_1}\right)^2 + \left(\frac{\partial y}{\partial \xi_1}\right)^2}, \qquad h_2 = \sqrt{\left(\frac{\partial x}{\partial \xi_2}\right)^2 + \left(\frac{\partial y}{\partial \xi_2}\right)^2}$$

However, if the transformation is in particular a conformal mapping from the $\xi_1 + i\xi_2$ plane to the $x + iy$ plane then the Cauchy-Riemann equations hold, that is

$$\frac{\partial x}{\partial \xi_1} = \frac{\partial y}{\partial \xi_2}, \qquad \frac{\partial x}{\partial \xi_2} \approx -\frac{\partial y}{\partial \xi_1}$$

and therefore $h_1 = h_2$ which reduces (2) to

$$\frac{\partial}{\partial \xi_1}\left(y\, \frac{\partial \phi}{\partial \xi_1}\right) + \frac{\partial}{\partial \xi_2}\left(y\, \frac{\partial \phi}{\partial \xi_2}\right) = 0 \tag{A3}$$

Even though (A3) is formally no simpler than (A1) it is possible to find general mappings which greatly simplify the surface boundary condition by relating the given profile to one of a number of canonical forms in an auxiliary (ξ_1, ξ_2) plane. Specifically the class of mappings which map airfoil-like profiles into the unit circle have been found to be of great utility in two dimensions and so are considered further for this application.

A3. UNIT CIRCLE MAPPING

According to Riemann's fundamental mapping theorem any profile whose contour encloses a singly-connected domain (in the usual engineering sense of e.g. Woods [A6]) can be mapped into the unit circle. However, for airfoils and axisymmetric bodies of interest to engineering, the types of mapping of sufficient generality and simplicity to be useful are quite constrained. The role of these constraints has been discussed by James [A4] and need not be elaborated in detail here. Briefly, the desired characteristics are that: (a) the mapping should reflect the existence of a finite trailing-edge angle discontinuity $(\pi - \tau)$, (b) the mapping derivative must $\rightarrow 1$ as $|z| \rightarrow \infty$, (c) the profile must be closed, and (d) the mapping derivative must have neither zeros nor singularities on* or outside the unit circle.

---

*In the general theory of mapping methods certain boundary singularities may arise, but they are not of interest in this application.

Let $\zeta = \xi + i\eta$ be the unit circle plane then it is easy to show that a mapping which conforms to (a) — (d) is of the type

$$\frac{dz}{d\zeta} = \left(1 - \frac{1}{\zeta}\right)^{1-\tau/\pi} g(\zeta) \tag{A4}$$

where $g(\zeta)$ is an analytic function with neither zeros nor singularities outside C (the unit circle) and which $\to 1$ as $|\zeta| \to \infty$. Many different forms of $g(\zeta)$ can be used to generate profiles, but for the present purpose the more general representation of $g(\zeta)$ as an expansion

$$g(\zeta) = 1 + \frac{(1 - \tau/\pi)}{\zeta} + \frac{a_2}{\zeta^2} + \ldots \tag{A5}$$

is appropriate. That the first coefficient a_1 is $(1 - \tau/\pi)$ is a consequence of the closure condition (c).

It is possible to prove in general that if the origin in the z-plane is located at the trailing edge then, as a consequence of (A4) and (A5),

$$z = \zeta \left(1 - \frac{1}{\zeta}\right)^{2-\tau/\pi} \left[1 + a_2 S_1\left(\frac{1}{\zeta}\right) + a_3 S_2\left(\frac{1}{\zeta}\right) + \ldots\right] \tag{A6}$$

where $S_1\ S_2 \ldots$ are polynomials of a particularly simple form. The nature of these polynomials is not important here since (A6) will not be used directly; however, it does show that very awkward fractional powers will arise in the analysis of the differential equation (A3) through the y factor which is the imaginary part of z. In order to test the utility of this theory it was first investigated for the cases which do not give rise to fractional powers, namely

$$\tau = \pi \quad \text{(blunt)} \qquad \frac{dz}{d\zeta} = g(\zeta) = 1 + \frac{a_2}{\zeta^2} + \frac{a_3}{\zeta^3} + \ldots \tag{A7}$$

$$\tau = 0 \quad \text{(cusp)} \qquad \frac{dz}{d\zeta} = \left(1 - \frac{1}{\zeta}\right) g(\zeta) = \left(1 - \frac{1}{\zeta}\right)\left(1 + \frac{1}{\zeta} + \frac{a_2}{\zeta^2} + \ldots\right) \tag{A8}$$

and the remainder of this study deals only with these forms. Fortunately, the exclusion of fractional powers is not very important for most engineering applications, because those bodies of practical interest which are not truly blunt (like ellipsoids) usually have small values of τ/π for which the rear stagnation region (where the velocity falls very sharply to zero) is very localized. Hence, it is of little importance since the boundary layer tends to "smudge" the details very close to the trailing edge and the question of the

43

"proper" combined flow in this region is an unsolved problem well beyond the scope of this work.

If the forms in (A7) and (A8) are reorganized and integrated both yield a series

$$z = C + \zeta - \frac{B_1}{\zeta} - \frac{B_2}{\zeta^2} - \ldots \tag{A9}$$

where C is an arbitrary real constant (again choosing the trailing edge as the origin of z) and, for:

$$\tau = \pi \quad \text{(blunt)}, \qquad B_1 = a_2, \qquad B_2 = a_3/2, \ldots$$
$$\tau = 0 \quad \text{(cusp)}, \qquad B_1 = a_2 - 1, \quad B_2 = (a_3 - a_2)/2, \ldots \tag{A10}$$

Naturally in dealing with the unit circle in the ζ-plane it is expedient to use the angular variable (ω) so that

$$\zeta = re^{i\omega}, \qquad r = 1 \quad \text{represents the profile}$$

but z is not, of course, an analytic function of $r + i\omega$, so to circumvent this it is necessary to use the variable

$$\zeta = e^\sigma \qquad \text{where} \qquad \sigma = \lambda + i\omega, \quad r = e^\lambda \tag{A11}$$

For axisymmetric bodies the reflection symmetry ensures that all the a_n and B_n coefficients are real so that using (A11) in (A9) gives the general form of y as

$$y(\lambda,\omega) = e^\lambda \sin \omega + B_1 e^{-\lambda} \sin \omega + B_2 e^{-2\lambda} \sin 2\omega + \ldots \tag{A12}$$

to be used in the differential equation

$$\frac{\partial}{\partial \lambda} \left(y \frac{\partial \phi}{\partial \lambda} \right) + \frac{\partial}{\partial \omega} \left(y \frac{\partial \phi}{\partial \omega} \right) = 0 \tag{A13}$$

with the boundary conditions

$$\phi \sim e^\lambda \cos \omega \quad \text{as} \quad \lambda \to \infty$$
$$\left(\frac{\partial \phi}{\partial \lambda} \right) = 0 \qquad \text{when} \quad \lambda = 0 \tag{A14}$$

44

Although this is a properly posed problem which has so far defied analytic solution, the reduction presented in this section is by no means exhaustive; it is merely the simplest. Thus the question of convergence has been tacitly ignored. Experience has shown that this breakdown is adequate for most purposes, but it is clear that when $\tau = 0$, $dz/d\zeta$ has a higher order zero at the trailing edge than when $\tau = \pi$. If, then, convergence is adequate for the blunt cases when using (A9) or (A12) (which effectively disguises the zero factor) it will be less so for the cusp cases. Furthermore, (A9) shows quite clearly that one should remove a zero factor from the expression for z in both cases for even better convergence. However, it is not possible to consider all these ramifications here. As will be seen the basic method summarized in (A12), (A13) and (A14) is remarkably good and behaves exactly as these conjectures would lead one to expect.

A4. SOME REMARKS ON DIFFERENT ITERATIVE SCHEMES

One classical method of solution is to seek a sequence of approximations ϕ_0, ϕ_1, ϕ_2 such that

$$\phi = \phi_0 + \phi_1 + \phi_2 + \ldots$$

and, by substitution into (A13), separate a series of differential equations each of which can be solved for the individual orders. The number of different ways in which this kind of analysis can be effected is quite remarkable, but the varying forms of the successive ϕ_n functions and the manner and rate of their convergence is even more surprising. Since the natural and obvious assumptions do not work, it would be remiss not to include some brief discussion of the general character of such schemes.

(a) For instance, (A13) can be expressed in the form

$$y\nabla^2\phi + y_\lambda\phi_\lambda + y_\omega\phi_\omega = 0 \tag{A15}$$

or symbolically as

$$yD\phi + dyd\phi = 0 \tag{A16}$$

Then by identifying the successive terms of $y = y_0 + y_1 + \ldots$ as $y_0 = e^\lambda \sin \omega$, $y_1 = e^{-\lambda} \sin \omega$, $y_2 = e^{-2\lambda} \sin 2\omega \ldots$, and expanding (A16)

one is led to an array which can be arranged as:

$$y_0 D_0 + y_0 D_1 + y_0 D_2 + \ldots + dy_0 d\phi_0 + dy_0 d\phi_1 + dy_0 d\phi_2 + \ldots$$

$$y_1 D_0 + y_1 D_1 + y_1 D_2 + \ldots + dy_1 d\phi_0 + dy_1 d\phi_1 + dy_1 d\phi_2 + \ldots \qquad = 0$$

$$y_2 D_0 + y_2 D_1 + y_2 D_2 + \ldots + dy_2 d\phi_0 + dy_2 d\phi_1 + dy_2 d\phi_2 + \ldots$$

$$\cdots \qquad\qquad\qquad \cdots \qquad\qquad\qquad (A17)$$

The simplest scheme which successively annihilates the left hand side of (A17) appears to be

$$D_0 = 0$$
$$y_0 D_1 = -dy_0 d\phi_0$$
$$y_0 D_2 = -y_1 D_1 - dy_0 d\phi_1 - dy_1 d\phi_0 \qquad (A18)$$

$$\cdots$$

and it is worth noting that each equation is of Poisson form and so readily solvable. Furthermore, although (A18) is not unique in any sense because any number of known y_n's could be appended to the right sides, it is at least consistent inasmuch as each order does not introduce higher harmonics than required for the Laplacian part. That is,(A18) could well be solved by the assumptions

$$\phi_0 = f_0(\lambda) \cos \omega, \qquad \phi_1 = f_1(\lambda) \cos \omega, \qquad \phi_2 = f_2(\lambda) \cos 2\omega, \ldots$$

and, proceeding in this manner with the proper boundary conditions, readily leads to

$$\phi_0 = 2 \cosh \lambda \cos \omega$$

$$\phi_1 = -(1 + \lambda)e^{-\lambda} \cos \omega$$

$$\phi_2 = \left\{ (1 + \lambda + \frac{1}{2} \lambda^2)e^{-\lambda} - \frac{1}{4} B_1 \left[(1 + 4\lambda)e^{-\lambda} + e^{-3\lambda} \right] \right\} \cos \omega$$

and rapidly increasing complexity. It is clear that this scheme suffers from obvious defects, among which the crucial ones are: (1) the analysis increases rapidly in complexity and still requires solution of nonhomogeneous differential equations at each step and so cannot be mechanized, (2) the convergence

46

in a qualitative sense is poor since ϕ_2 has only just introduced a B coefficient — merely the first — and varies only as $\cos \omega$. Part of the inadequacy of this scheme arises from the fact that each equation of (A18) has an essentially two-dimensional character so that the "rate of introduction of axisymmetry" is poor.

(b) Kaplan's scheme is much more sophisticated and has an axisymmetric character in each approximation right from the beginning. It can be represented in terms of the symbology of (A17) by the sequence

$$(y_0 + y_1)D_0 + (dy_0 + dy_1)d\phi_0 = 0$$

$$(y_0 + y_1)D_1 + (dy_0 + dy_1)d\phi_1 = -y_2D_0 - dy_2d\phi_0 \quad \text{(A19)}$$

$$(y_0 + y_1)D_2 + (dy_0 + dy_1)d\phi_2 = -y_2D_1 - y_3D_0 - dy_2d\phi_1$$
$$\cdots \qquad\qquad\qquad - dy_3d\phi_0$$

which certainly penetrates the array faster than (A18). In fact this scheme not only introduces B_2 and $\cos 2\omega$ in ϕ_2, but the first term is representative of flow around an ellipsoid, not merely an ellipse, and all the left-side operators have a more nearly axisymmetric character.

Unfortunately this improvement in the character of each term has been bought at the expense of enormous increase of complexity. Using separation of variables on each equation of (A19) leads to left sides which give rise to two Legendre equations involving the Legendre functions of both kinds. The function of second kind (Q_n) is awkward to handle, and the occurrence of such combinations in the nonhomogeneous part of each equation leads to appalling complexity even for the third function ϕ_3. Thus further terms by analysis would be effectively impossible and computer mechanization unthinkable. However, it is interesting to note that, even so, Kaplan's approximation gave a remarkably good answer for a Joukowski profile of revolution. This provided an important stimulus to the work reported here, and is discussed further in paragraph 8 c . Kaplan's method in general also made it clear that iterative/analytic methods of the type discussed above could never lead to general analytical solutions unless some means could be found to make each succeeding order depend only on algebraic steps rather than ones involving

47

differential equations. For algebraic operations there is some hope of computer mechanization so that the generality criteria of section 1 could then be met; but where each step still involves partial differential equations there is none.

(c) The obvious assumption consistent with (a) and (b) above is

$$\phi = f_0(\lambda) + f_1(\lambda) \cos \omega + f_2(\lambda) \cos 2\omega + \ldots \qquad (A20)$$

since ϕ must clearly be an even periodic function. However, substituting this into (A13) and separating the harmonics leads to an infinite sequence of equations each of which contains linear differential operators of second order. Solution of such a system in practical terms seems out of the question, and its intractable nature arises from the strong coupling between equations — in the sense that the expression for f_n contains all f's for other values of n. This in turn is a consequence of the addition formulas for trigonometric products and so cannot be avoided by any assumption of the form (A20).

(d) It appears therefore that (A20) is precisely the wrong kind of assumption, and of course, the coupling problem arising from (A20) can be alleviated by using Chebyshev* polynomials instead of trigonometric series, since then the major algebraic steps reduce to manipulations with power series. Putting

$$\xi = \cos \omega, \qquad \eta = e^{\lambda}$$

then, the analog of (A20) is

$$\phi = g_0(\eta) + g_1(\eta)\xi + g_2(\eta)\xi^2 + \ldots \qquad (A21)$$

which greatly reduces the coupling problem but doesn't solve it. In fact, use of (A21) leads to a system in which the equation for g_n involves g_{n+2} which is again undesirable since each differential equation cannot be solved outright in general terms which might conceivably lead to a reduction to algebraic steps.

---

*In a quick spot-survey of 16 mathematics textbooks and assorted dictionaries, the author found 8 different spellings. This was the most popular being quoted on 37.5% of occasions!

Examining the reduction to a suitable ξ, η form shows what the proper procedure should be. Noting that y has factor $\sin \omega$, (A12), let Y be defined as

$$y = \sin \omega \cdot Y \qquad (A22)$$

where

$$Y(\xi, \eta) = \eta + \frac{B_1}{\eta} + \frac{B_2}{\eta^2} U_1(\xi) + \ldots \qquad (A23)$$

and $U_n(\xi)$ is the Chebyshev polynomial of second kind, viz.

$$U_n(\xi) = \frac{\sin(n + 1)\omega}{\sin \omega}$$

Using (A22) and (A23) in (A13) then gives the transformed differential equation

$$Y \{\nabla^2 \phi - \xi \phi_\xi\} + \eta^2 Y_\eta \phi_\eta + (1 - \xi^2) Y_\xi \phi_\xi = 0 \qquad (A24)$$

with the boundary conditions

$$\phi_\eta = 0 \quad \text{when} \quad \eta = 1$$
$$\phi \sim \xi \eta \text{ when } \quad \eta \to \infty \qquad (A25)$$

But if (A21) is applied to (A24) it can immediately be seen that the offending factor which produces a shifting upward of powers is the term $(1 - \xi^2)\phi_{\xi\xi}$ coming from transformation of the $\nabla^2 \phi$. On the other hand the η-part, $\eta^2 \phi_{\eta\eta} + \eta \phi_\eta$ preserves the same powers in each differential operator.

A5. THE ASSUMPTION FOR ϕ

(a) On the basis of section A4d above, the assumption

$$\phi = \eta F_0(\xi) + \frac{1}{\eta} F_1(\xi) + \frac{1}{\eta^2} F_2(\xi) + \ldots \qquad (A26)$$

is more logical than (A21) although both (A20) and (A21) appeal more immediately to intuition. Using (A26) it is possible to produce a system which can be reduced entirely to programmable algebraic steps. This reduction is elementary but involved, and only the important stages can be recorded here.

Putting (A26) progressively into (A24) leads to the first step that

$$\nabla^2 \phi - \xi \phi_\xi = \eta \Delta_0 + \frac{1}{\eta} \Delta_1 + \ldots \frac{1}{\eta^n} \Delta_n + \ldots$$

49

where Δ_n is the differential expression

$$\Delta_n \equiv (1 - \xi^2)F_n'' - 2\xi F_n' + n^2 F_n , \quad n \geq 1$$

The temptation to use this as a basis for iteration (as opposed to the use of the contribution from $\nabla^2\phi$ alone) on the grounds that it may introduce non-two-dimensional effects quicker if one divided (A24) by Y, can be resisted very easily by noting that the first member would be

$$\Delta_0 \equiv (1 - \xi^2)F_0'' - 2\xi F_0' + F_0 = 0 \tag{A27}$$

which does not have a solution proportional to ξ as it must if (A25) is to be satisfied.

Continuing the development, we note instead that the product term involving $\nabla^2\phi$ can be reduced in the following way. Write

$$Y = \eta \left\{ 1 + \frac{B_1}{\eta^2} + \frac{B_2 U_1}{\eta^3} + \ldots \right\} = \eta \left\{ 1 + \frac{\beta_1}{\eta^2} + \frac{\beta_2}{\eta^3} + \ldots \right\} = \eta(1 + \beta)$$

and

$$\nabla^2\phi - \xi\phi_\xi = \eta \left\{ \Delta_0 + \frac{\Delta_1}{\eta^2} + \frac{\Delta_2}{\eta^3} \ldots \right\} = \eta(\Delta_0 + \Delta)$$

say, so that the product becomes

$$Y \{\nabla^2\phi - \xi\phi_\xi\} = \eta^2(1 + \beta)(\Delta_0 + \Delta) = \eta^2(1 + \beta\Delta_0 + \Delta + \beta\Delta)$$

where the final term $\beta\Delta$ is $O(\eta^{-4})$. The other two terms in (A24) yield similar expressions with final products of $O(\eta^{-4})$; in detail, if

$$y_\eta = 1 - \frac{\beta_1}{\eta^2} - \frac{2\beta_2}{\eta^3} \ldots = 1 - \tilde{\beta}$$

$$\phi_\eta = F_0 - \frac{F_1}{\eta^2} - \frac{2F_2}{\eta^3} \ldots = F_0 - \tilde{F}$$

then

$$\eta^2 Y_\eta \phi_\eta = \eta^2 \{1 - \tilde{\beta}\}\{F_0 - \tilde{F}\} = \eta^2 \{F_0 - \tilde{\beta}F_0 - \tilde{F} + \tilde{\tilde{\beta}}\tilde{F} \}$$

and, if

$$Y_\xi = \eta \left\{ \frac{\beta_1'}{\eta^2} + \frac{\beta_2'}{\eta^3} + \ldots \right\} = \eta\beta'$$

$$\phi_\xi = \eta \left\{ F_0' + \frac{F_1'}{\eta^2} + \frac{F_2'}{\eta^3} + \ldots \right\} = \eta(F_0' + F')$$

then

$$(1 - \xi^2)Y_\xi\phi_\xi = \eta^2(1 - \xi^2)\{\beta'F_0' + \beta'F'\}$$

so that ultimately a factor η^2 can be cancelled and the differential equation reduced to

$$\{\Delta_0 + \beta\Delta_0 + \Delta + F_0 - \tilde{\beta}\tilde{F}_0 - \tilde{F} + (1 - \xi^2)\beta'F_0'\} + [\beta\Delta + \tilde{\beta}\tilde{F} + (1 - \xi^2)\beta'F'] = 0 \tag{A28}$$

which can be written for convenience of discussion as

$$\{H\} + [G] = 0 \tag{A29}$$

In this expression the collection G contains only terms of at least $O(\eta^{-4})$ and the collection H starts from order zero. This separation of the higher-order products turns out to be a very important step, since isolated study of the dependence of G on the functions F_n shows how the whole solution can be reduced to mechanizable algebraic steps.

(b) However, the structure of G can be appreciated only by first examining the behavior of H. Interpreting H from (A27) and the definitions of $\Delta, \beta, F, \tilde{F}$ shows that

$$H = (\Delta_0 + F_0) + \frac{H_1}{\eta^2} + \frac{H_2}{\eta^3} + \ldots \tag{A30}$$

where

$$H_n = \Delta_n - \eta F_n + \Delta_0\beta_n - F_0\eta\beta_n + (1 - \xi^2)F_0'\beta_n' \tag{A31}$$

Since G is $O(\eta^{-4})$ it follows that the solutions for the first three F_n's are independent of G and are given by

$$H_0 = 0, \qquad H_1 = 0, \qquad H_2 = 0 \tag{A32}$$

51

and in particular the first of these according to (A29) and the definition of Δ_0 (A27) yields

$$(1 - \xi^2)F_0'' - 2\xi F_0' + 2F_0 = 0$$

This is a Legendre equation of degree 1 with the solutions

$$F_0 = AP_1(\xi) + BQ_1(\xi)$$

where $P_1(\xi)$ and $Q_1(\xi)$ are the Legrendre polynomials of degree 1 and A, B are arbitrary constants. In fact,

$$P_1(\xi) = \xi, \qquad Q_1(\xi) = \frac{1}{2}\,\xi\,\ln\left(\frac{\xi + 1}{\xi - 1}\right) - 1$$

and since the second kind $[Q_1(\xi)]$ gives a logarithmic singularity at $\xi = \pm 1$ we set $B = 0$ on the grounds that ϕ must be a smooth function. Then choosing $A = 1$ gives

$$F_0 = \xi, \qquad \Delta_0 = -\xi \tag{A33}$$

so that the first term of (A26) becomes $n\xi$ which generates a proper free stream as $n \to \infty$, as it should according to (A25).

Substituting this back into (A31) shows that H_n can be reduced to

$$H_n = \Delta_n - nF_n - (n + 1)\xi\beta_n + (1 - \xi^2)\beta_n'$$

$$= L_n - B_n\{(n + 1)\xi U_{n-1}(\xi) - (1 - \xi^2)U_{n-1}'(\xi)\}$$

where L_n is the Legendre differential operator of degree $(n - 1)$,

$$L_n = (1 - \xi^2)F_n'' - 2\xi F_n' + n(n - 1)F_n \tag{A34}$$

Furthermore, the expression $\{\ \}$ is a well-known identity

$$(n + 1)\xi U_{n-1}(\xi) - (1 - \xi^2)U_{n-1}'(\xi) = nU_n(\xi)$$

so that, finally

$$H_n = L_n - nB_n U_n$$

and therefore the complete sequence of solutions from (A29) must satisfy

$$L_1 = B_1 U_1$$
$$L_2 = 2B_2 U_2$$
$$L_3 = 3B_3 U_3 - G_3$$
$$\cdots$$
$$L_n = nB_n U_n - G_n \qquad \text{(A35)}$$
$$\cdots$$

where we have written

$$G = \frac{G_3}{n^4} + \frac{G_4}{n^5} + \cdots$$

since, as already noted, G is $O(n^{-4})$.

(c) With regard to the G_n quantities arising from the higher-order products it can be seen from (A28) that

$$G = \beta\Delta + \tilde{\beta}\tilde{F} + (1 - \xi^2)\beta'F'$$

and each of these products can be expanded into a power series in $1/n$ by using the definitions of β, Δ etc. to give

$$G_{n+2} = \sum_{r=1}^{n} B_r \{U_{r-1}\Delta_{n+1-r} + r(n + 1 - r)U_{r-1}F_{n+1-r} + (1 - \xi^2)U'_{r-1}F'_{n+1-r}\} \qquad \text{(A36)}$$

The details of how this can be simplified sufficiently to enable algebraic computation to be affected for arbitrary n will be considered later (section 9). For the moment the important feature is that G_n depends only on F_{n-2}, Δ_{n-2}, etc., so the only coupling is to functions already known from previous lower orders — which is, of course, the vital point of contrast to all the other iterative/analytical methods discussed in Section 4.

Now the general solution of $L_n = 0$ which remains finite at $\xi = \pm 1$ is

$$\alpha_n P_{n-1}(\xi)$$

where α_n is an arbitrary constant. Furthermore, a particular solution of

$$L_n = nB_n U_n(\xi)$$

is

$$F_n = -B_n T_n(\xi)$$

since

$$(1 - \xi^2)T_n'' - 2\xi T_n' + n(n - 1)T_n = -nU_n$$

where $T_n(\xi)$ is the Chebyshev polynomial of first kind

$$T_n(\xi) = \cos n\omega$$

Thus $F_1, F_2, \Delta_1, \Delta_2$ are polynomials in ξ and so, therefore, is G_3 according to (A36). However, it is not necessarily obvious that every F_n is thereby a polynomial since F_3 involves the particular solution for a right side (G_3) which is (essentially) an arbitrary polynomial rather than a special form. But the highest degree in G_3 is 1 so we could represent the problem for F_3 as

$$L_3 = 3B_3 U_3 - p_1; \qquad\qquad p_1 = A\xi + B \quad \text{(say)}$$

to emphasize this aspect. A particular solution for

$$L_3 = p_1, \qquad\qquad F_3 = q_1 \qquad \text{(say)}$$

is $q_1 = (1/4)A\xi + (1/6)B$ which is still of degree 1 only. The highest degree in G_4 is ξ^2, but now we know that the highest degree in G_5 is still only ξ^3 because the solution for F_3 did not increase the degree of p_1.

Proceeding in this manner it is clear that <u>if</u> a particular solution q_{n-2} can be found for the equation

$$L_n = p_{n-2}$$

where p_{n-2} is at most of degree ξ^{n-2} then every F_n will be a polynomial of degree $\leq n$.

(d) To see that this is the case, consider the superposition of solutions of

$$L_n(q) = \xi^{m-1} \qquad (A36)$$

where q is assumed to be a power series

$$q = q_1 + q_2\xi + q_2\xi^2 + \ldots \qquad (A37)$$

which may or may not terminate*. Operating on (A37) with L_n, and equating ξ coefficients gives the system of equations

$$\left.\begin{array}{l} Nq_1 + 2.1q_3 = 0 \\ (N - 2.1)q_2 + 3.2q_4 = 0 \\ \qquad \bullet \ \bullet \ \bullet \\ \{N - m(m - 1)\}q_m + m(m + 1)q_{m+2} = 1 \\ \qquad \bullet \ \bullet \ \bullet \end{array}\right\} \quad N = n(n - 1) \qquad (A38)$$

whose solution depends on the value of m in relation to n.

If $m = n$ then q_{m+2} can be found from (A38) and therefore all the higher coefficients displaced by two. There is no way to find the coefficients displaced by one, nor those for m, $m-2$, $m-4$, $\ldots$. However, since we are only interested in finding any special solution these can be taken as zero and the recursive computation of q_{m+4}, q_{m+6} $\ldots$ provides a satisfactory procedure — except for the fact that this sequence does not terminate.

Evidently if $m > n$ all coefficients up to $m + 2$ must again be taken as zero with the same consequences.

Fortunately, the case for $m < n$ is different since $q_{n+2} = 0$ and we may take all powers n, $n-2$, $\ldots$ as zero until m is reached. Therefore, the recursive sequence starts with q_m and descends, viz.

---

*The choice of numbering in the coefficients may appear a little unusual, but this particular system will be used frequently since it is consistent with the computer numbering and numerical steps.

$$q_m = \frac{1}{\{N - m(m - 1)\}}$$

(A39)

$$q_{m-2} = -\frac{(m - 2)(m - 1)}{\{N - (m - 2)(m - 3)\}} q_m$$

$$\cdot \cdot \cdot$$

until q_1 or q_2 is reached.

Thus it is possible to obtain a special solution to (A36) which is a polynomial of degree $m - 1$ provided m does not exceed $n - 1$. As can be seen from section c, this is just the case required where the polynomial on the right (p_{n-2}) is of degree at most $n - 2$.

Therefore, we have established inductively that:

1. $G_n = p_{n-2}$ is of degree at most $n - 2$

2. q_{n-2} is of degree at most $n - 2$

3. F_n is always a polynomial of degree at most n

On this basis it is more convenient to use the p, q notation and write the system of equations (A35) as

$$L_1 = B_1 U_1$$
$$L_2 = 2B_2 U_2$$
$$L_3 = 3B_3 U_3 - p_1 \qquad\qquad\text{(A40)}$$
$$\cdot \cdot \cdot$$
$$L_n = nB_n U_n - p_{n-2}$$
$$\cdot \cdot \cdot$$

The solution of this system is, according to section c, and the above discussion,

$$F_1 = \alpha_1 P_0(\xi) - B_1 T_1(\xi)$$
$$F_2 = \alpha_2 P_1(\xi) - B_2 T_2(\xi)$$
$$F_3 = \alpha_3 P_2(\xi) - B_3 T_3(\xi) - q_1(\xi) \qquad\qquad\text{(A41)}$$
$$\cdot \cdot \cdot$$
$$F_n = \alpha_n P_{n-1}(\xi) - B_n T_n(\xi) - q_{n-2}(\xi)$$
$$\cdot \cdot \cdot$$

All of these are elementary polynomials and the only items standing in the way of a general automatic computation scheme are the details of the p_n, q_n calculations and the manner in which the boundary conditions must be satisfied in order to determine the constants α_n.

Both of these items together with the general behavior of the solution can be clarified by a brief examination of the first few approximations.

A6. STRUCTURE OF THE FIRST FEW TERMS

(a) Having seen that $\phi_0 = nF_0$ gives a free stream, it is instructive to see next what the inclusion of the next two terms yields since these are still independent of any $p \to q$ operations. Let ϕ_1 denote the approximation up to F_1 so that

$$\phi_1 = n\zeta + \frac{1}{n}\left(\alpha_1 - B_1\zeta\right) = n \cos \omega + \frac{1}{n}\left(\alpha_1 - B_1 \cos \omega\right)$$

from (A41). Then

$$\left(\frac{\partial \phi_1}{\partial n}\right)_{n=1} = -\alpha_1 + (1 + B_1) \cos \omega$$

and it is clear that there is no choice of α_1 which makes this vanish for all ω unless it happens that $B_1 = -1$, $B_n = 0(n > 1)$. In that case if $\alpha_1 = 0$ the mapping represents a zero thickness (plate) profile parallel to the stream direction.

Taking the next term

$$\phi_2 = n\xi + \frac{1}{n}\left[\alpha_1 - B_1 T_1(\xi)\right] + \frac{1}{n^2}\left[\alpha_2\xi - B_2 T_2(\xi)\right]$$

$$= \frac{1}{n}\alpha_1 + \left(n - \frac{B_1}{n} + \frac{\alpha_2}{n^2}\right)\cos \omega - \frac{B_2}{n^2}\cos 2\omega$$

so that

$$\left(\frac{\partial \phi_2}{\partial n}\right)_{n=1} = -\alpha_1 + (1 + B_1 - 2\alpha_2) \cos \omega - 2B_2 \cos 2\omega$$

57

It is impossible to choose α_1 and α_2 to make this vanish for all ω unless $B_2 = 0$. If B_2 <u>is</u> zero, then the choice

$$\alpha_1 = 0$$

$$\alpha_2 = \frac{1 + B_1}{2}$$

gives

$$\phi_2 = \left(\eta - \frac{B_1}{\eta} + \frac{1 + B_1}{2\eta^2} \right) \cos \omega \tag{A42}$$

The case of ellipsoids is considered in more detail in the next section, but at this point it is worth noting that if every $B_n = 0$ (including B_1) the mapping generates a circular profile and under these circumstances

$$\phi_2 = \left(\eta + \frac{1}{2\eta^2} \right) \cos \omega = \left(r + \frac{1}{2r^2} \right) \cos\omega$$

which is the correct potential for a sphere.

For any other body ϕ_2 is an approximation. It is <u>not</u> correct for an ellipsoid when $B_1 \neq 0$ even though every other B_n is zero for such a body. It is this curious feature that makes the ellipsoids worth further study in their own right. If $B_2 \neq 0$ then ϕ_2 is a poor approximation in general because the boundary condition will be in error in the $\cos 2\omega$ term.

(b) Since it is not difficult to work out p_1 and p_2 by hand we next consider ϕ_4. Leaving out the details, the calculated values of p_1 and p_2 obtained from (A36) and F_1, F_2 are:

$$p_1 = 2B_1\alpha_1, \qquad\qquad p_2 = (4B_1\alpha_2 + 6B_2\alpha_1)\xi$$

and then the procedure of section 5d gives

$$q_1 = \frac{B_1\alpha_1}{3}, \qquad\qquad q_2 = \frac{1}{5} (2B_1\alpha_2 + 3B_2\alpha_1)\xi$$

so that the whole solution for ϕ_4 is

$$\phi_4 = \eta\xi + \frac{1}{\eta} (\alpha_1 P_0 - B_1 T_1) + \frac{1}{\eta^2} (\alpha_2 P_1 - B_2 T_2) + \frac{1}{\eta^3} \left(\alpha_3 P_2 - B_3 T_3 - \frac{\alpha_1 B_1}{3} \right)$$
$$+ \frac{1}{\eta^4} \left(\alpha_4 P_3 - B_4 T_4 - \frac{1}{5} [2B_1\alpha_2 + 3B_2\alpha_1]\xi \right) \tag{A43}$$

Putting the Legendre polynomials in terms of $\cos n\omega$ and applying the boundary condition then gives for each frequency in decreasing order

$$-\frac{5}{2}\,\alpha_4 + 3B_3 = 0$$

$$-\frac{9}{4}\,\alpha_3 + 2B_2 = 0$$

$$-\frac{3}{2}\,\alpha_4 + \frac{4}{5}\,(2B_1\alpha_2 + 3B_2\alpha_1) - 2\alpha_2 + B_1 + 1 = 0 \tag{A44}$$

$$-\frac{3}{4}\,\alpha_3 + \alpha_1 B_1 - \alpha_1 = 0$$

with, as before, the understanding that the $\cos 4\omega$ term cannot be accounted for. The first two equations give immediate solutions

$$\alpha_4 = \frac{6}{5}\,B_3, \qquad\qquad \alpha_3 = \frac{8}{9}\,B_2$$

and then the last two reduce to the 2×2 matrix

$$(8B_1 - 10)\alpha_2 + 12B_2\alpha_1 = 9B_3 - 5(1 + B_1)$$

$$3(B_1 - 1)\alpha_1 = 2B_2$$

which can be solved as

$$\alpha_1 = -\frac{2}{3}\,\frac{B_2}{1 - B_1}$$

$$\alpha_2 = \frac{1}{(8B_1 - 10)}\left[9B_3 + \frac{8B_2^2}{1 - B_1} - 5(1 + B_1)\right] \tag{A45}$$

This shows that the α_n coefficients will not in general depend linearly on the B_n coefficients, and that some kind of small matrix solution will be required for higher-order terms. In fact, the algebra up to the 4×4 matrix solution was carried out by hand, but only a few key points are recorded for use in the next section.

The structure of ϕ_6 itself in terms of F_n, is clear enough from the basic formula (A26) together with (A41). Expressions for q_1 and q_2 have already been given and the results for q_3 and q_4 follow from the calculation of p_3 and p_4 through (A36) and the procedure of section 5d. The results are:

$$q_3 = C_0 + C_2\xi^2; \qquad q_4 = D_1\xi + D_3\xi^3$$

where

$$C_0 = -\frac{1}{140}\left[30B_1\alpha_3 - 4B_2\alpha_2 + (28B_1^2 + 44B_3)\alpha_1\right]$$

$$C_2 = \frac{1}{14}\left[9B_1\alpha_3 + 10B_2\alpha_2 + 16B_3\alpha_1\right] \tag{A46}$$

$$D_1 = -\frac{1}{84}\left[56B_1\alpha_4 + 30B_2\alpha_3 + \left(\frac{108}{5}B_1^2 + 24B_3\right)\alpha_2 \right.$$
$$\left. + \left(100B_4 + \frac{312}{5}B_1B_2\right)\alpha_1\right]$$

$$D_3 = \frac{1}{18}\left[20B_1\alpha_4 + 21B_2\alpha_3 + 24B_3\alpha_2 + 40B_4\alpha_1\right]$$

Satisfaction of the boundary condition on the surface leads to six equations for the six α_n constants which again break down into two explicit formulas for α_5 and α_6, viz.

$$\alpha_6 = \frac{5 \times 128}{6 \times 63}B_5, \qquad \alpha_5 = \frac{4 \times 64}{5 \times 35}B_4 \tag{A47}$$

and 4 simultaneous equations for α_1, α_2, α_3, α_4

$$\alpha_3(45B_1 - 63) + \alpha_2(50B_2) + \alpha_1(80B_3) = 64B_4 - 56B_2$$

$$\alpha_3(75B_1 - 105) + \alpha_2(270B_2) + \alpha_1(140 - 140B_1 - 180B_3 + 140B_1^2) = -144B_4$$

$$\alpha_4(60B_1 - 90) + \alpha_3(63B_2) + \alpha_2(72B_3) + \alpha_1(120B_4) = 100B_5 - 108B_3 \tag{A48}$$

$$\alpha_4(420B_1 - 63) + \alpha_3(1305B_2) + \alpha_2 C_{43} + \alpha_1 C_{44} = 1000B_5 - 420(1 + B_1)$$

where the two coefficients C_{43} and C_{44} are

$$C_{43} = (-840 + 672B_1 + 1800B_3 - 648B_1^2)$$

$$C_{44} = (1008B_2 + 1210B_4 - 1872B_1B_2)$$

These clumsy results are included only for the algebraic arguments of the next section and for completness in the sense that they are invaluable guides in working out and checking general automatic computing schemes.

60

A7. COMPARISON WITH ELLIPSOID SOLUTIONS

(a) The reason that it is worthwhile considering ellipsoids in detail is, of course, that they represent the only simple general class of parametrically varying axisymmetric bodies with exact solutions. Furthermore, there is a curious feature involved when comparing the classical exact solutions with the sequence ϕ_0, ϕ_2, ϕ_4 ... developed in the foregoing sections. This arises in the following way. With all $B_n = 0$ except B_1, separation of real and imaginary parts in (A9) and putting $\lambda = 0$ gives

$$x_s = (1 - B_1) \cos \omega, \qquad y_s = (1 + B_1) \sin \omega$$

if we choose to take $C = 0$ and so shift the origin to the usual central point for ellipses. Thus, keeping the x-axis always aligned with the flow,

semi-major axis = $a = 1 - B_1$

semi-minor axis = $b = 1 + B_1$

showing that $-1 \leq B_1 \leq +1$, with $B_1 = 0$ giving a circular profile as noted in section 6b, and $-1 \leq B_1 \leq 0$ giving the usual range of thickness ratios representing "ovary" ellipsoids. Now it is apparent that the foregoing theory gives ϕ_0, ϕ_2, ϕ_4 ... directly in terms of B_1 irrespective of whether B_1 is $>$ or < 0. However, the classical results (e.g., Milne-Thomson [A7]) show that the analytical <u>form</u> of solution is different according as $a > b$ or $a < b$, i.e., according as $B_1 < 0$ or $B_1 > 0$.

This situation can be clarified by "expanding" the classical solutions in some way and showing that the expansions so obtained agree with $\phi_0 \phi_2 \phi_4$ ... irrespective of the sign of B_1.

(b) The classical solutions can be expressed by means of elliptic coordinates as follows:

o   When $a > b$ $(-1 \leq B_1 \leq 0)$ put $B_1 = -e^{-2\mu}$ and write $\gamma = \cosh(\lambda + \mu)$, $\gamma_0 = \cosh \mu$ then

$$\phi = 2e^{-\mu} \cos \omega \left\{ \gamma - \frac{\gamma/2 \ln[(\gamma + 1)/(\gamma - 1)] - 1}{1/2 \ln[(\gamma_0 + 1)/(\gamma_0 - 1)] - [\gamma_0/(\gamma_0^2 - 1)]} \right\}$$

(A49)

o   When $a < b$ $(1 \geq B_1 \geq 0)$ put $B_1 = e^{-2\mu}$ and write $\sigma = \sinh (\lambda + \mu)$, $\sigma_0 = \sinh \mu$ then

$$\phi = 2e^{-\mu} \cos \omega \left\{ \sigma - \frac{[\sigma \tan^{-1}(1/\sigma) - 1]}{[\tan^{-1}(1/\sigma_0) - \sigma_0/(\sigma_0^2 + 1)]} \right\} \tag{A50}$$

A reasonable supposition is that if (A49) and (A50) are capable of yielding expansions which can be matched to ϕ_0, ϕ_2, ϕ_4 ...,   then the case of large λ should be the one to examine. The first term of (A49) is

$$e^{-\mu} \{e^{\lambda+\mu} + e^{-\lambda-\mu}\} \cos \omega = (e^\lambda + e^{-2\mu}e^{-\lambda}) \cos \omega = \left(\eta - \frac{B_1}{\eta}\right) \cos \omega$$

in the earlier notation. Thus, temporarily denoting the constant in (A49) by h we have

$$\phi = \cos \omega \left[\left(\eta - \frac{B_1}{\eta}\right) - h \left(\frac{\gamma}{2} \ln \frac{\gamma + 1}{\gamma - 1} - 1\right) \right]$$

If λ and μ are both taken as large then $\lambda + \mu$ is large and it is natural to put $\epsilon = e^{-(\lambda+\mu)}$ and find the expansion for small ϵ. The term in $\lambda + \mu$ is then expressible as

$$\frac{\gamma}{2} \ln \frac{\gamma + 1}{\gamma - 1} - 1 = \frac{1}{2} \left(\frac{1}{\epsilon} + \epsilon\right) \ln \left(\frac{1 + \epsilon}{1 - \epsilon}\right) - 1 \sim \frac{4}{3} \epsilon^2 + \frac{8}{15} \epsilon^4 + \frac{12}{35} \epsilon^6 + \ldots$$

or, since $\epsilon^2 = e^{-2\mu}e^{-2\lambda} = -B_1/\eta^2$,

$$\phi = \cos \omega \left[\left(\eta - \frac{B_1}{\eta}\right) + h \left(\frac{4B_1}{\eta^3} \frac{1}{2} - \frac{8B_1^2}{15} \frac{1}{\eta^4} + \frac{12B_1^3}{35} \frac{1}{\eta^6} - \ldots\right) \right] \tag{A51}$$

In order to derive consistent comparisons for individual orders from (A51) it is convenient to proceed in a slightly unusual manner because of the apparently very complicated nonlinear dependence of the $\phi_4\phi_6$ terms on B_1 through the α_n constants (see e.g. (A43) and (A44) for ϕ_4 and α_4). Since h is the constant appropriate to an infinite number of terms, it seems reasonable to argue that one should designate h_2, h_4, h_6 as the constants appropriate to the orders η^{-2}, η^{-4}, η^{-6} and then these can be determined by noting that every order must individually satisfy the surface boundary condition. This procedure is certainly consistent with the philosophy under-lying the structure of $\phi_2\phi_4\phi_6$.

62

For instance, on this basis (A51) yields

$$\phi_2 = \cos \omega \left[\left(\eta - \frac{B_1}{\eta} \right) + h_2 \frac{4B_1}{3} \frac{1}{\eta^2} \right] \tag{A52}$$

and then we must have

$$h_2 = \frac{3(1 + B_1)}{8B_1} \tag{A53}$$

Similarly ϕ_4 and ϕ_6 are given by (A51) with

$$h_4 = \frac{-15(1 + B_1)}{8B_1(4B_1 - 5)} ; \qquad\qquad h_6 = \frac{105(1 + B_1)}{8B_1(35 - 28B_1 + 27B_1^2)} \tag{A54}$$

For the other case (A50) let the constant be denoted by k then

$$\phi = \cos \omega \left[\left(\eta - \frac{B_1}{\eta} \right) - k(\sigma \tan^{-1} \frac{1}{\sigma} - 1) \right]$$

and again let $\varepsilon = e^{-(\lambda+\mu)}$ so that

$$(\sigma \tan^{-1} \frac{1}{\sigma} - 1) = \frac{1}{2} \left(\frac{1}{\varepsilon} - \varepsilon \right) \tan^{-1} \frac{2\varepsilon}{1 - \varepsilon^2} - 1 \sim -\frac{4}{3} \varepsilon^2 + \frac{8}{15} \varepsilon^4 - \frac{12}{35} \varepsilon^6 + \ldots$$

This time

$$\varepsilon^2 = e^{-2\mu} e^{-2\lambda} = B_1/\eta^2$$

and if this is substituted into the expansion above the same expression as
(A51) results. Since the constants k_2, k_4, k_6 ... would be chosen by the
same argument it follows that (A51) through (A54) represent the successive
orders of approximation for both cases, thus resolving one aspect of the
curious feature mentioned in section a.

(c) Next it is necessary to show that the ϕ_2, ϕ_4, ϕ_6 of section 6 are
consistent with (A51) through (A54). In the case of ϕ_2 it is obvious by
inspection on comparing (A42) with (A52). For ϕ_4 put B_2, B_3 to zero and
then α_3 and α_4 are zero according to (A44). Furthermore, according to
(A45) $\alpha_1 = 0$ and

$$\alpha_2 = - \frac{5(1 + B_1)}{(8B_1 - 10)}$$

63

so that if these results are substituted into (A43) the formula for ϕ_4 becomes

$$\phi_4 = \cos \omega \left[\left(\eta - \frac{B_1}{\eta} \right) - \frac{5(1 + B_1)}{8B_1 - 10} \left(\frac{1}{\eta^2} - \frac{2B_1}{5\eta^4} \right) \right] \tag{A55}$$

which can be seen to be identical to (A51) with h_4 given by (A54).

Finally, for ϕ_6 with all B_n coefficients zero except B_1, the equations (A47) and (A48) for the α_n's reduce to

$$\alpha_6 = 0, \quad \alpha_5 = 0, \quad \alpha_4 = 0, \quad \alpha_3 = 0, \quad \alpha_1 = 0$$

and

$$\alpha_2 = \frac{105(1 + B_1)}{(210 - 168B_1 + 162B_1^2)}$$

Then the expression for ϕ_6 becomes quite simple because q_3 and q_4 simplify to

$$q_3 = 0, \qquad q_4 = -\frac{9}{35} B_1^2 \alpha_2 \xi$$

thus giving

$$\alpha_6 = \cos \omega \left[\left(\eta - \frac{B_1}{\eta} \right) + \alpha_2 \left(\frac{1}{\eta^2} - \frac{2}{5} B_1 \frac{1}{\eta^4} + \frac{9}{35} B_1^2 \frac{1}{\eta^6} \right) \right] \tag{A57}$$

Using the α_2 given by (A56) in (A57) it is easy to see that this result agrees with (A51) and (A54) showing that the classical expansions agree with the algebraically derived approximations ϕ_2, ϕ_4, ϕ_6 of this theory for ellipsoidal bodies.

(d) Finally, the comparisons will be complete if we can show that the constants h_2, h_4 and h_6 are progressively better approximations to h and k, the exact constants appropriate to an infinite number of terms. Denoting $e^{-\mu}$ by ε (small), the first form of constant from (A49) is

64

$$h = \frac{2e^{-\mu}}{\{1/2 \ \ln \ [(\gamma_0 + 1)/(\gamma_0 - 1)] - [(\gamma_0)/(\gamma_0^2 - 1)]\}}$$

$$= - \frac{1}{\epsilon^2 [8/3 + (24/5)\epsilon^2 + (48/7)\epsilon^4 \ ...]} \qquad \text{(A58)}$$

which can be written in the forms

$$h = \frac{1}{B_1 [8/3 - (24/5)B_1 + (48/7)B_1^2 - ...]} = \frac{(1 + B_1)}{B_1 [8/3 - (32/15)B_1 + (72/35)B_1^2 \ ...]}$$
$$\text{(A59)}$$

since $\epsilon^2 = e^{-2\mu} = -B_1$. Progressively including higher-power terms in [ ] gives

$$h_2 = \frac{3(1 + B_1)}{8B_1} \ , \qquad h_4 = \frac{15(1 + B_1)}{B_1 (40 - 32B_1)} \ , \qquad h_6 = \frac{105(1 + B_1)}{8B_1 (35 - 28B_1 + 27B_1^2)}$$

which are identical to (A53) and (A54). The expansion for k in ϵ^2 is the same as (A58) except for alternating signs which give exactly (A59) again since this time $\epsilon^2 = +B_1$.

Thus both forms of classical formula give the same expansion for the constants of each type. Of course the two forms for the classical formulas result from the same general argument in more general complex variables so none of this is really very surprising. Nevertheless this topic cannot be discussed further here. We have shown that ellipsoidal bodies are correctly represented by the sequence of potentials in this theory. It is more appropriate to inquire about the convergence of this sequence, and this can best be discussed in terms of the velocity.

A8. FORMS OF THE VELOCITY

(a) The general theory for ϕ as given in sections A1 through A7 will be of little value unless we can be sure that the velocity — and in particular the surface velocity — can be computed accurately — without problems from the trailing edge singularity for instance. For the present it is only the surface velocity $(\lambda = 0)$ which is of interest, and denoting magnitude by Q

65

we have from section 3

$$Q(0,\omega) = -\frac{1}{h_1(0)} \left(\frac{\partial \phi}{\partial \omega}\right)_{\lambda=0}$$

In the case of the conformal mapping used here

$$h_1 = h_2 = \left|\frac{dz}{d\zeta}\right|$$

and on the surface $\zeta = e^{i\omega}$ so that

$$h_1(0) = \left|\frac{dz_s}{d\omega}\right| = \frac{ds}{d\omega}$$

where s is the arc length along the profile measured from the trailing edge (which is taken as the origin in all general computations). Thus using s as a subscript for surface value

$$Q_s = -\frac{\partial \phi_s/\partial \omega}{ds/d\omega} \tag{A60}$$

and the need for caution arises from possible zero values of $ds/d\omega$ as a consequence of the assumed forms for the mapping derivative [(A7) and (A8)].

Setting $\zeta = e^{i\omega}$ in (A7) and (A8) gives

$$\tau = \pi \text{ (blunt)} \quad \frac{ds}{d\omega} = \left[(1 + a_2 \cos 2\omega + \ldots)^2 + (a_2 \sin 2\omega + \ldots)^2\right]^{1/2} \tag{A61}$$

$$= 0 \text{ (cusp)} \quad \frac{ds}{d\omega} = 2 \sin \frac{\omega}{2} \left[(1 + \cos \omega + a_2 \cos 2\omega + \ldots)^2 + (\sin \omega + a_2 \sin 2\omega + \ldots)^2\right]^{1/2} \tag{A62}$$

so that $ds/d\omega$ does indeed vanish at $\omega = 0$ when $\tau = 0$. It is convenient to note that (A61) and (A62) can be expressed in terms of the surface modulus of the $g(\zeta)$ function of section 3 for both cases, that is:

$$\frac{ds}{d\omega} = |g_s(\omega)| \qquad \text{if} \qquad \tau = \pi$$

$$\frac{ds}{d\omega} = 2 \sin \frac{\omega}{2} |g_s(\omega)| \qquad \text{if} \qquad \tau = 0$$

<div align="right">(A63)</div>

<div align="center">66</div>

where $|g_s(\omega)|$ is a positive periodic function which has no zeroes or infinities – as is obvious from (A61) and (A62).

Now the form of ϕ given by (A26) and (A41) has the natural terms consisting of $\cos n\omega$ and powers of $\xi = \cos \omega$. These latter can always be expressed in terms of $\cos \omega$, $\cos 2\omega$ ... by using the reverse transformation for the Chebyshev polynomial of first kind, so that it is always possible to express ϕ in the form

$$\phi = G_0(n) + G_1(n) \cos \omega + G_2(n) \cos 2\omega + \dots$$

by a simple reorganization. Consequently,

$$\frac{\partial \phi}{\partial \omega} = - \left[G_1(n) \sin \omega + 2G_2(n) \sin 2\omega + \dots \right]$$

from which a factor $\sin \omega$ can be entracted leaving a modulation term which is a function of the Chebyshev polynomials of second kind. That is,

$$\frac{\partial \phi}{\partial \omega} = - \sin \omega\, G(\xi, n) \tag{A64}$$

where

$$G(\xi, n) = G_1(n) + 2G_2(n)U_1(\xi) + 3G_3(n)U_2(\xi) + \dots \tag{A65}$$

so that the velocity from (A60), (A63), (A64) can be written

$$Q_s = \frac{\sin \omega\, G(\xi, 1)}{|g_s(\omega)|} \qquad\qquad \text{if} \qquad\qquad \tau = \pi \quad \text{(blunt)}$$

$$= \frac{\cos\,(\omega/2)\,G(\xi, 1)}{|g_s(\omega)|} \qquad\qquad \text{if} \qquad\qquad \tau = 0 \quad \text{(cusp)}$$

and both of these forms are computationally trouble free for all ω. As expected blunt bodies have stagnation points at both ends, whereas a body with a cusp trailing edge has a finite nonzero velocity at that trailing edge ($\omega = 0$).

67

(b) For the ellipsoids the results of section 7 can be used to give some idea of the maximum velocity convergence. It is interesting to compare the successive terms with the two-dimensional value which can be denoted as the zero-th order approximation very conveniently. The complete solution for two dimensions is, of course,

$$\phi_0 = \left(\eta + \frac{1}{\eta}\right) \cos \omega = 2 \cosh \lambda \cos \omega$$

so that, dropping the now unnecessary "s" subscript, the zero-th order approximation to surface velocity is

$$Q_0 = \frac{2 \sin \omega}{|g_s(\omega)|} \qquad \text{or} \qquad G_0 = 2 \qquad (A65)$$

irrespective of the shape. For the order 2, 4, 6 terms on ellipsoids the G function surface values follow from (A42), (A55), and (A57) leading to the sequence

$$
\begin{aligned}
G_0 &= 2 \\
G_2 &= (1 - B_1) + \frac{1}{2}(1 + B_1) \\
G_4 &= (1 - B_1) + \frac{1}{2}(1 + B_1)\left(\frac{5 - 2B_1}{5 - 4B_1}\right) \\
G_6 &= (1 - B_1) + \frac{1}{2}(1 + B_1)\left(\frac{35 - 14B_1 + 9B_1^2}{35 - 28B_1 + 27B_1^2}\right)
\end{aligned}
\qquad (A66)
$$

As an illustration, the case of ellipsoids of fineness ratios $a/b = 3/1$ and $a/b = 1/3$ are given in the table below. Exact values for G are computed from (A49) and (A50) by setting $\lambda = 0$ to give the slightly simplified forms:

$$G = \frac{4e^{-\mu}}{2 \cosh \mu - \sinh^2 \mu \, \ln[(\cosh \mu + 1)/(\cosh \mu - 1)]} \; ; \; B_1 < 0 = -e^{-2\mu}(a > b)$$

$$= \frac{2e^{-\mu}}{\cosh^2 \mu \, \tan^{-1}(1/\sinh \mu) - \sinh \mu} \; ; \qquad B_1 > 0 = e^{-2\mu} \, (a < b)$$

whilst the values of $|g_s(\omega)|$ at $\omega = \pi/2$ corresponding to the point of maximum velocity are:

68

when $\qquad a = \frac{3}{2}$, $\qquad b = \frac{1}{2}$ $\qquad$ then $B_1 = -\frac{1}{2}$; $\left|g_s\left(\frac{\pi}{2}\right)\right| = \frac{3}{2}$

when $\qquad a = \frac{1}{2}$, $\qquad b = \frac{3}{2}$ $\qquad$ then $B_1 = +\frac{1}{2}$; $\left|g_s\left(\frac{\pi}{2}\right)\right| = \frac{1}{2}$

The results are summarized in the table below with the % errors defined as

$$\% \text{ error} = \frac{(\text{approx value} - \text{exact value}) \times 100}{\text{exact value}}$$

Table of G Values and Maximum Velocities for Various Orders
of Approximation on Two Ellipsoids

	Slender Ellipsoid $a/b = 3$			Blunt Ellipsoid $a/b = 1/3$		
Order	G values	Q_{max} Values	Q_{max} % Error	G Values	Q_{max} Values	Q_{max} % Error
0	2.0	1.333333	+18.8	2.0	4.0	+45.8
2	1.75	1.166667	+4.0	1.25	2.5	-8.8
4	1.714286	1.142860	+1.9	1.50	3.0	+9.4
6	1.698431	1.132300	+0.9	1.317568	2.635136	-3.9
Exact	1.682953	1.121970	-	1.371324	2.742648	-

As an illustration not too much should be deduced from these tabular
values. Perhaps we should just remark here that the signs oscillate for the
excessively blunt case $(a/b = 1/3)$, but not for the more usual type of body
$(a/b = 3/1)$, and that convergence is adequate but not impressive. In
section 9 detailed results will be presented for a variety of bodies so
judgment should be deferred until then.

(c) Before passing onto general computation one other remark concerning
accuracy is worth drawing attention to. Naturally the convergence of velocity
is crucially dependent on the convergence of the B_n coefficients. Some idea
of the behavior of these numbers can be gained by brief consideration of the
Joukowski profile case on which Kaplan (section 4) obtained such good answers
with a scheme essentially sensitive only to B_3. A Joukowski profile has the
exact modulating function

69

$$g(\zeta) = 1 + \frac{1}{\zeta - d} + \frac{d(1-d)}{(\zeta - d)^2}$$

(see [A4]) where d is real for a symmetric case and $0 < d < 1$. Therefore, the expansion coefficients are

$$a_n = nd^{n-1} - (n-1)d^n; \qquad B_n = -d^{n-1}(1-d)^2$$

When $|d|$ is small it is clear that the convergence of the B_n numbers is good. For instance in the case quoted by Kaplan $d = 0.15$, giving

$$B_1 = -0.7225, \quad B_2 = -0.1084, \quad B_3 = -0.01626, \quad B_4 = -0.00244$$

The dominant "ellipsoid-effect" or leading term is proportional to $1 + B_1 = 0.2775$ so the amplitude ratio of the first neglected term in Kaplan's calculation would be essentially proportional to

$$\frac{0.00244}{0.2775} < \frac{1}{100}$$

which goes some way toward explaining the satisfactory results obtained with such limited sensitivity to the infinite sequence of B_n coefficients.

However, it is not difficult to get cases of practical importance in which the B_n convergence is very much worse than this, as will be seen in section 10, where test cases for the general solution having deliberately chosen peculiarities are presented.

A9. GENERAL CALCULATION SCHEME

(a) The overall structure of the general calculation scheme is based on the sequence of operations already described algebraically in the earlier sections (5 through 6). The computer program was written in Fortran IV for use on the Douglas IBM 370/168 system and can be regarded as proceeding by the following stages:

1. Input B_n coefficients and other data necessary.

2. Compute double subscripted arrays for the coefficients of special polynomial used $(P_n(\xi), T_n(\xi), \ldots)$.

3. Fill the first three orders F_1, F_2, F_3 of the solution variables
    using the algebraic answers discussed in Section 5b and c. All
    solution polynomials, unlike the special polynomials in 2, are
    functions of the α_n constants and so must be represented by
    3 subscript arrays which store the coefficients. Thus, F, p, q, ...
    are all typically represented as

$$F_n(\xi) = F_{n,1}(\xi) + F_{n,2}(\xi)\alpha_1 + \ldots + F_{n,n+1}(\xi)\alpha_n$$

where each polynomial $F_{n,i}(\xi)$ is of the form

$$F_{n,i}(\xi) = f_{n,i,1} + f_{n,i,2}\xi + \ldots f_{n,i,n+1}\xi^n$$

so that the coefficient array $f_{n,i,k}$ requires storage N, N + 1,
N + 1 if N is the highest order desired. Since three subscripted
arrays use a lot of core space, some trouble was taken in the program
to minimize the number of such arrays actually used. The current
version only requires two; but even so a great deal more could be
done to improve the efficiency of this particular version of
program.

4. Starting with $n = 4$ each F_n coefficient array is computed using
    (A41) and the p and q functions of order up to $n-2$. In
    addition the p function of next highest order is computed at
    this stage and the coefficients stored for future use.

5. A subroutine computes q coefficients from p coefficients by
    using the algorithm of section 5d and these are also stored for
    future use as in 4.

6. When the F_n functions have been computed up to the order desired
    (N say), a separate subroutine handles satisfaction of the boundary
    conditions by first converting $f_{n,i,k}$ to $\tilde{f}_{n,i,k}$ such that

$$F_{n,i}(\xi) = \tilde{f}_{n,i,1} + \tilde{f}_{n,i,2}T_1 + \tilde{f}_{n,i,3}T_2 + \ldots \tilde{f}_{n,i,n+1}T_n$$

which is an appreciable simplification at this stage since T_k is
merely $\cos k\omega$. Using the arguments of section 6, a set of $N-2$
simultaneous equations for the α_n constants follows, which can be

71

solved by a simple standard matrix inverse of low order operating wholly within core.

7.   A final subroutine computes and outputs the surface potential and velocities using the formulas of section 8.

This description of the essential steps followed by the program is only intended as an outline for discussion purposes; but most of the programming involved in the ommitted details is elementary and does not deserve comment.

However, one aspect of this scheme does deserve brief amplification.

(b) The central operation which includes all the "difficult" part of the whole theory (essentially all the nonlinear aspects) is the computation of p from the extant F_n functions according to (A36). It has already been remarked that not only does the whole theory hinge on the fact that each F depends (via p) only on previously computed F's, but that also it is possible to prove that $F_n(\varepsilon)$ is a polynomial of degree at most n (section 5c, d). However, the boundary condition procedure can always be reduced to a matrix inverse of order $(N-2) \times (N-2)$ with α_N and α_{N-1} determined directly, because, in fact, the p_{n-2} which effects F_n is actually only of order $n-3$ rather than $n-2$.

In section 5c it was noted that if the special solutions q were polynomials given a polynomial p of degree at most $n-2$, then the validity of the whole procedure could be proved inductively. That $p_n(\equiv G_{n+2})$ itself is of degree at most n is obvious from (A36), but the additional vanishing of the highest order term requires a little closer examination. Denoting $n-2$ by m, (A36) can be rewritten

$$p_m = \sum_{r=1}^{m} B_r \ \{U_{r-1}\Delta_{m+1-r} + r(m + 1 - r)U_{r-1}F_{m+1-r} + (1 - ^2)U'_{r-1}F'_{m+1-r}\}$$
(A67)

and each major contribution is a product of two polynomials. A special polynomial product subroutine keeps track of the coefficients for this frequently used operation, but for the highest order terms alone the answer can be written down directly. Nevertheless (A67) is not the best form of either the numerical construction or the algebraic scrutiny. Using the expression for

Δ_n in terms of F_n (section 5a), it is easy to reorganize (A67) into

$$p_m = \sum_{r=1}^{m} B_r \left[\frac{d}{d\xi} (1 - \xi^2) U_{r-1} F'_{m+1-r} + (m + 1)(m + 1 - r) U_{r-1} F_{m+1-r} \right] \qquad (A68)$$

which is the form actually used in the program. Furthermore, it is obvious from the structure of F_n (A41) that the highest order term is always contributed by $-B_n T_n(\xi)$ and so is always

$$-2^{n-1} B_n$$

Consequently the second part of (A68) contributes to ξ^m the amount

$$- \sum_{r=1}^{m} B_r B_{m+1-r} (m + 1)(m + 1 - r) 2^{m-1} \qquad (A69)$$

The highest order term in $U_{r-1} F'_{m+1-r}$ is, by the same reasoning,

$$-B_{m+1-r}(m + 1 - r) 2^{m-1} \xi^{m-1}$$

so that the contribution to ξ^m from the first part of (A68) must be

$$+ \sum_{r=1}^{m} B_r B_{m+1-r}(m + 1)(m + 1 - r) 2^{m-1}$$

which exactly cancels (A69), showing that the ξ^m term in p_m vanishes. Thus the computing scheme can, as explained, make use of this information to keep the α_n-matrix as small as possible. The cases of $N = 4$ and 6 as worked out in section 6b are illustrations of this feature.

A10. SOME EXAMPLES OF DIRECT VELOCITY CALCULATIONS

(a) In order to test the theory a number of profiles were generated by using a modification of the "pole airfoil" theory reported in [A4]. This procedure is extremely flexible since poles and zeros of the mapping derivative can be chosen at will within the unit circle in order to generate bumps and dimples on the profile. The point of all this is, of course, to provide test cases of sufficient character to reveal more information about the accuracy

73

than can be obtained, for instance, by only using Joukowski profiles. We have already seen that this can be very misleading (section 8c) and since most common test shapes are members of this larger class of pole airfoils (profiles) it is considered to be a useful adjunct to the whole theory.

For the test cases described below the form of $dz/d\zeta$ started out as a quotient of isolated linear groups, viz.

$$\frac{dz}{d\zeta} = \frac{(\zeta - c_1)(\zeta - c_2) \ldots (\zeta - c_m)}{(\zeta - d_1)(\zeta - d_2) \ldots (\zeta - d_m)} \qquad |c_n|, \quad |d_n| \leq 1 \qquad (A70)$$

where the first factor can be used to generate blunt or cusped shapes — since the latter is the only allowable example of the singularity being on the surface; the choice then being

$$c_1 = 1, \qquad d_1 = 0$$

to give the usual type of cusp.

Otherwise various criteria apply to the choice of c_1, c_2, ..., d_1, d_2, ... required to generate specific effects which need not be explained here in detail (see [A4]), except to note that the generation of extreme surface convolutions can only be achieved in general by having some $|c_n|$ and some $|d_n|$ very close to unity.

Equation (A70) can be expressed as

$$\frac{ds}{d\zeta} = 1 + \sum_{k=1}^{m} \frac{\lambda_k}{\zeta - d_k} \qquad |d_k| < 1 \qquad (A71)$$

which is the fundamental pole form where the quantities λ_k are the pole strengths. A simple partial fraction program determined these strengths from (A70), and then (A71) can be used to give an exact formula for the shape. In addition (A71) lends itself to an immediate expansion which is uniformly convergent in $|\zeta| \geq 1$ since every $|d_k| < 1$, viz.

$$\frac{dz}{d\zeta} = 1 + \frac{a_1}{\zeta} + \frac{a_2}{\zeta^2} + \ldots \qquad (A72)$$

74

where

$$a_n = \sum_{k=1}^{m} \lambda_k d_k^{n-1} \tag{A73}$$

These coefficients show that the ultimate rate of convergence is controlled by the largest $|d_k|$ and therefore it follows from the remarks above that extreme convolutions will have poor convergence. In the context of this work, of course, everything depends on the significance of the words "extreme" and "poor." This subject is best left to the examples given below, except to note in passing that the B_n coefficients used for the theory here are defined directly from (A72) by integration. Thus

$$z = C + \zeta - \frac{B_1}{\zeta} - \frac{B_2}{\zeta^2} - \ldots$$

agreeing with (A9), and so

$$B_n = \frac{a_{n+1}}{n} ; \qquad n = 1, 2, \ldots$$

(remembering that $a_1 = 0$ for closure) which shows that the B_n coefficients converge faster than the a_n coefficients.

It should be noted that this system of test cases generates exact shapes and exact B_n coefficients whose rate of convergence can be controlled and studied. Clearly this is necessary for the testing phase, but it does not represent a bias in favor of the current method. Any profile enclosing a schlict singly-connected domain can be mapped into the unit circle, and it is a trivial matter to write such a mapping program and to make the associated B_n coefficients available for input to this theory. In this sense neither is the special system used here a restriction of generality. A mapping program is available for finding these coefficients, but was not used in the cases described below. This question will be considered further in the discussion of the inverse (design) mode (section 11).

b.1. The first figure (Fig.A1) shows what might be described as a very bland basic case (body 1) in which the profile was a smooth blunt shape generated by

75

$$c_1 = 0.9, \qquad c_2 = -0.5$$

$$d_1 = 0, \qquad d_2 = 0.4$$

The velocity distribution based on only 10 B_n coefficients is shown compared with the very accurate "higher-order Neumann" method of Hess [A2]. Evidently, agreement is good for a trivial investment of computer effort because the "hardest" task involved in this theory for only 10 terms is the inversion of an 8×8 matrix*. For the Neumann runs and output stations of the method of this appendix, 101 points on the half body were used. Of course, the blandness of this case leads one to suspect that it is particularly favorable to the kind of theory advocated here, just as the Joukowski case used by Kaplan (see section 8c) turned out to be particularly favorable in that context. In fact, the rate of convergence for this case is unduly good. At the 64th station (very close to the maximum velocity) the zero-th order approximation (two-dimensional) is 1.520655 and the succeeding orders are:

Order	Q_s
2	1.226915
4	1.227366
6	1.225472
8	1.225760
10	1.225739

showing precisely the kind of weighted choice one should avoid in test cases!

2. However, the results obtained for the second body (Fig. 2) continue to show excellent agreement even though only 10 terms are used. This body is a perturbation of the basic case (1) in which a bump was generated deliberately near the nose — as can be seen from Fig. A2. The resultant sharp peak in velocity is produced accurately in detail and appears to be a good demonstration of the excellent convergence properties of the method.

---

*There is little point in trying to isolate proper computer CPU times from these runs because they are so small that the figures are largely obscured by various accounting and other semioptional features. For instance, in this run the CPU time was quoted as 0.011 minutes and the I/O as 0.044, but velocities of order 0, 2, 4, 6, 8 and 10 were individually computed and stored which is typical of many options not always needed.

3. Body No. 3 is a further perturbation of even more extreme character (Fig. A3). As can be seen, the velocity shows quite violent response to the artificially created bump-dip-bump, but the theory again gives remarkably good results with only 10 terms when compared with the higher-order Neumann. Obviously, this case is a still better demonstration of the relative insensitivity of the basic method to higher order B_n convergence.

4. The final case is interesting because it shows how a cusp is handled by the theory. The body is essentially similar to case 2 except that the B_n sequence terminates at B_3 and that there is a cusp. It can be seen (Fig. A4) that agreement (again with 10 terms) is excellent everywhere except close to the trailing edge. A much greater number of terms is required to give a good answer in the immediate locality of the cusp. This is exactly what would be expected on the grounds of the discussion given at the end of section 2 where it was pointed out that if the structure of the B_n coefficients gave good answers for the nonsingular (blunt) case then obviously it would be less satisfactory for cases where a further zero term should be extracted.

These cases cannot be considered exhaustive and evidently further work should be done, particularly for arbitrary bodies where the mapping program to determine the B_n coefficients is required first. To some extent the design cases considered next relieve any residual anxiety that perhaps the above results were subtly (unintentionally) biased in favor of this theory. Accepted at face value, however, the above results show very clearly the excellent convergence and economy of the theory.

A11. DESIGN (INVERSE) OPERATION

(a) As pointed out in Section 1, one of the important advantages of analytical solutions in engineering is the readiness with which they can usually be converted to a design (inverse) mode. In the context of airfoil theory it happens that the design problem, where a desired velocity is given and an associated shape determined, is both exact mathematically and non-iterative. Airfoils designed in this way are those which — in a least

77

squares sense — give velocities "closest" to the desired input and as such have recently proven to be of great practical value [A8].

In fact, interest in design methods for axisymmetric flow was one of the original stimuli for this study, particularly as there was no design procedure of any kind available at the start of this work except in two dimensions. However, recently a procedure for designing axisymmetric shapes by simply iterating a direct (Neumann type) method has finally been perfected by Bristow [A9] and we are fortunate to be able to compare a few cases of Bristow's method and the procedure advocated here.

But first a brief description of the inverse mode for the current theory is needed. Once again the important feature is the decoupling of the purely geometric aspect and the velocity aspect. In two dimensions this decoupling is complete, whereas for axisymmetric flow the gradient of ϕ still depends on the B_n coefficients. Thus, unlike the two-dimensional case, the design procedure for axisymmetric flow is iterative. The steps used in the current program version are very similar in character to those needed to determine the B_n coefficients (i.e., the mapping) from a given profile, or to find the flow about a given (two-dimensional) airfoil. As such they constitute an iterative scheme belonging to a general class whose convergence and accuracy properties have excellent precedents from two-dimensional experience. Briefly the procedure is based upon the central idea that if $ds/d\omega$ can be found at a certain stage then the appropriate a_n coefficients can be calculated directly by employing a transformation which is common in two-dimensional mapping theory. Looking at (A61) and (A62) it might be thought that, given $ds/d\omega$, there is no way to determine the a_n coefficients directly, but this is not the case. The argument by which these coefficients can be determined is typical of the great power and flexibility of mapping methods and is rarely appreciated as such.

(b) Briefly, if $dz/d\zeta$ is given by series of the forms (A7) and (A8), then

$\tau = \pi$ (blunt) $\qquad \ln \dfrac{dz}{d\zeta} = \ln g(\zeta) = g(\zeta)$

$\tau = 0$ (cusp) $\qquad \ln \dfrac{dz}{d\zeta} = \ln \left(1 - \dfrac{1}{\zeta}\right) + \ln g(\zeta) = \ln \left(1 - \dfrac{1}{\zeta}\right) + f(\zeta)$

and in both cases $g(\zeta)$ is an analytic function for $|\zeta| \geq 1$ which $\to 1$ as $|\zeta| \to \infty$. Thus $f(\zeta)$ is an analytic function for $|\zeta| \geq 1$ which $\to 0$ as $|\zeta| \to \infty$ and can be represented by

$$\ln g(\zeta) = \ln \left(1 + \frac{a_1}{\zeta} + \frac{a_2}{\zeta^2} + \ldots\right) = f(\zeta) = \frac{b_1}{\zeta} + \frac{b_2}{\zeta^2} + \ldots \qquad (A74)$$

In a relation of this form the determination of the a_n coefficients given the b_n or vice versa is a purely algebraic procedure which is easy to compute. On the other hand, the connection between the surface values of f_s and g_s is $f_s = \ln g_s$ so that if $f_s = u_s + iv_s$ (say) then

$$u_s = \ln g_s ; \qquad v_s = \arg g_s$$

Therefore, using (A63), the first of these gives

$$u_s = \ln \frac{ds}{d\omega} \qquad (\tau = \pi)$$

$$= \ln \frac{ds}{d\omega} - \ln \left(2 \sin \frac{\omega}{2}\right) \qquad (\tau = 0)$$

from which u_s can be calculated. But according to (A74) u_s is the real part of the b_n series with real coefficients (for the axisymmetric case — by symmetry) giving

$$u_s = b_1 \cos \omega + b_2 \cos 2\omega + \ldots \qquad (A75)$$

where $b_1 = a_1 = 0$ if $\tau = \pi$ or $b_1 = a_1 = 1$ if $\tau = 0$ due to the closure condition (A5).

Thus it follows that the b_n coefficients can be determined directly by Fourier analysis of u_s and therefore the a_n coefficients indirectly by inversion of (A74) as remarked before. In addition, the magnitude of b_1 is clearly a measure of "compatibility" at any stage of the iteration or, in the particular case of two-dimensional design, a direct measure of the plausibility of the desired velocity distribution.*

---

*The inverse problem is not unique in either two-dimensional or axisymmetric flow. The best one can expect is some minimum measure of closeness to the desired input and a least squares Fourier criterion has been found very satisfactory in two dimensions (see, e.g. [A8].

(c) The steps in the iterative design mode for the theory developed here
can then be described in the following terms:

Step 1. Guess a set of B_n coefficients. The runs described below all
use those for body 1 (section 10d) as a starting system.

Step 2. Calculate $\partial\phi_s/\partial\omega$ by using (A64) and (A65). For this step the
major part of the basic direct program as described in section 9a
is used as a subroutine. Only number 7 is left off.

Step 3. Use (A60) to give $ds/d\omega$ and hence $u_s(\omega)$.

Step 4. Find the b_n coefficients from (A75) by Fourier analysis of
$u_s(\omega)$ according to section b above. For this step a small Fast
Fourier transform subroutine tailored for ordinary engineering usage
in Fortran IV was used. (In a modern computer context this has to be
recognized as one of the big advantages of Fourier methods in
general).

Step 5. From the b_n coefficients calculate the a_n coefficients and
hence the B_n coefficients which in turn define the new velocity
and associated profile.

Limits on convergence were defined by testing the RMS changes in y_j, x_j and
Q_j. Experience has shown that usually velocity is the more sensitive param-
eter and that it is very important not to impose a too stringent requirement
on accuracy. In fact, a limit of 0.001 is quite sufficient for most engineer-
ing purposes and is usually safe. The importance of adequate caution for itera-
tive procedures of this kind derives from the fact that such schemes very often
contain numerical steps of a very commonplace nature (e.g., interpolations, quad-
ratures, ...) which are in fact much less accurate than the overall theory or
truncation thereof; but which frequently get overlooked. This remark does not,
of course, apply to the Fast Fourier Transform routine used here which returns
11 significant digits. However, this particular theory does have a nonlinear
dependence on the B_n coefficients, no scaling on the higher-order contributions
(where the coefficients of the Legendre and Chebyshev polynomials become large)
and a very early truncation. These are reasons enough for not overdoing the
convergence criterion.

A12. RESULTS OF INVERSE CALCULATIONS

(a) As an obvious first check the inverse mode was run on all the direct
cases described before (section A10). Convergence was remarkably good again
with only 10 terms, and most of the results could not be distinguished from
the input on any reasonably plottable scales. Body 3 was the only one with
sufficient character to be interesting and it was the first one to be run
with direct comparison with the method of Bristow [A9]. Hence it is the only
one worth more discussion here.

In fact, Fig. 5 shows the original exact body and exact velocity (higher-
order Neumann) used for input to the design process. It also shows the results
of 13 cycles of the current thoery compared with 20 cycles of Bristow's method.
From this figure it appears that after 20 cycles the Bristow method still has
a long way to go and that quite small deviations in velocity near the nose are
associated with quite large errors in overall thickness.

On the other hand, the method advocated here is very good after only 13
cycles (with no under-relaxation factor, see section b below). Furthermore,
it is quicker since the CPU times were approximately in the ratio 1:10.

(b) Another case of design operation is shown in Fig.A6. It is particularly
interesting in that it represents a more typical situation in which the designer
inputs the very crude straight line distribution (Fig. A6) knowing full well
that it is impossible in detail, but that it represents the kind of levels and
gradients he requires. This figure shows that after 7 cycles of the current
theory and 20 cycles of Bristow's the desired input is very nearly being
achieved. However, it is clear that the two body shapes do differ near the
trailing edge. This is a reflection of the same situation as encountered in
section a above — namely that the Bristow method approaches more slowly to
the limit, a fact that is made apparent on Fig. A6 by noting the closeness of
the agreement between the higher-order Neuamnn answers for the 7 cycle body and
the 7-cycle velocities. Once again the CPU times were approximately in the
ratio 1:10.

Some details about this run are worth noting. Firstly, it should not be thought that such a close match to the desired input is possible in general. The case shown is one which was known to be close to a "real" velocity distribution by experimentation. Had the desired initial rise and trailing edge values been associated with a level of say 1.2 instead of 1.05, then the design theory would have shown how far from possible such a request was. It would also have returned some "closest" match, leaving it up to the designer to use this information to introduce a compromise. Secondly, the remarkably good convergence shown for the current theory may not always be achieved in practice. Fig. A7 shows the behavior of the B_1 coefficient and RMS y error as functions of cycle number with and without an under-relaxation parameter of 1/2 whose need was rather obviously indicated. There are some intuitive grounds for regarding an "average" as a good choice; but, of course, there is no mathematical ground for assuming that this value is optimum in any rigorous sense. Obviously more experience with the method is desirable. Thirdly, it should be noted that by ordinary engineering (fluid mechanic) standards, these straight line inputs are excessively crude having discontinuities in slope and other features quite uncharacteristic of analytic functions. It is therefore a very convincing argument in favor of mapping and Fourier analysis methods that they can treat such unfavorable distributions smoothly and accurately.

A13. CONCLUSIONS

A theory for the general solution of axisymmetric incompressible potential flow in terms of analytic functions of elementary type has been presented. For the cases usually of importance to engineering (blunt and cusp trailing edges) comparison with existing numerical methods has shown that with only 10 terms excellent results can be obtained for negligible expenditure of computer time on bodies with more character than usually encountered. When used in the design (inverse) mode the method is apparently quite satisfactory being both quicker and more accurate than the iterative-Neuamnn algorithm of Bristow which is (as far as is known) the only alternative nonlinear design process for axisymmetric flow.

Clearly more work needs to be done to explore the full range of this method, and, maybe it would be worthwhile studying the solutions for arbitrary $(0 \leq \tau \leq \pi)$ trailing edge angles. The results so far are certainly encouraging.

APPENDIX A. REFERENCES

A1. VonKarman, T.: Calculation of Pressure Distribution on Airship Hulls. NACA T.M.574, 1930 (from Abhandlungen aus dem Aerodynamischen Institut an der Technischen Hochschule Aachen, No. 6, 1927).

A2. Hess, J.L. and Martin, R.P.: Improved Solution for Potential Flow about Arbitrary Axisymmetric Bodies by the Use of a Higher Order Surface Source Method. Part I. Theory and Results. NASA CR 134694, McDonnell Douglas Report No. MDC J6627-01, July 1974.

A3. Kaplan, C.: On a New Method for Calculating the Potential Flow Past a Body of Revolution. NACA Report No. 752, 1943.

A4. James, R.M.: A General Class of Exact Airfoil Solutions. J. of Aircraft, Vol. 9, No. 8, Aug. 1972.

A5. Anon: Studies on the Problem of Development of Bodies of Revolution Having Minimum Resistance at High Reynolds Numbers. McDonnell Douglas Tech. Proposal 73D-473T, Nov. 1973.

A6. Woods, L.C.: The Theory of Subsonic Plane Flow. Cambridge Aeronautical Series, III, C.U.P., 1961.

A7. Milne-Thomson, L.M.: Theoretical Hydrodynamics. 2nd Edition, MacMillan, N.Y., 1950.

A8. Smith, A.M.O.: High-Lift Aerodynamics. 37-th Wright Brothers Memorial Lecture, AIAA Paper No. 74-939, August 1974.

A9. Bristow, D.R.: A Solution to the Inverse Problem for Incompressible Axisymmetric Potential Flow. AIAA Paper 74-520, June 1974.

HIGHER ORDER NEUMANN

●●●●● ANALYTICAL (10 TERMS)

VELOCITIES

SHAPE

Qs

1.5

1.0

0.5

0

y

1.0

0.5

0

x

0

-0.5

-1.0

-1.5

-2.0

-2.5

-3.0
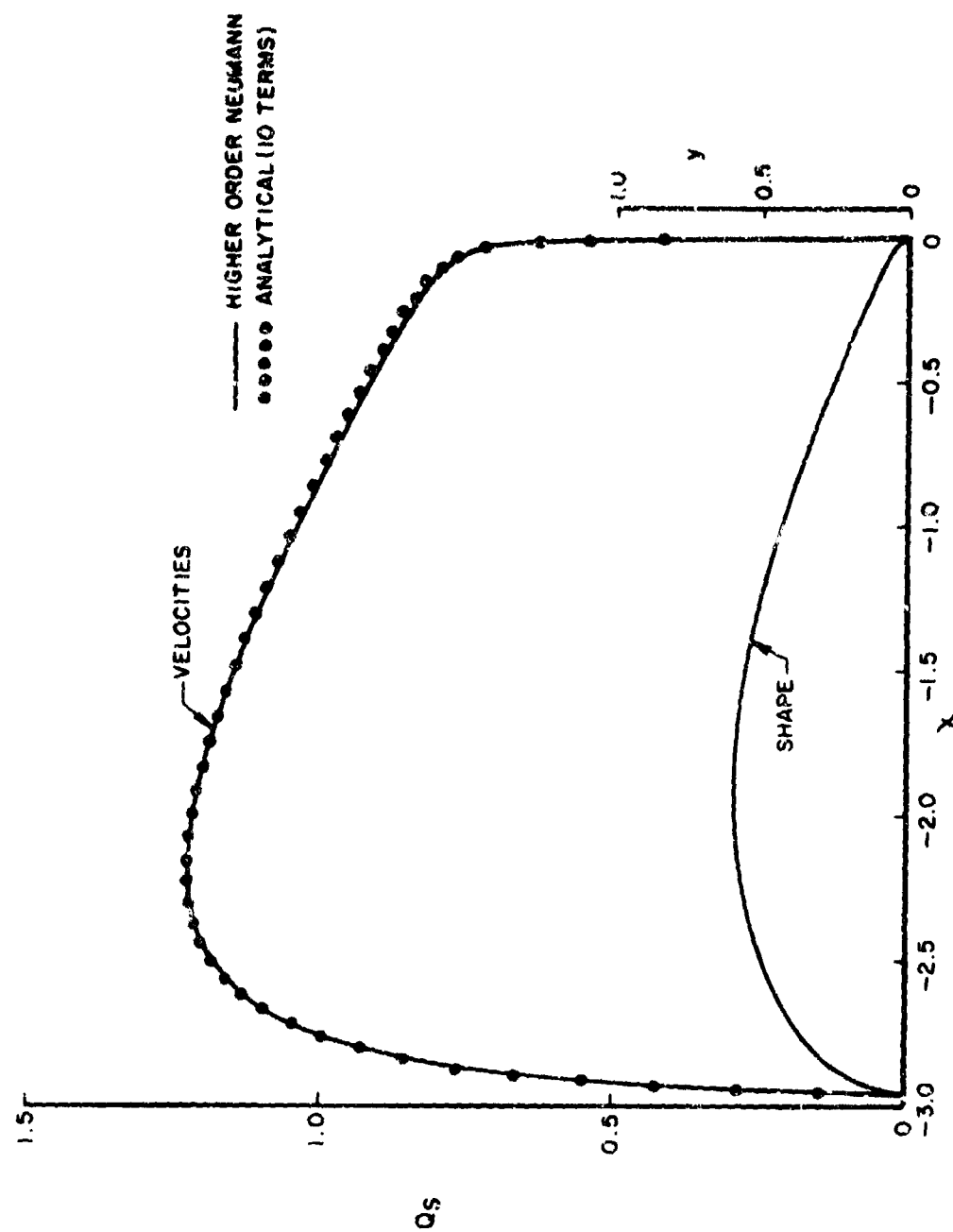
Figure A1. A bland blunt two-pole body (Body 1) showing the velocity distribution for 10 terms vs x compared with the higher order Neumann method.

84
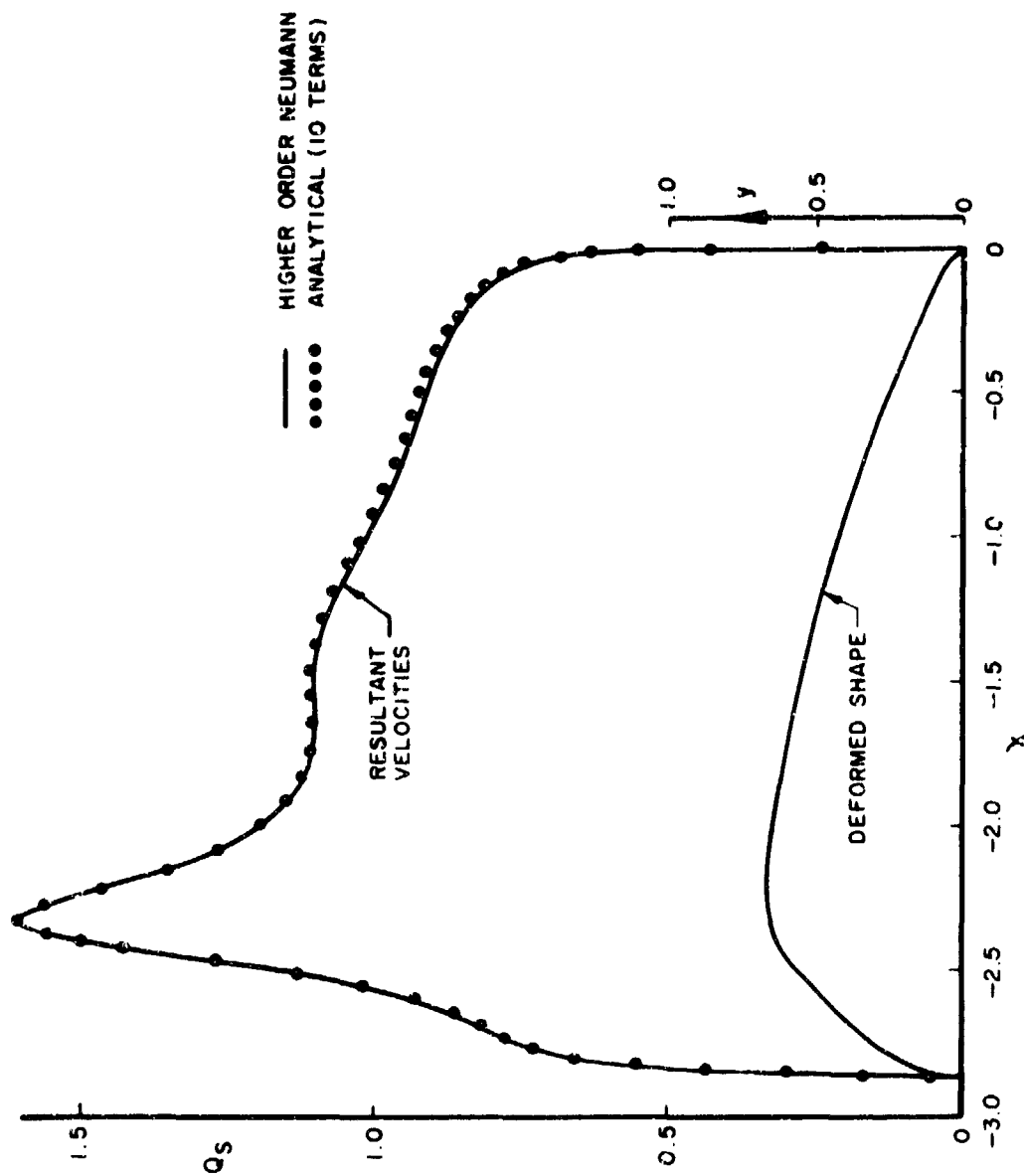
Figure A2. A deformed version (Body 2) of Body 1 showing how the velocity distribution for only 10 terms faithfully reproduces the sharp peak caused by the lump deformation.

85
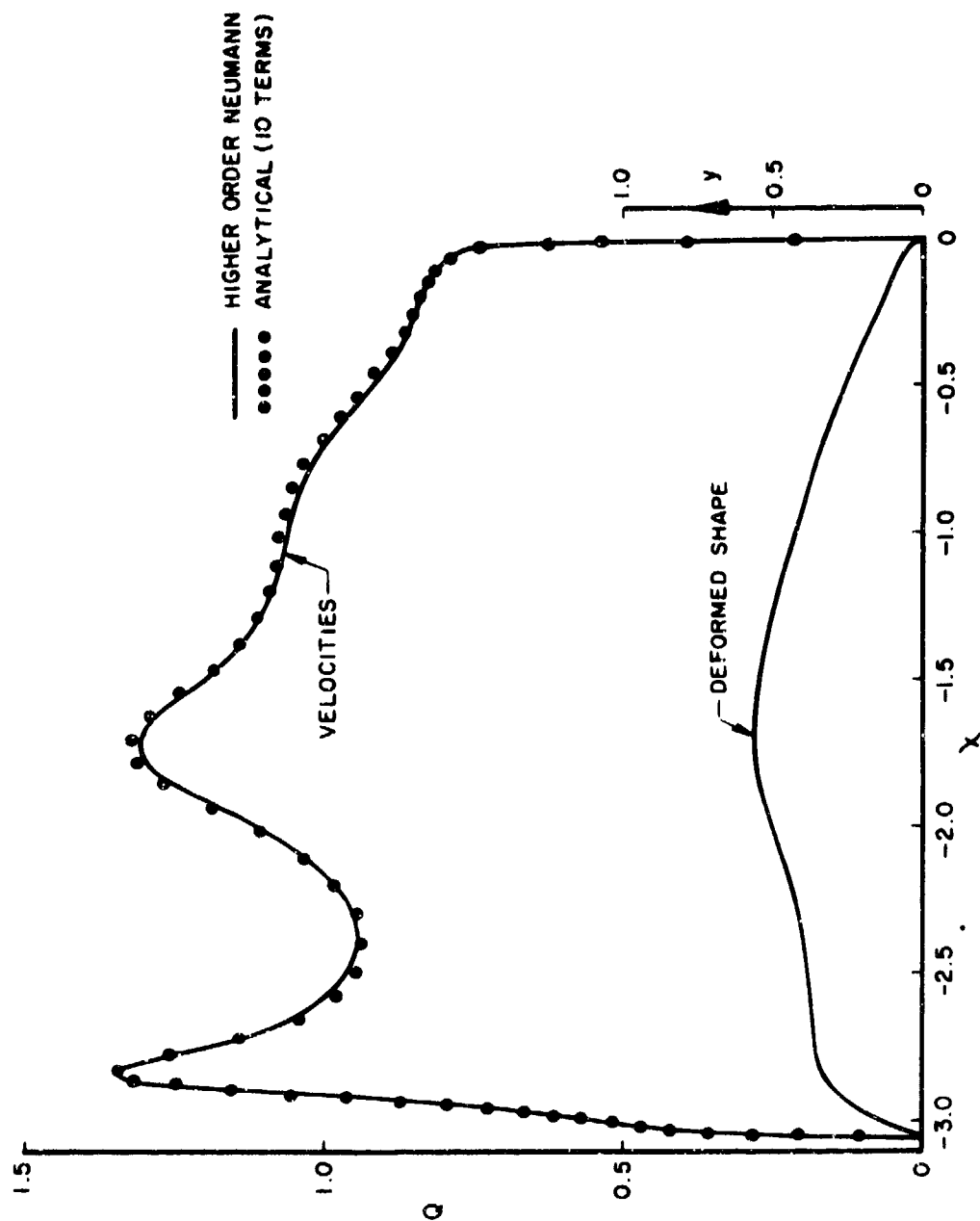
Figure A3. A more extreme deformation of the basic shape showing how the complicated velocity distribution is again well matched with only 10 terms when compared with the higher order Neumann method.
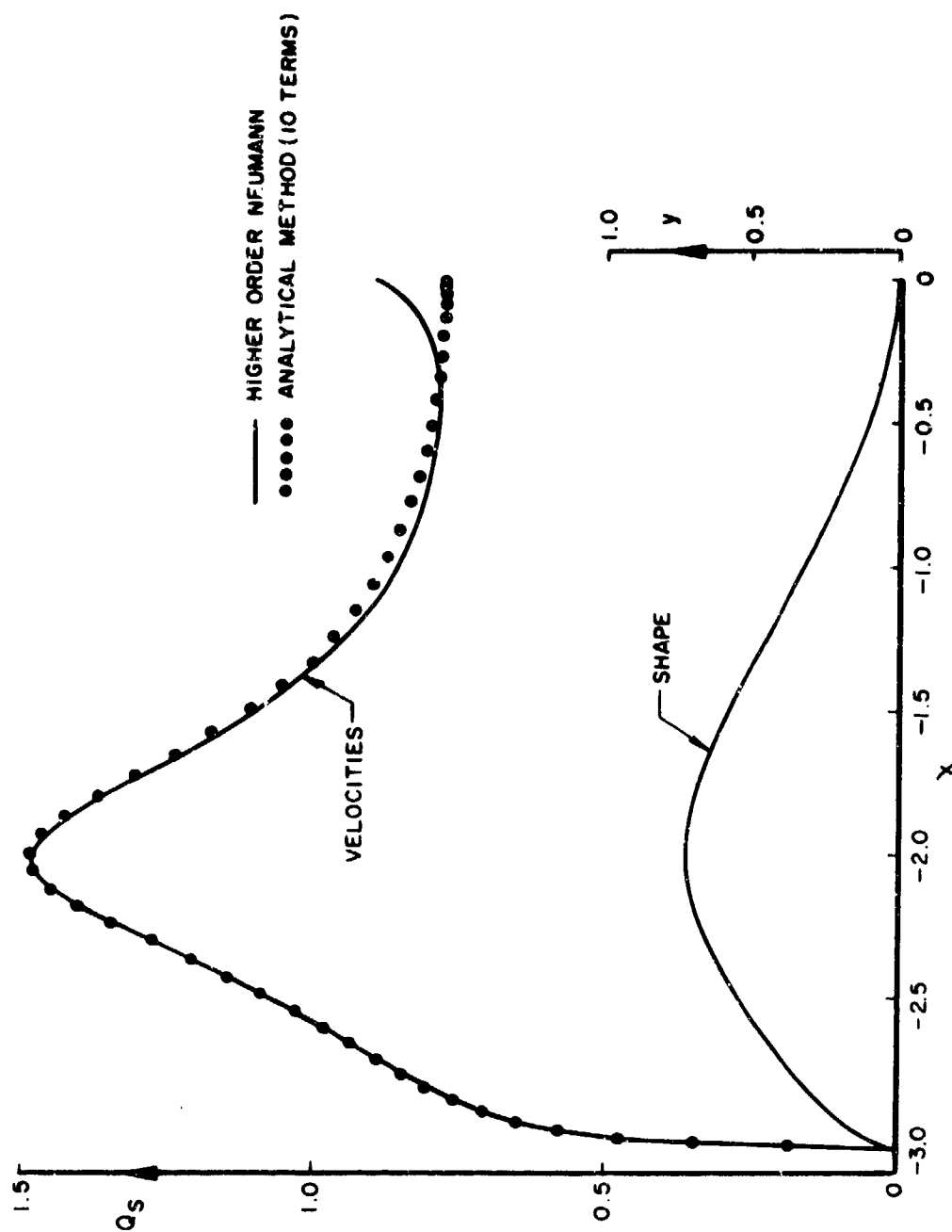
Figure A4. A body generated by a terminating B-sequence with a cusp trailing edge showing the analytical solution (10 terms) compared with the higher order Neumann method.

87
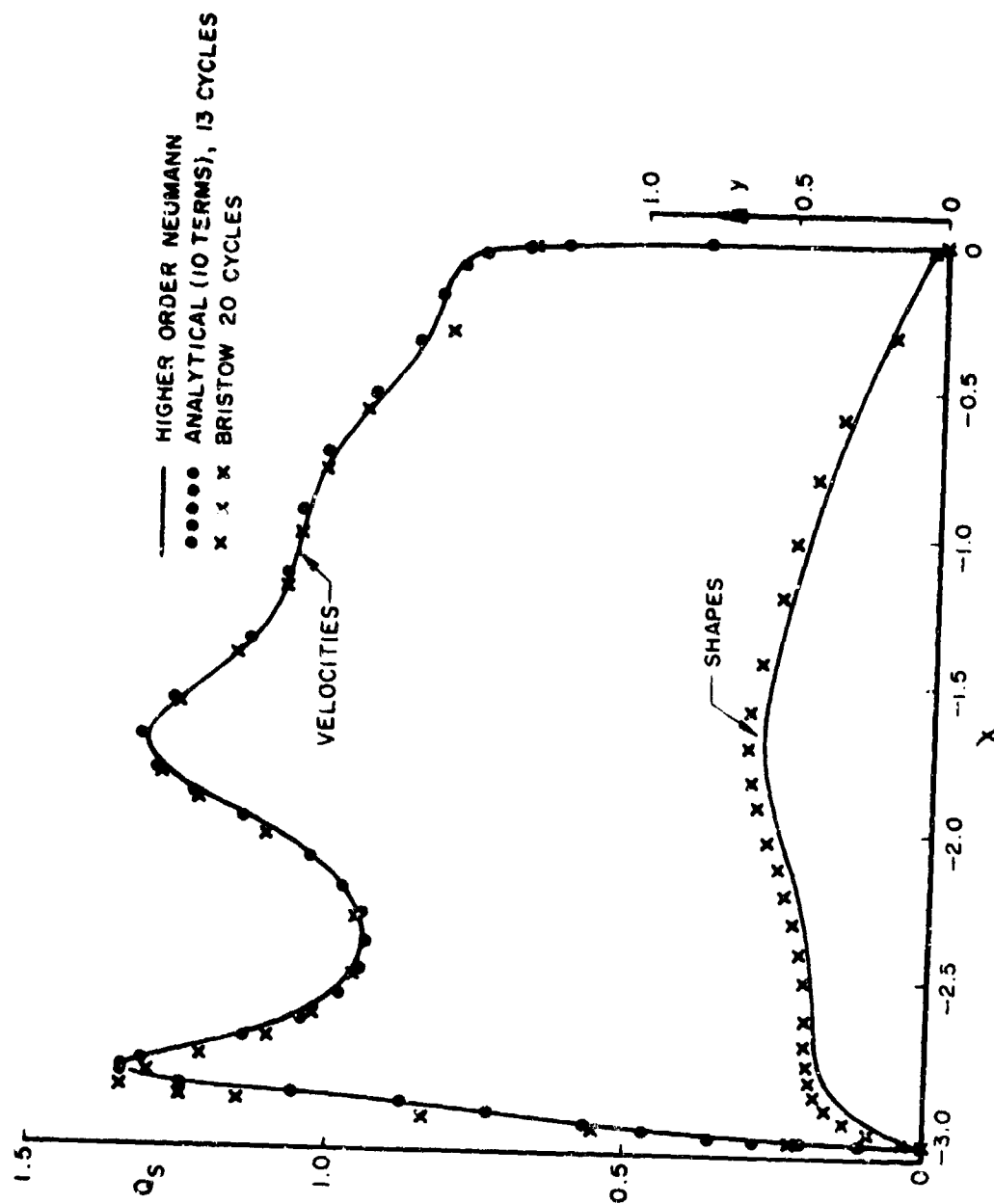
Figure A5. Inverse solution procedure applied to Body 3 (Fig. A3) showing the present method (13 cycles) and Bristow's method (20 cycles) compared with the higher order Neumann results.

88
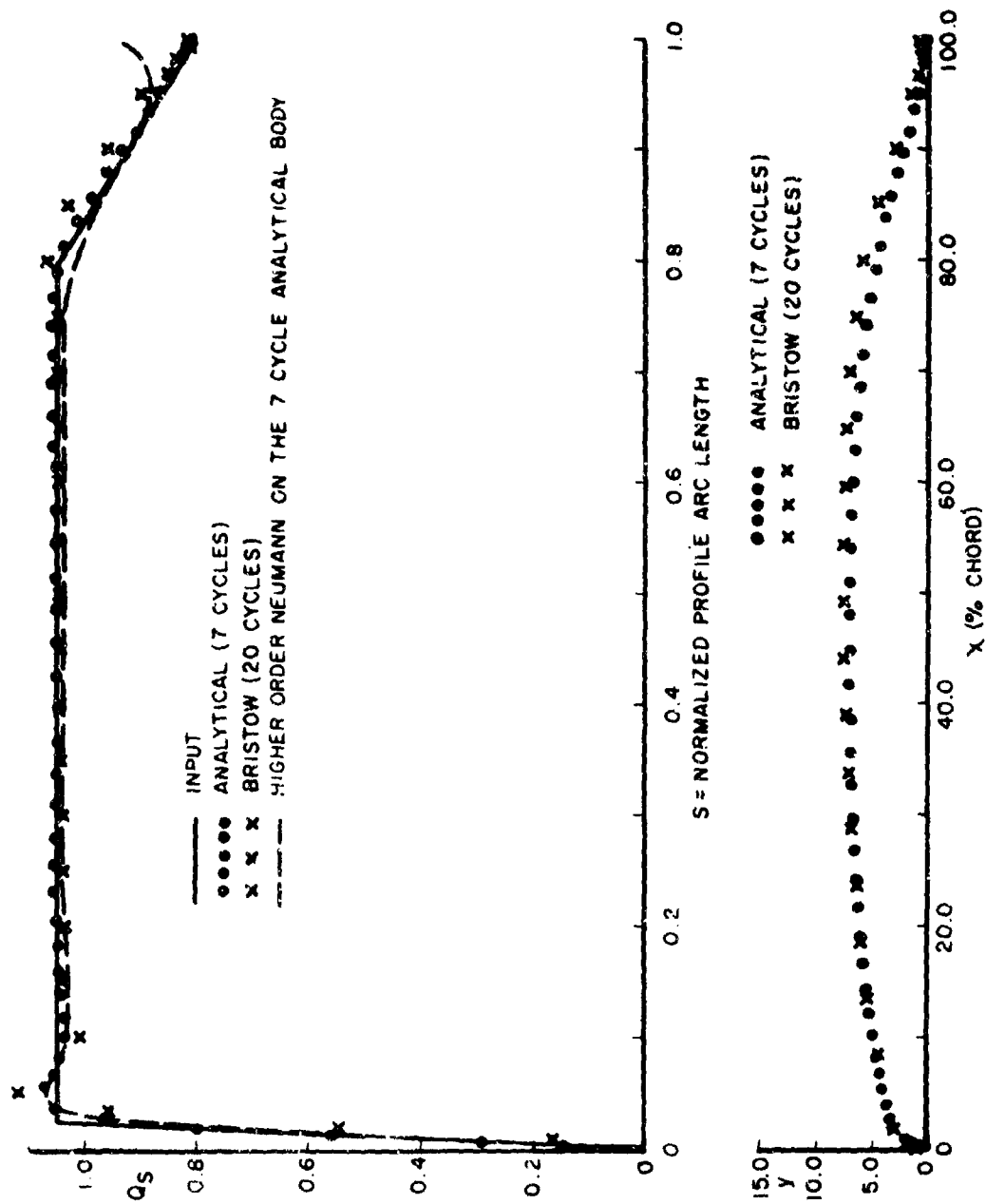
Figure A6. Input velocity (linear segments) and results from the analytic method (7 cycles) and Bristow (20 cycles).
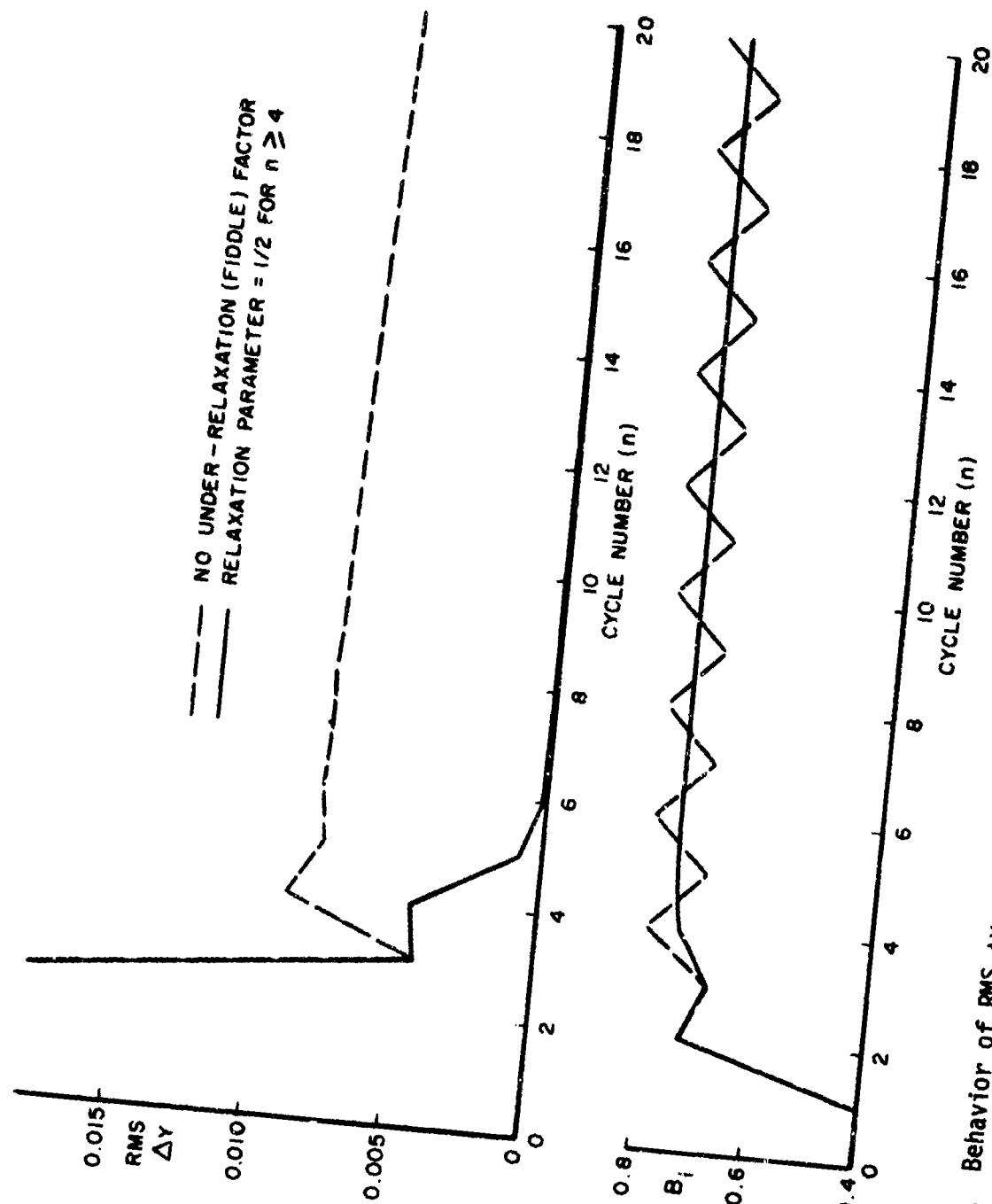
Figure A7. Behavior of RMS Δy error and B_1 coefficient as functions of cycle number with and without an under relaxation parameter of 1/2 applied to the case of Fig. A6.

90

APPENDIX B

A NUMERICAL STUDY OF SOME OPTIMUM DRAG CONFIGURATIONS IN TWO DIMENSIONS

B1. INTRODUCTION

As a contribution to the overall investigation of minimum drag bodies of revolution, certain two-dimensional studies were undertaken. The main purpose of these was to gain insight into the possibilities inherent in the mapping approach to profile definition which, it was felt, might yield a sufficient injection of analyticity into the whole problem for a genuine variational analysis to become possible. As a technique for separating geometrical and flow aspects, conformal mapping is of great importance in two dimensions, and its value in axisymmetric flow as a simplifying mechanism can be judged by Appendix A where an analytic method for flow analysis or design of bodies of revolution is developed ab initio by using unit circle mapping. At very least this kind of mapping constrains the allowable form of velocity in such a way as to focus attention on relatively few parameters characterizing "mode functions" of the correct type.

Although it would seem that this is a necessary prerequisite for introduction of calculus of variations, it was found that in the time available, no concrete variational approach could be formulated for the axisymmetric case. However, the two-dimensional pilot studies did, indeed, lead to a number of interesting results and advances in understanding which can be summarized as follows:

a. A two-dimensional complete variational formulation does appear to be possible. However, development of the underlying mathematical techniques is insufficient for such a problem to be solved at the present time. Variational methods using complex variable function theory appear to be both much more subtle than the conventional real variable methods and totally unexplored. We shall not, therefore, discuss this subject further here.

b. It is possible to reduce both the axisymmetric and two-dimensional problems to minimization problems involving a definite sequence of parameters to be chosen such as to minimize certain combinations of integrals.

c. A very simple computer program was written to find solutions of such
    minimization problems, and the two-dimensional applications of this
    program under various restricted circumstances led to some interesting
    results — not the least of which was the inherent feasibility of this
    approach for the unique definition of the minimum drag shape given
    enclosed area or volume.

The work described in (b) and (c) was not completed owing to insufficient time,
but the feasibility is adequately illustrated by the results described below.

B2. TWO DIMENSIONAL DRAG INTEGRAL

According to Thwaites[B1] as interpreted by A.M.O. Smith, the drag of a
two-dimensional symmetric shape in wholly turbulent flow can be expressed by
Spence's integral as

$$C_{D_c} = \frac{Drag}{(1/2)\rho U_\infty^2 c} = 2\left[0.02429R^{-1/5} \int_0^{p/c} Q^4 d\left(\frac{s}{c}\right)\right]^{5/6} \tag{B1}$$

where p is the half perimeter, c the chord and Q the surface velocity
divided by U_∞ expressed as a function of arc length s. In this formula the
Reynolds number R is based on chord so

$$R = U_\infty c/\nu \tag{B2}$$

where U_∞, ν have their usual significance. (B1) can also be written

$$C_{D_c} = 2(0.0452R^{-1/6})\left[\frac{1}{c}\int_0^p Q^4 ds\right]^{5/6} \tag{B3}$$

where the expression in ( ) is the Blasius formula for a flat plate and the non-
dimensional group in [ ] is a convenient parameter worth a name, viz.

$$I_D = \frac{1}{c}\int_0^c Q^4 ds \tag{B4}$$

92

In making comparative geometric studies it is clear that both the chord and free-stream velocity should be kept constant, but(B3) alone is not very useful as it stands, since $I_D \geq 1$ so that minimization of C_{D_C} will always yield the flat plate solution. Alternatives which could conceivably be useful from a practical engineering standpoint would keep (say) enclosed area, maximum thickness or perimeter constant as well. Some experience with these has shown that the area constraint produces the most desirable type of optima, and the remainder of this study is concerned only with drag optima for constant area, chord and free stream.

As far as the conversion of this to a readily computed form in terms of the mapping theory is concerned, the area factor must be nondimensionalized in order that body size should not be an influence, so a sensible parameter for minimization is

$$C_{D_A} = C_{D_C} \frac{c}{\sqrt{A}} \qquad \text{where} \quad A = \text{total enclosed area}$$

But the quantity most easily computed is the half area integral which can be readily expressed by

$$A = 2 \int_0^c y\,dx$$

and then

$$\frac{A}{2c^2} = \frac{1}{c^2} \int_0^c y\,dx = I_A \qquad \text{(say)} \tag{B5}$$

giving from (B3) and (B4)

$$C_{D_A} = (0.0452R^{-1/6}) \cdot z^{1/2}\, I_D^{5/6}/I_A^{1/2} \tag{B6}$$

Finally for reasons of partial comparisons with other results it was decided that the integrals based on the complete configuration should be used, which would give

93

$$C_{D_A} = (0.0452R^{-1/6})\ 2^{1/6}(2I_D)^{5/6}/(2I_A)^{1/?}$$

with the purely geometric expression

$$F = \frac{(2I_D)^{5/6}}{(2I_A)^{1/2}} = 2^{1/3}\ \frac{I_D^{5/6}}{I_A^{1/2}} \tag{B7}$$

separable as a measure of configuration efficiency. In terms of F then

$$C_{D_A} = (0.0452R^{-1/6})\ 2^{1/6}F \tag{B8}$$

and the work described below is concerned with the minimization of F.

B3. MAPPING FORMAT

In Appendix A a fairly complete description of the mapping format required for transformation of the profile in the z-plane to the unit circle in the ζ-plane is given. Although the basic philosophy concerning constraints on this mapping function is unchanged for the application here, an appreciable generalization is desirable. Thus the work of Appendix A was restricted to circumstances under which it was feasible (possible) to work out complete solutions for general axisymmetric flow, and in fact only blunt noses with either blunt or cusped trailing edges were actually analyzed.

As far as the numerical analysis of the integrals of section B2 are concerned, however, it is sensible to begin by stating the most general case — that for which finite angles τ_1 and τ_2 are permitted at both ends of the body. Under these circumstances the mapping derivative can be written

$$\frac{dz}{d\zeta} = \left(1 - \frac{1}{\zeta}\right)^{\mu_1}\left(1 + \frac{1}{\zeta}\right)^{\mu_2}\left[1 + \frac{a_1}{\zeta} + \frac{a_2}{\zeta^2} + \ldots\right] \tag{B9}$$

where

$$\mu_1 = 1 - \tau_1/\pi, \qquad \mu_2 = 1 - \tau_2/\pi$$

and

$$a_1 = \mu_1 - \mu_2$$

94

in order to ensure closure. In addition it can be shown by symmetry that for profiles representing a body of revolution every a_n coefficient must be real and, of course, the surface behavior of the derivative is obtained by setting $\zeta = e^{i\omega}$ for points on the unit circle. In fact the connection between the mapping derivative on the surface and the arc length is of central importance, and follows from the observation that, if subscript "s" denotes surface value, then

$$\frac{dz_s}{d\omega} = ie^{i\omega} \frac{dz_s}{d\zeta_s} \tag{B10}$$

and so

$$\frac{ds}{d\omega} = \left| \frac{dz_s}{d\zeta_s} \right| , \qquad \theta_s = -\frac{\pi}{2} + \omega + \text{Arg}\left(\frac{dz_s}{d\zeta_s} \right) \tag{B11}$$

where s is the profile arc length measured from the trailing edge, and θ_s is the geometric surface angle (or flow angle).

There are a number of different formulas which can be used for the various integrals arising in section B2 which will be very useful in deriving certain special and exact cases. However, there is very little that can be done with the fundamental integral

$$I_D = \frac{1}{c} \int_0^c Q^4 ds$$

unlike the chord and area. Thus for this integral we note that the surface velocity (in two dimensions only) can be written

$$Q = \frac{2 \sin \omega}{ds/d\omega}$$

so that

$$I_D = \frac{1}{c} \int_0^\pi \frac{2^4 \sin^4 \omega}{(ds/d\omega)^3} d\omega \tag{B12}$$

Putting $\zeta = e^{i\omega}$ in (B9) and (B11) then gives

$$\frac{ds}{d\omega} = \left(2 \sin \frac{\omega}{2} \right)^{\mu_1} \left(2 \cos \frac{\omega}{2} \right)^{\mu_2} \left[(1 + a_1 \cos \omega + a_2 \cos 2\omega + \ldots)^2 + (a_1 \sin \omega + a_2 \sin 2\omega + \ldots)^2 \right]^{1/2} \tag{B13}$$

95

and the best that can be done with I_D is then

$$I_D = \frac{1}{c} \int_0^\pi \frac{(2 \sin \omega/2)^{4-3\mu_1} (2 \cos \omega/2)^{4-3\mu_2} \, d\omega}{[(1 + a_1 \cos \omega + a_2 \cos 2\omega + \ldots)^2 + (a_1 \sin \omega + a_2 \sin 2\omega + \ldots)^2]^{3/2}} \tag{B14}$$

So far no way has been found to avoid direct numerical evaluation of this formula except in certain special cases.

Obviously if the necessary number of coefficients is large and the number of quadrature points must be large for sufficient accuracy, the evaluation of (B14) for the many permutations required to ace the minimum of F could become a very tedious and costly operation. Therefore, there is a strong incentive to find both more accurate (specific) quadrature formulas than (say) Simpson's rule, and methods of evaluation at least for A and c which do not require further quadratures. The topic of special quadrature formulas is considered later (section 9b), but the obvious alternatives for c and A can be derived immediately from (B9) by using the expansion in powers of $1/\zeta$ valid when $|\zeta| \geq 1$.

Thus by truncating each group in (B9) it is a trivial matter to find the triple product coefficients A_n in the formula

$$\frac{dz}{d\zeta} = 1 + \frac{A_2}{\zeta^2} + \frac{A_3}{\zeta^3} + \ldots \tag{B15}$$

by using the polynomial product subroutine mentioned in Appendix A. Then it is easy to prove from (B15) that

$$c = - \int_0^\pi \frac{dx}{d\omega} \, d\omega = 2\left(1 - A_2 - \frac{A_4}{3} - \frac{A_6}{5} - \ldots\right) \tag{B16}$$

and

$$A = 2 \int_0^\pi y \frac{dx}{d\omega} \, d\omega = \pi\left(1 - A_2^2 - \frac{A_3^2}{2} - \frac{A_4^2}{3} - \frac{A_5^2}{4} - \ldots\right) \tag{B17}$$

96

both of which may be useful computational formulas provided the convergence is adequate. As will be seen the convergence is quite often poor, but (B16) and (B17) do have a theoretical interest in certain special cases quite apart from their general computational promise.

The most general case has not been computed fully since it was not realized in the early stages of this study that it would be necessary to incorporate an option providing for finite closure angles at both ends. This feature greatly increases the program complexity through the poor convergence of the zero factors

$$\left(1 - \frac{1}{\zeta}\right)^{\mu_1} \qquad \text{and} \qquad \left(1 + \frac{1}{\zeta}\right)^{\mu_2}$$

and the associated revised general optimization program has not been properly tested, although preliminary results have been obtained. This phase is described further in section B9 where it properly belongs, because most of the subtleties necessary for the general scheme* were learned from the preliminary study of special cases. Therefore, it is both easier and more logical to discuss the special cases first — more or less in the order in which they were developed.

B4. ELLIPSES

A natural starting point for such optimization studies is the ellipse profile because its characterization is so simple in terms of the mapping theory. Furthermore, not only does it appeal to the intuition as a low drag shape, but in fact it was <u>known</u> to have good properties (see e.g., Figure 14 and section 8 in this report).

In the early stages it was thought that perhaps the ellipse could be established analytically as the optimum case with a continuous θ (as opposed to trick "fairings"), on the grounds that the ellipse family is the only blunt ended symmetric class $(\tau_1 = \tau_2 = \pi)$ which also has every a_n coefficient zero except a_2. This conjecture did not turn out to be correct,

*including, of course, the necessity for its introduction at all!

but it was possible to produce analytic expressions for every phase of the ellipse study and so give invaluable guidance for accuracy requirements on the later numerical work.

The essential formulas come from (B9) by first setting $\mu_1 = \mu_2 = 0$ which gives

$$\frac{dz}{d\zeta} = 1 + \frac{a_2}{\zeta^2} + \frac{a_3}{\zeta^3} + \ldots \tag{B18}$$

as the defining formula for all symmetric blunt-ended bodies. Then the ellipse family is defined by further putting $a_3 = a_4 = \ldots = 0$ so

$$\frac{dz}{d\zeta} = 1 + \frac{a_2}{\zeta^2} ; \qquad z = C + \zeta - \frac{a_2}{\zeta} ; \qquad C \text{ real}$$

Choosing $C = 0$ to put the origin at the center and then setting $\zeta = e^{i\omega}$ gives the surface coordinates as

$$x_s = (1 - a_2) \cos \omega, \qquad y_s = (1 + a_2) \sin \omega$$

so that

    a = semi-major axis = $1 - a_2$

    b = semi-minor axis = $1 + a_2$

and the range of a_2 is $-1 \le a_2 \le +1$. Clearly the likely (slender) range of low drag shapes corresponds to $a_2 < 0$ and obvious limiting cases are the streamwise flat plate $(a_2 = -1)$ and the circle $(a_2 = 0)$.

Now the structure of $ds/d\omega$ from (B13) is

$$\frac{ds}{d\omega} = \sqrt{1 + 2a_2 \cos 2\omega + a_2^2} = \sqrt{a^2 \sin^2 \omega + b^2 \cos^2 \omega}$$

from which it is clear that for the range $a_2 < 0$ (or $b < a$) of interest here, integrands involving $ds/d\omega$ can be expressed in terms of complete elliptic integrals by choosing the modulus as

$$k^2 = 1 - b^2/a^2$$

thus giving the complementary modulus k', where

$$k'^2 = 1 - k^2 = b^2/a^2$$

as the fineness ratio. Then the perimeter/chord ratio is

$$p = \frac{1}{c} \int_0^\pi \frac{ds}{d\omega} \, d\omega = E$$

and the fundamental I_D integral can be written

$$I_D = \frac{(1 + k')^4}{k^4} [(2 - k^2)E - 2k'^2K]$$

where E and K are the standard complete elliptic integrals. Since, in addition,

$$I_A = \frac{\pi}{8} k'$$

these results can be used to calculate the behavior of the comparison factor F of (B7) with great precision as a function of the fineness ratio $k' = b/a$.

The limiting values behave as expected. Firstly, as $k' \to 0$ ($k \to 1$), $I_A \to 0$ but K behaves as $\ln 4/k'$. The limiting value of the last term is nonetheless zero since it is multiplied by k'^2. Furthermore $E(1) = 1$ so the limiting value of I_D is 1 as it should be according to the definition (B3) since $k' = 0$ is the flat plate case.

As $k' \to 1$ the profile tends to circularity and $I_A \to \pi/8$ as it should according to (B5). Some care is needed with I_D as $k \to 0$ owing to the k^{-4} factor, but it turns out that

$$(2 - k^2)E - 2k'^2K \sim \frac{3\pi}{16} k^4 + O(k^6)$$

99

giving the limiting value

$$I_D(0) = 3\pi$$

which implies that a circular cylinder in turbulent flow has a drag coefficient $(3\pi)^{5/6}$ x flat plate of the same chord — provided, of course, that separation is ignored

In any event Fig.B1 shows the ellipse curve as a function of fineness ratio (f) with the clearly defined minimum at about $f = k' = 0.22$. Anticipating somewhat, it can be seen that this curve has very nearly the lowest minimum of all those on Fig. B1.

B5. SOME CUSPED AIRFOILS

No study like this is complete without the Joukowski airfoil. This shape also offers some hope of complete analytic evaluation, but there are others of even simpler form. These are all of intrinsic interest because the cusped trailing edge removes the possible objection that any wholly blunt shape deduced as an optimum by this integral formulation would always be liable to poor practical performance due to separation.

The Joukowski profile is a member of the more general class known as pole airfoils which are mentioned in Appendix A and discussed in more detail in [B2]. The single pole airfoil is, strictly speaking, the simplest member of this class and so will be considered first.

(a)   A single pole airfoil is characterized by $\tau_1 = 0$, $\tau_2 = \pi$ and

$$\frac{dz}{d\zeta} = \left(1 - \frac{1}{\zeta}\right)\left(1 + \frac{1}{\zeta - d}\right) , \qquad |d| \leq 1 \tag{B19}$$

d being real for the symmetric case. The second factor can be expanded to give the a_n coefficients as

$$a_n = d^{n-1}$$

100

but again (as a check case) a more direct evaluation was used for I_D, only the area being computed from the series. Thus, instead of expanding (B19) the modulus of $1 + 1(\zeta - d)$ can be calculated on the surface and used in (B11) to give

$$\frac{ds}{d\omega} = 2 \sin \frac{\omega}{2} \left[\frac{d^2 + 4(1 - d) \cos^2 \omega/2}{(1 + d)^2 - 4d \cos^2 \omega/2} \right]$$

so that substituting in (B12) and using the transformation $\xi = \cos \omega/2$ yields

$$I_D = \frac{64}{c} \int_0^1 \left[\frac{(1 + d)^2 - 4d\xi^2}{d^2 + 4(1 - d)\xi^2} \right]^{3/2} \xi^4 d\xi$$

Since the chord is given by

$$c = 2 + \frac{1 - d}{d} \ln \left(\frac{1 + d}{1 - d} \right)$$

and the thickness by

$$t = 2y_{max} = \sqrt{(3 - d)(1 + d)} - 2 \left(\frac{1 - d}{d} \right) \sin^{-1} \left(\frac{d\sqrt{3 - d}}{2} \right)$$

computation was straightforward, but I_D was evaluated by using a 101 point Simpson routine on looking at the above formula. The results are shown on Fig. B1 and clearly exhibit a minimum at about $f = 0.2$. Somewhat disappointingly the drag is evidently much greater than for the ellipse.

(b) In the pole format a Joukowski profile takes the form

$$\frac{dz}{d\zeta} = \left(1 - \frac{1}{\zeta} \right) \left[1 + \frac{1}{\zeta - d} + \frac{d(1 - d)}{(\zeta - d)^2} \right]; \quad (0 \leq d \leq 1)$$

again with d real. Following the same steps as for the single pole case leads to

$$I_D = \frac{64}{c} \int_0^1 \frac{[(1 + d)^2 - 4d\xi^2]^3 \xi^4 d\xi}{[4d^2 - 4(2d - 1)\xi^2]^{3/2}} \tag{B20}$$

with

$$c = \frac{4}{1 + d}$$

$$t = \frac{2d \sin \omega_0 (1 - \cos \omega_0)}{1 - 2d \cos \omega_0 + d^2} \quad ; \quad \cos \omega_0 = \frac{(1 - d + d^2) - \sqrt{1 - d^2 + d^4}}{2d}$$

Again (B20) was evaluated by a 101 point Simpson quadrature, but this time an exact integration was possible and was carried out. It served to show that the results obtained by the numerical procedure were quite adequate. The results are given on Fig. Bl and exhibit a very similar behavior to the single pole case with a somewhat higher drag.

(c) The final experiment in cusped trailing edges was a single parameter airfoil which is, in a sense, the cusped analog of the ellipse since it is defined by all $a_n = 0$ except a_2 so that

$$\frac{dz}{d\zeta} = \left(1 - \frac{1}{\zeta}\right)\left(1 + \frac{1}{\zeta} + \frac{a_2}{\zeta^2}\right), \quad a_2 \quad \text{real} \tag{B21}$$

On the basis of the kind of argument advanced intuitively for the ellipse, namely that it should be some kind of optimum since all the higher order modulations due to a_n are absent, it might be expected that (B21) would be superior to both the Joukowski and single pole profiles since they both have an infinite sequence of a_n coefficients.

However, some doubt can be cast on this idea immediately because the modulating $g(\zeta)$ factor in (B21) is

$$g(\zeta) = \frac{\zeta^2 + \zeta + a_2}{\zeta^2} = \frac{(\zeta - \zeta_1)(\zeta - \zeta_2)}{\zeta^2}$$

where

$$\zeta_1, \zeta_2 = -\frac{1}{2} \pm \sqrt{\frac{1}{4} - a_2}$$

If $a_2 \leq 1/4$ both zeros are real and since no zero can lie outside the unit circle the overall permissible range of a_2 is $0 \leq a_2 \leq 1$. When the roots

102

become complex the profile starts to bulge and unlike all the previous cases the limiting form at $a_2 = 1$ has two symmetrically disposed cusps just downstream of the leading edge! Consequently, it is clear that (even without separation) this shape will have very poor drag characteristics for a_2 appreciably greater than $1/4$.

Forwarned by this argument the numerical result comes as no surprise. Using

$$c = 4\left(1 - \frac{1}{2} a_2\right)$$

$$t = \frac{3\sqrt{3}}{2} a_2$$

and the original form of I_D (i.e., (B14)) with a Simpson quadrature gives the curve shown on Fig. B1. Evidently the characteristics are much worse than the previous cusped cases, which serves to show very clearly the naiveté of the conjectures made before about optima coming from having as many a_n coefficients as possible vanish. Further very surprising evidence concerning this situation is provided by the next section.

B6. INITIAL OPTIMIZATION FOR BLUNT BODIES

The evidence of section B5 lent weight to the idea that the really good shapes would have fore and aft symmetry. Furthermore, there was at least a suspicion that the cusp was an undesirable feature quite apart from its unsymmetrical role in the airfoils studied. Therefore, it was natural to consider the problem of minimizing F only for blunt ended shapes. Under these circumstances $\tau_1 = \pi$, $\tau_2 = \pi$ so that $\mu_1 = 0$, $\mu_2 = 0$ and the fundamental formulas become simplified mainly because then

$$A_n = a_n$$

so that (B16) and (B17) could be used directly without undue fears about convergence. In fact (B7), (B8), (B14), (B16) and (B17) show that F is a function only of the a_n numbers for blunt ended shapes, and a definite cut-off for the a_n sequence consistent with some optimistic belief about convergence is obviously a necessity for any numerical work.

103

On this basis a computer program was written to effect the minimization, and it can be described very simply as follows:

(a) It was decided that rather than try sophisticated gradient, steepest descent, etc. methods, a very simple "boxing" procedure to progressively narrow in on the minimum of $F(a_1, a_2, \ldots a_n)$ would be adequate, mainly because of the conviction that it only needed to be done once in order to isolate the optimum. This very simple program works by the following steps which depend only on a subroutine to evaluate F given a set of a_n values.

Step 1. Input an initial guess for the a_n values and a starting step size h.

Step 2. Increase a_1 to $a_1 + h$. If F has decreased, move on to a_2. If F has increased, try $a_1 - h$. If this also gives an increase, leave a_1 alone and move on to a_2. Continue this process to a_n.

Step 3. After one pass as in step 2, repeat the cycle to see if the changed values of a_2, a_3, $\ldots$ have changed the decision regarding a_1. Continue this checking until a _complete_ pass does not change F.

Step 4. Decrease h by a factor of 10 and start again at step 2.

Step 5. When h has been reduced to desired accuracy, stop.

It can be seen that each completed cycle (end of step 3) means that to within the current value of h, it is not possible for the program to detect a further decrease in F, which implies that the local minimum is contained within a hypercube (box) of volume h^n. The division of h by 10 each time is a particularly convenient mode of operation since then each completed cycle defines another decimal place.

Various runs were tried to test this program using special test functions of several variables and the direct results already reported for F depending on only one variable. It was very soon appreciated that high accuracy for the quadratures was necessary if a large number of terms were to be isolated,

104

since the whole process hinges on the detection of a <u>genuine</u> change of F due to a change of a_n as opposed to variations caused by numerical error. This topic will be discussed later (Section B9); it is sufficient to record here that 50 - 101 quadrature points were adequate for 20 - 30 a_n coefficients with h as small as 0.00001. For this particular version of the program further description is not necessary because of the results that it led to immediately.

Of course, in the case of the ellipse it was not necessary to worry about accuracy of quadrature formulas since all the necessary calculations were exact. Under these circumstances it was a trivial exercise to determine the optimum ellipse by the minimization program and the result when cycled down to $h = 0.0000001$ was

$$a_2 = -0.6375691, \quad f = t/c = 0.2213225, \quad F = 7.7122530$$

This is shown on Fig. B2 compared with some other "good" profiles.

(b) The first two serious attempts to find general optima were with 10 and 20 a_n coefficients. Since the result obtained with the 20 term case was a repeat of the 10 term with greater accuracy, we shall not discuss the 10 term at all. In fact, both runs were first carried out without the 5/6 power on I_D, but this only changes the details not the nature of the answers.

First it was observed that as h was decreased through each cycle all the odd coefficients decreased rapidly which implies very clearly that fore and aft symmetry is a necessary requirement. After 5 cycles ($h = 0.00001$) the following even coefficients were obtained:

$$a_2 = -0.71513$$
$$a_4 = -0.09447$$
$$a_6 = -0.04134$$
$$a_8 = -0.02384$$
$$a_{10} = -0.01567$$
$$a_{12} = -0.01111$$
$$a_{14} = -0.00825$$
$$a_{16} = -0.00628$$
$$a_{18} = -0.00480$$
$$a_{20} = -0.00349$$

It was noted that this body did have a slightly lower F than the best ellipse by about 0.15%, but by far the most striking feature of the coefficients was their poor convergence. On plotting the shape it was noted that the "bluntness" was confined to an exceedingly local region near the ends, with the overall aspect having every appearance of a finite angle wedge ended body. By a very crude protractor estimate, a τ_1 value of about 50° was obtained from the plot leading to $\tau_1/\pi \sim 0.28$ or $\mu_1 = \mu_2 \sim 0.72$. In view of the leading coefficient in the above table, the obvious requirement for fore and aft symmetry and the poor convergence, it was only natural to compare the table values with the expansion of

$$\left(1 - \frac{1}{\zeta^2}\right)^\mu = 1 - \frac{\mu}{\zeta^2} - \frac{\mu(1 - \mu)}{2!} \ \frac{1}{\zeta^4} - \dots$$

for $\mu = 0.72$. The values of these coefficients are

$$a_2 = -0.72$$
$$a_4 = -0.1008$$
$$a_6 = -0.0430$$
$$a_8 = -0.0245$$
$$a_{10} = -0.0161$$
$$a_{12} = -0.0115$$
$$a_{14} = -0.0087$$
$$a_{16} = -0.0068$$
$$a_{18} = -0.0055$$
$$a_{20} = -0.0045$$
$$\cdot \ \cdot \ \cdot$$

On comparing the two sets of values and remembering that the "minimization" sequence was truncated and that the estimate for τ was very crude, it was hardly possible to avoid the inference that the minimization procedure was leading to a limiting form of solution described by

$$\frac{dz}{d\zeta} = \left(1 - \frac{1}{\zeta^2}\right)^\mu , \qquad \mu \sim 0.72$$

Inasmuch as such bodies would have finite trailing edge angles and characteristic rates of convergence as shown above, this discovery was singularly unwelcome as well as surprising. It meant, at least, that much more serious

106

thought would have to be given to the structure of subroutines designed to
evaluate F for use in the minimization program. However, this is once again
best discussed in Section B9, since it is a topic relevant to the most general
program and the important details can, in any case, be best appreciated by
examining the simpler special solutions with finite closure angles first.

B7. CANONICAL WEDGE END PROFILE

If the ellipse can be considered as the canonical blunt end shape on the
grounds that it has only one a_n coefficient, then the class suggested in
Section B6 as the tentative limit of the minimization procedure, namely

$$\frac{dz}{d\zeta} = \left(1 - \frac{1}{\zeta^2}\right)^\mu, \qquad 0 \le \mu \le 1 \tag{B22}$$

can certainly be regarded as the canonical wedge end profile since it has none.
Once again the temptation exists to jump to the conclusion that because there
are no a_n coefficients this profile must be the optimum; but having been
wrong twice before (section B4 and B5c) it is possible to defer judgment on
this issue.

The consequences of (B22) are quite interesting. Since all the a_n
coefficients are zero the expansion of (B22) gives the A_n coefficients
immediately as

$$A_n = \frac{\mu(1 - \mu) \cdots (n - 1 - \mu)}{n!}$$

so that

$$\left| \frac{A_{n+1}}{A_n} \right| = \frac{n - \mu}{n + 1} \sim 1 - \frac{\mu + 1}{n} + 0\left(\frac{1}{n^2}\right)$$

and therefore the expansion is uniformly convergent [B3] when $|\zeta| \ge 1$ if

$$\mu > 0 \quad \text{or} \quad n > \tau$$

which covers all cases of interest here. Hence (B16) and (B17) are apparently
trivial calculations to give area and chord. Furthermore, from (B10) and (B11)

$$\frac{ds}{d\omega} = (2 \sin \omega)^{\mu}; \qquad \theta_s = -\frac{\tau}{\pi}\left(\frac{\pi}{2} - \omega\right)$$

and so

$$Q_s = (2 \sin \omega)^{\tau/\pi}$$

which are all unusually simple.

However, the most important feature is that the drag integral also turns out to be an analytic result. This can be seen from the combination of the above results because

$$I = \int_0^{\pi} Q^4 \frac{ds}{d\omega} d\omega = \int_0^{\pi} (2 \sin \omega)^{3\epsilon+1} d\omega$$

where we have used ϵ for τ/π as a convenience so

$$\mu = 1 - \epsilon$$

Using $\phi = \pi/2 - \omega$ this can be written as

$$I = -2^{3\epsilon+1} \int_{-\pi/2}^{\pi/2} (\cos \phi)^{3\epsilon+1} d\phi$$

and then by using the expansion* $(-\pi/2 \leq \phi \leq \pi/2)$

$$\cos^{\nu}\phi = \frac{1}{2^{\nu-1}} \frac{\Gamma(\nu + 1)}{\Gamma[(1/2)\nu + 1]^2} \left[\frac{1}{2} + \frac{\nu}{\nu + 2} \cos 2\phi + \frac{\nu(\nu - 2)}{(\nu + 2)(\nu + 4)} \cos 4\phi + \ldots\right]$$

it follows that

$$I = \frac{\Gamma(3\epsilon + 2)\pi}{\Gamma[(3\epsilon/2) + (3/2)]^2}, \qquad I_D = I/c$$

another remarkably simple result. It can be seen that this has the correct behavior in the limits since

a. $\epsilon = 0$ gives $I = \Gamma(2)\pi/\Gamma(3/2)^2 = 4$ which is correct for a mapped flat plate which always has a chord of 4 giving $I_D = 1$.

---

*This appears in [B3], p. 263, No. 40. It is also uniformly convergent when $\epsilon < 1$ and has the same asymptotic rate of convergence as the A_n expansion.

b. $\varepsilon = 1$ gives $I = \Gamma(5)\eta/\Gamma(3)^2 = 6\pi$ so $I_D = 3\pi$ since $c = 2$
     for the circle which is the correct result according to section B4.

By using these formulas the analytic behavior as recorded on Fig. B1 was easy to
calculate.

However, this calculation served to indicate a rather obvious weakness in
the expanded forms used for the chord and area. In order to determine the chord
accurately a lot of terms had to be used since the convergence of the A_n
sequence is poor. To some extent this was also true of the area but much less
severe. Thus, at a $f = t/c$ ratio of 0.215 it was necessary to use 200 terms
in (B16)!

The subroutine which generated the various formulas was also cycled through
the optimization program described before (section B6a) down to a step size of
$h = 0.0000001$, and gave the optimum case of this family as

$\varepsilon = 0.3397098$, $f = t/c = 0.2151623$, $F = 7.7007989$

In this application — as in the straightforward parametric variation to define
the curve of Fig. B1 — the slow convergence was not important since only one
parameter (μ or actually ε) was being varied, but the implication for
general studies with many parameters were not regarded as very encouraging.
This will be discussed further in section B9. For the moment we merely note
that the optimum member of this family (above) has a wedge half angle of about

$$0.3397098 \times 90 \sim 30.57°$$

and is shown on Fig. B2. According to section B6a, the value of F is certainly
lower than that of the optimum ellipse, but the gain is trivial since the C_{D_A}
ratio is only 1.0015 (see Fig. B2).

B8.   CIRCULAR ARC

Because of the evident importance and different nature of wedge-end
profiles it was decided that at least one other case should be investigated.
It is known that the profiles generated by segments of circles can be analyzed
exactly and in fact the basic solution is given by Milne-Thomson [B4]. However,

109

one of the reasons for considering this case was to compare the known theory with the mapping format used here — in order to get a better understanding of the convergence situation. This was considered necessary because section B7 shows how poorly the zero factors converge when expanded naively, but this was no guarantee that a modulating term containing a_n coefficients would not make the situation worse still. Obviously such information and test cases would be important in designing an overall subroutine suitable for the most general minimization applications.

Therefore, some detail had to be added to Milne-Thomson's exposition and this turned out to be very fruitful since an exact formula (no quadratures) was found for the drag integral. This case then became the most important test problem since it had all the features desired for the most general program and all the relevant formulas exact.

Hence some explanation cannot be avoided and, whilst circular arc profiles are a natural aspect of Karman-Trefftz mappings, the coaxial circle method of Milne-Thomson is preferrable since it (eventually) suggests the forms which permit exact evaluation of the Q^4 integral. Briefly, the classical procedure is to start from bipolar coordinates defined in the $z = x + iy$ plane as sketched, whence
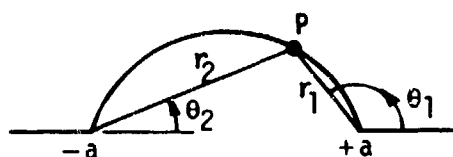
$$\ln \frac{z + a}{z - a} = \ln \frac{r_2}{r_1} + i(\theta_2 - \theta_1)$$

and then denote

$$\mu = \ln \frac{r_2}{r_1} ; \quad \lambda = \theta_2 - \theta_1; \quad \nu = \mu + i\lambda$$

so that profiles of constant λ are circular arcs. The mapping

$$z = a \coth \frac{1}{2} \nu \tag{B23}$$

then maps the lines $-\infty \leq \mu \leq +\infty$, $0 \geq \lambda \geq -2\pi$ into a connected sequence of shapes consisting of the real axis and a piece of circular arc which can either be concave or convex from a chosen side.

110

(a) There are many ways to get fluid motions into such a system (see e.g., Milne-Thomson), but one of the most fruitful is to consider various $W \rightarrow \nu$ mappings where

$$W = \phi + i\psi = \text{complex potential}$$

In particular the relation

$$W = \frac{2a}{m} \coth \left(\frac{\nu}{m}\right) \tag{B24}$$

is interesting because separating real and imaginary parts gives

$$\psi = \frac{-(2a/m)\ \sin\ (2\lambda/m)}{\cosh\ (2\mu/m) - \cos\ (2\lambda/m)} \quad , \quad \phi = \frac{(2a/m)\ \sinh\ (2\mu/m)}{\cosh\ (2\mu/m) - \cos\ (2\lambda/m)} \tag{B25}$$

the first of which vanishes for

$$\lambda = 0, \quad \pm \frac{m\pi}{2}, \ \pm\ m\pi, \ \ldots$$

Leaving aside some slightly subtle details about branches, it can be shown that if $0 \le m \le 2$ then the cases $\lambda = 0$, $\lambda = -m\pi/2$ give flows having the real axis and one of the above sequence of circular arcs as streamlines.

Although it is not possible to eliminate ν directly to give a $W(z)$ relation in general, the two limiting cases of interest to this work can be done, viz.

when $m = 2$, $w = z$ (infinite plate along $y = 0$)
when $m = 1$, $w = z + a^2/z$ (semicircle)

and evidently the range of interest is $1 \le m \le 2$.

(b) The complex velocity is, however, expressible in terms of ν for all cases since

$$q = u - iv = \frac{dW}{dz} = \frac{dW}{d\nu}\frac{d\nu}{dz} = \frac{4}{m^2} \frac{\sinh^2 \nu/2}{\sinh^2 \nu/m}$$

so that the surface velocity magnitude can be written

$$Q_s = \frac{4}{m^2} \left(\frac{\cosh \mu - 1}{\cosh 2\mu/m - 1} \right), \qquad x^2 > a^2$$

<div align="right">(B26)</div>

$$= \frac{4}{m^2} \left(\frac{\cosh \mu - \cos m\pi/2}{\cosh 2\mu/m + 1} \right), \qquad -a \leq x \leq +a$$

which are reasonable enough formulas in terms of the parameter μ. However, to relate these to the unit circle plane contained in $\zeta = \xi + i\eta$ it is necessary to find a mapping which maps the unit semicircle into one of the segments and has the same distant regions. Evidently a mapping of the same kind as (B23) must suffice, and by considering, therefore

$$\zeta = c \coth \frac{\nu}{n}$$

it is easy to show that the choice $n = 2m$, $c = 1$ is required giving

$$\zeta = \coth \frac{\nu}{2m} \qquad \text{or} \qquad e^{\nu/m} = \frac{\zeta + 1}{\zeta - 1}$$

Comparing this with (B24) and noting that the distant fields match only when $m = 2a$ gives the relation

$$\frac{z + m}{z - m} = \left(\frac{\zeta + 1}{\zeta - 1} \right)^m; \qquad m = 2 - \varepsilon = 1 + \mu \qquad (B27)$$

which is the usual Karman-Trefftz form.

By means of (B26) and (B27) the surface velocity can be expressed in terms of the usual unit circle angular variable since we get

$$e^{\mu/m} = \cot \frac{\omega}{2}$$

and then

$$Q_s = \frac{4^{1-\varepsilon}}{m^2} (2 \sin \omega)^\varepsilon \left(\cos^{2m} \frac{\omega}{2} + \sin^{2m} \frac{\omega}{2} + 2 \cos \varepsilon \frac{\pi}{2} \cos^m \frac{\omega}{2} \sin^m \frac{\omega}{2} \right)$$

which is fine for specific computation of Q_s on the profile, but not of much general use.

Much more significant is that by using ϕ as the independent variable an exact form for the basic drag integral can be found. Thus, from (B25) with $\lambda = -m\pi/2$ and $m = 2a$

$$\phi = \frac{2 \sinh 2\mu/m}{\cosh 2\mu/m + 1} = 2 \tanh \frac{\mu}{m}$$

giving

$$e^{\mu/m} = \sqrt{\frac{2 + \phi}{2 - \phi}}, \qquad (-2 \le \phi \le 2 \text{ on the surface})$$

whilst

$$I = \int_0^p Q^4 ds = \int_{-2}^2 Q^4 \frac{ds}{d\phi} d\phi = \int_{-2}^2 Q^3 d\phi \qquad (B28)$$

and Q can be written (with $\beta = \cos \epsilon\pi/2$)

$$Q = \frac{1}{4m^2} \left[(2 + \phi)^m + (2 - \phi)^m + 2\beta(4 - \phi^2)^{m/2} \right] (4 - \phi^2)^{\epsilon/2} \qquad (B29)$$

Substituting (B29) into (B28) and accounting for many symmetries in groups of terms gives, finally,*

$$I = \frac{2^9}{m^6 \Gamma(8)} \left[\Gamma(7 - \tfrac{3\epsilon}{2})\Gamma(1 + \tfrac{3\epsilon}{2}) + 6\beta\Gamma(6 - \epsilon)\Gamma(2 + \epsilon) + 3(1 + 4\beta^2)\Gamma(5 - \tfrac{\epsilon}{2})\Gamma(3 + \tfrac{\epsilon}{2}) \right.$$
$$\left. + 2\beta(3 + 2\beta^2)\Gamma(4)\Gamma(4) \right] \qquad (B30)$$

The other quantities needed for direct evaluation are the chord and area. These are given very simply by

$$c = m \qquad (B31)$$

and

---

*It is, again, easy to show that (B30) gives the same correct limiting values of I_D in the flat plate and semicircle cases as before, but there is no point in giving the details here.

113

$$A = m^2 \left(\frac{\theta \tan \theta - \sin^2 \theta}{\tan \theta \sin^2 \theta} \right) \tag{B32}$$

where θ is half the closure angle $(\theta = \tau/2)$. Note that for small values of θ, $A \to 0$ of $0(\theta)$, in fact

$$A \sim m^2 \left[\frac{2}{3} \theta + \frac{4}{45} \theta^3 + 0(\theta^5) \right]$$

Putting (B30), (B31) and (B32) together, the circular arc curve of Fig.B1 was produced by completely analytic steps. These formulas were also run through the minimization program down to $h = 0.0000001$ with the resulting optimum given as:

$$\epsilon = 0.2693423 \ (\tau \sim 48.5^0), \quad f = 0.2147540, \quad F = 7.7239339$$

As can be seen from Fig.B1 the drag characteristics are (slightly) less desirable than either the ellipse or canonical wedge end profiles. Fig.B2 shows the optimum shape compared with the optima of these other two families and also indicates that the drag ratio of the best circular arc is only 1.0030 x that of the best overall wedge end case.

(c) However, as pointed out before the greatest value of the circular arc is as a test case, because it has all the desired features of the general method. It remains therefore to cast the unit circle mapping (B27) into the format of this work. Differentiating gives

$$\frac{dz}{d\zeta} = \frac{4m^2 \ (\zeta + 1)^\mu (\zeta - 1)^\mu}{[(\zeta + 1)^m - (\zeta - 1)^m]^2} , \qquad \mu = 1 - \epsilon = m - 1$$

which can be reorganized to

$$\frac{dz}{d\zeta} = \left(1 - \frac{1}{\zeta^2} \right)^\mu \left\{ \frac{2m}{\zeta[(1 + 1/\zeta)^m - (1 - 1/\zeta)^m]} \right\}^2 = \left(1 - \frac{1}{\zeta^2} \right)^\mu g(\zeta)$$

showing that the modulating $g(\zeta)$ part is

$$g(\zeta) = \frac{4m^2}{\zeta^2} \left[(1 + \frac{1}{\zeta})^m - (1 - \frac{1}{\zeta})^m \right]^{-2}$$

This can be expanded in powers of $1/\zeta^2$ since

$$(1 + \frac{1}{\zeta})^m - (1 - \frac{1}{\zeta})^m = \frac{2m}{\zeta} \left(1 + \alpha_2 \frac{1}{\zeta^2} + \alpha_4 \frac{1}{\zeta^4} + \dots \right)$$

where

$$\alpha_2 = \frac{\mu(\mu - 1)}{3!} , \qquad \alpha_4 = \frac{\mu(\mu - 1)(\mu - 2)(\mu - 3)}{5!} , \dots$$

so that

$$g(\zeta) = \left(1 + \frac{\alpha_2}{\zeta^2} + \frac{\alpha_4}{\zeta^4} + \dots \right)^{-2} = 1 - \frac{2\alpha_2}{\zeta^2} - \frac{(2\alpha_4 + 3\alpha_2^2)}{\zeta^4} - \dots$$

These coefficients can be computed to any reasonable order by using existing subroutines which operate on series and, as expected, $g(\zeta)$ itself does not converge impressively. For instance, with $\mu = 0.9$ (which is certainly part of a reasonable test range) the 40th coefficient of $(1 + 1/\zeta)^\mu$ is 0.00008737 and the 40th coefficient of $g(\zeta)$ is 0.00004556, so the rate of convergence is about the same as for the singular factors. The combined 40th term is 0.00034836 showing, as anticipated, that product of the poorly convergent singular factors with the $g(\zeta)$ sequence only makes things worse. All this information is germane to the structure of the general minimization program. This topic is discussed next.

B9. GENERAL MINIMIZATION PROGRAM

(a) The numerical work described in sections B4 - B9 (Fig. B4) succeeded in establishing that the canonical wedge end optimum (section B7) was clearly the best of all the families and optima considered. However, as remarked before on a number of occasions (e.g., section B5c) we were loath to jump to the conclusion that this was the optimum just because of its extreme simplicity. Not only were such hasty arguments disproved by further calculations before (e.g., section B5c), but also it should be noted that the circular arc, which

was introduced merely as a further check case and which has a complicated and poorly convergent structure in terms of the a_n coefficients, nevertheless gives an optimum very close to the canonical shape. Moreover another factor had entered the picture at this point. The complex calculus of variations theory had been completed — admittedly on a very tentative basis. However, neither the ellipse (special case for $\tau = \pi$) nor the canonical wedge end profile satisfied the resulting differential equations supposedly defining the real extremum*. Although not conclusive, this fact together with the above arguments was sufficient to indicate that further numerical minimization studies were needed, and that they must encompass the complete system as outlined originally in section B3.

As has been noted before the convergence for the series in the general case is not adequate for them to be used to determine the area and chord. General operation of the numerical scheme described in section B6a requires a large number of passes for (say) the determination of 20 - 40 coefficients, and procedures adequate for only one parameter have to be reconsidered owing to the computing costs — even though this particular calculation only needs to be done once in principle. In this context it is also worth noting that if this is true in two dimensions, it is obviously even more important for the axisymmetric case.

(b) At first it was hoped that the convergence difficulty could be circumnavigated by replacing the series for chord and area by quadratures. A new program was written on this basis using various different numerical methods:

> Simpson's rule
> Cubic spline fits
> Fast Fourier transform fits

to carry out the quadratures. Even using 201 points not one of these was remotely accurate enough when compared with the circular arc exact solutions in the region of the various optima.

---

*No solutions for these equations have been found ab initio partly because of the speculative nature of their derivation. This phase of the work is simply not developed enough at the time of writing.

The reason for this failure of the conventional methods to give the kind of precision necessary for the minimization process to detect the influence of higher-order small coefficients is not hard to understand. All of such conventional methods depend very strongly on the fundamental axiom of classical numerical analysis -- that the data corresponds to a sufficiently smooth (differentiable) function. However, the functions to be integrated here are of the form (e.g., see (B14)).

$$I = \int_0^\pi (2 \sin \tfrac{\omega}{2})^p \ (2 \cos \tfrac{\omega}{2})^q \ f(\omega) \ d\omega \qquad (B33)$$

where $f(\omega)$ is smooth in the desired sense, but

$$0 \leq p, q \leq 1$$

Thus the singular factors cause a very rapid rise at the ends of the range and in fact the integrand of (B33) behaves as ω^p for small ω and so has an infinite derivative as $\omega \to 0$.

One way to get around this difficulty is the old (but very important) artifice of separating the singular terms and doing them analytically. A subroutine to affect this has been written and tested for integrals of the type shown in (B33). Its efficacy is staggering as can be seen from the results tabulated below on a simple test case where the complete answer is known, for instance $f(\omega) = 1$.

(c) The general program using this artifice for numerical quadrature has not been written but would not be difficult since the subroutines required and the basic operating process of the minimization part are all available. However, this program would not just be a repeat of that of section B6a with more accurate quadrature, since another very important feature for time and cost saving is that the old program computed the whole integrand each time, whereas it is obviously only necessary to update one term in (e.g.) the Fourier expansions each time an a_n coefficient is changed.

117

Table B1. % Error of I for Various Methods When $f(\omega) = 1$ (101 points)

Case		Simpson's Rule	Cubic Spline	Fast Fourier Transform	Separation of Singularity + Simpson's Rule
p	q				
0.1	0.1	-0.390048958	-0.396812512	-0.45374470	0.000000076
0.2	0.2	-0.224950593	-0.232855499	-0.267544643	0.000000236
0.3	0.3	-0.127376081	-0.134802905	-0.155229725	0.000000398
0.4	0.4	-0.070438403	-0.076724170	-0.088178328	0.000000521
0.5	0.5	-0.037729564	-0.042441076	-0.048640337	0.000000596
0.6	0.6	-0.019315228	-0.022617007	-0.025747832	0.000000620
0.7	0.7	-0.009221491	-0.011301525	-0.012755969	0.000000602
0.8	0.8	-0.003888859	-0.004997188	-0.005608282	0.000000546
0.9	0.9	-0.001220631	-0.001638814	-0.001845777	0.000000479
1.0	1.0	0.000000540	0.000002570	0.0	0.000000041

Since this would not be very difficult or costly it seems that it should be done if only to give, once and for all, the final optimum — and so define in a watertight manner the absolute lower limit on C_{D_A}. Not only will such studies not need to be repeated, but engineering compromises could then be organized on a firm objective basis.

B10. CONCLUSIONS

The studies carried out as described in sections B4 - B9 lead to the following straightforward conclusions:

a. A true optimum exists and can be found by a revised, more general version of the minimization program.

b. There is very little to choose between the class optima of ellipses, circular arcs and canonical wedge ends.

c. However the canonical wedge end is the best of these and it has finite (wedge) angles at the ends.

d. It would not be difficult to construct and run the general program (see a) to decide whether or not c is the absolute optimum.

e. Since the axisymmetric drag integral is similar, it should be possible to repeat this procedure using the theory of Appendix A and so define an axisymmetric true optimum.

B11. REFERENCES

B1. Thwaites, B. (ed.): Incompressible Aerodynamics. O.U.P., 1960.

B2. James, R.M.: A General Class of Exact Airfoil Solutions. J. of Aircraft, Vol. 9, No. 8, Aug. 1972.

B3. Whittaker, E.T. and Watson, G.N.: Modern Analysis. 4th Edition, C.U.P., 1952.

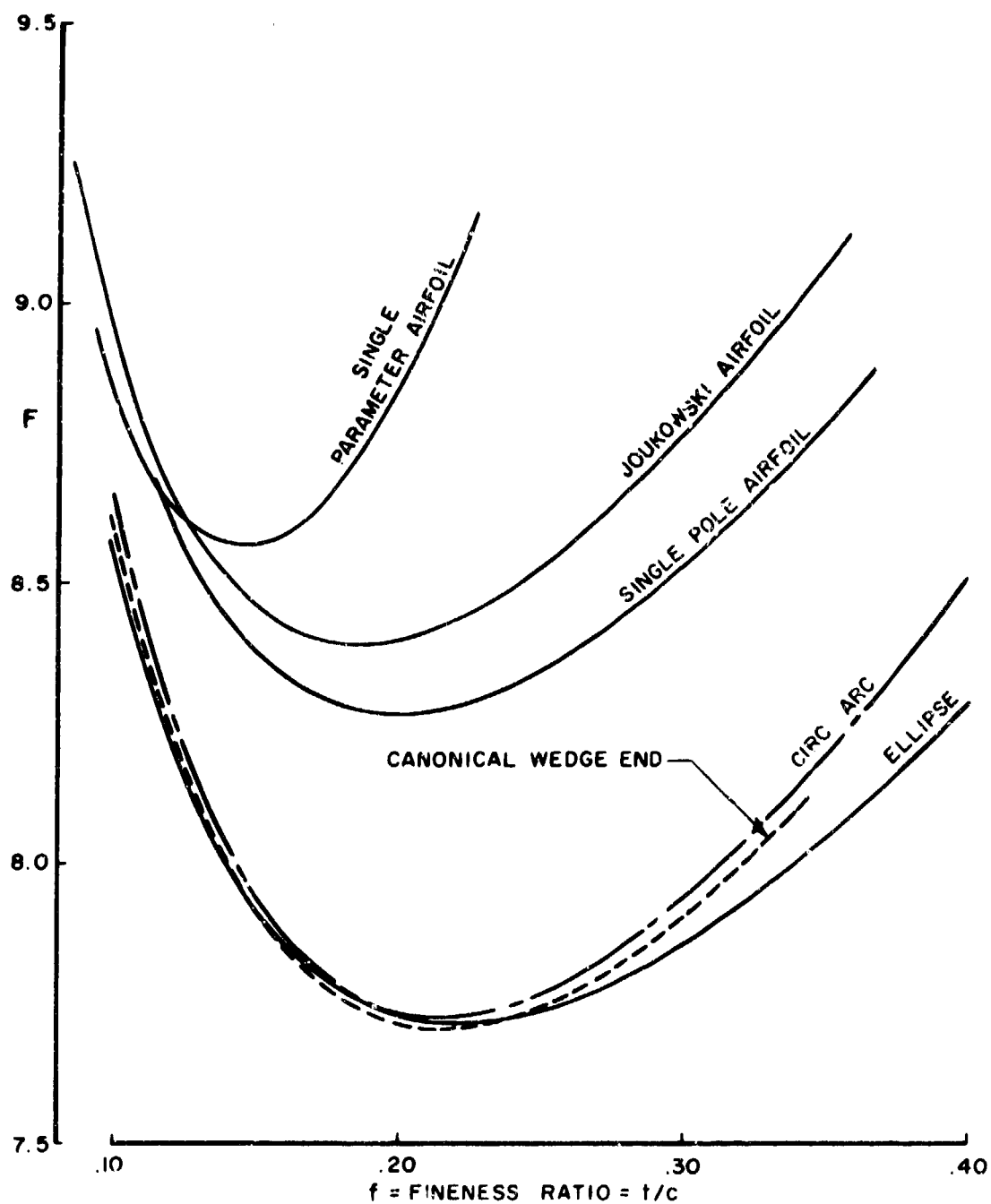B4. Milne-Thomson, L.M.: Theoretical Hydrodynamics. 2nd Edition, MacMillan, New York, 1950.

Figure B1. Geometric drag comparison factor F based on $\sqrt{\text{area}}$ for various two-dimensional special cases vs fineness ratio.
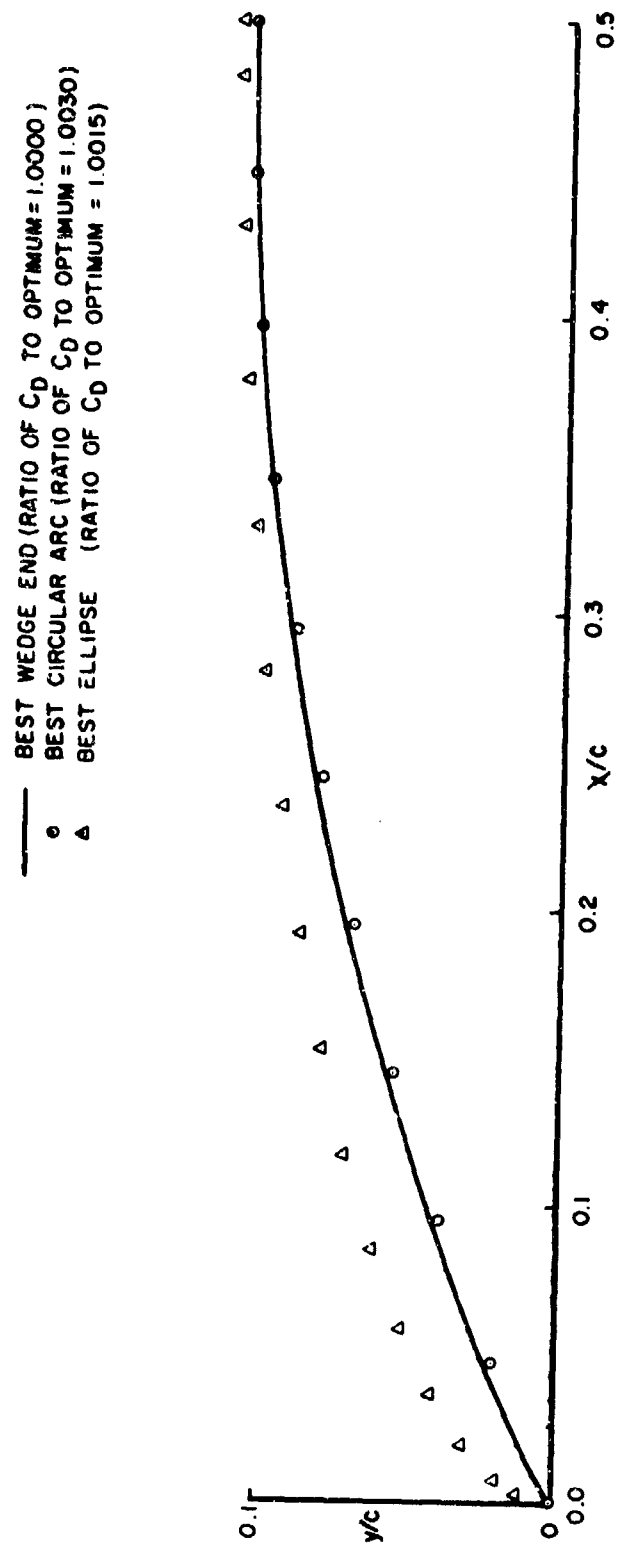
Figure B2. Comparison of the shapes of the three best special solutions from Fig. B1.

121